Application of Artificial Intelligence on Design Strategies to Optimize Urban Wind Energy

Stéphanie Higgins

A thesis in
The Department of
Building, Civil, and Environmental Engineering

Presented in Partial Fulfillment of the Requirements
for the Degree of Master of Applied Science
At
Concordia University
Montréal, Québec, Canada

December 2020

CONCORDIA UNIVERSITY

School of Graduate Studies

This is to certify that the thesis prepared

By: Stéphanie Higgins

Entitled: Application of Artificial Intelligence on Design Strategies to Optimize Urban Wind Energy

and submitted in partial fulfillment of the requirements for the degree of

Master of Applied Science (Building Engineering)

complies with the regulations of the University and meets the accepted standards with respect to originality and quality.

Signed by the final Examining Committee:

_____ Chair
Dr. Radu Zmeureanu

_____ Examiner
Dr. Lyes Kadem (External to program)

_____ Examiner
Dr. Hua Ge

_____ Thesis Supervisor
Dr. Theodore Stathopoulos

Approved by _____
Dr. Michelle Nokken, GPD
Department of Building, Civil, and Environmental Engineering

_____
Dr. Mourad Debbabi, Interim Dean
Gina Cody School of Engineering and Computer Science

Date: _____

ABSTRACT

Application of Artificial Intelligence on Design Strategies to Optimize Urban Wind Energy

Stéphanie Higgins

Maximizing urban wind energy capture constitutes a step towards self-sufficient buildings. Optimizing urban wind power requires knowledge of the environmental and building parameters modifying energy capture and tools for predicting urban wind behaviors.

This thesis main objective is to build a database to develop artificial intelligence (AI) programs to evaluate different design strategies and optimize urban wind energy. The database includes experimental wind tunnel velocities and turbulence intensities for terrain roughness, channeling effect, typical building shapes and several city configurations for several turbine locations. Wind velocities and turbulence intensities measured at the street-level and rooftop turbines on rectangular, U-shaped, and L-shaped buildings are further investigated with literature CFD results. Through the different combinations of experimental results and literature, a total of over 150 cases are added to the database. A decisional flow chart is developed using the results database and served as a results summary and an aid for programming the artificial intelligence (AI) networks. The elaborated database is implemented in an expert system and an artificial neural network. The AI programs are tested with city configurations models and a real case study, René-Lévesque Boulevard in downtown Montreal. Comparing the testing set to the actual experimental values, the data expert system predicts the modification in wind velocities with 68% - 98% accuracy. The feedforward artificial neural network developed is slightly more accurate than the

expert system, showing success rates from 76% to 99%. Thus, AI tools and the decisional flow chart approach may be used for a preliminary assessment of the different design strategies power capture in urban environment.

Acknowledgments

It is with recognition that I want to acknowledge several persons without whom my masters would not be the same. Their help has been primordial for the completion of this thesis.

The first person I want to thank for his support and guidance is my supervisor, Dr. Ted Stathopoulos. He motivated me, cultivated my interest in research and guided me towards my academic development. With his support, I was able to achieve something I never thought I would be able to do. I am thankful for his support for the past years.

I would like to make a special mention to my family and friends who unconditionally supported me through those years, I would like to show my appreciation for everything you did.

Table of contents

List of figures viii
List of tables x
Nomenclature xi
Chapter 1 Introduction 1
1.1 Background 1
1.2 Objectives 2
1.3 Outline 2
Chapter 2 Literature Review 3
2.1 Overview 3
2.2 Environmental Features 3
2.2.1 Terrain Roughness 3
2.2.2 Topography 5
2.2.3 Diurnal and Seasonal Cycles 8
2.2.4 Climate Change 9
2.3 Building features 10
2.3.1 Wind turbine types 10
2.3.2 Turbine placement 12
2.3.3 Roof slopes 15
2.3.4 Roof parapets 18
2.4 Guidelines and Summary 19
Chapter 3 Modeling Techniques Methodology 23
3.1 Overview 23
3.2 Wind Tunnel Testing 23
3.2.1 Boundary Layer Wind Tunnel 23
3.2.2 Wind Profile 25
3.2.2 Wind Tunnel Parametric Models 26
3.2.3 Overview 30
3.3 Artificial Intelligence 31
3.3.1 Expert System 31
3.3.2 Neural Network 32
4.1 Overview 37
4.2 Channeling 37

4.3 Building Shapes 42
4.4 Database city configurations 53
4.5 Database Accuracy Statistical Analysis 55
4.6 Summary 56
Chapter 5 Artificial Intelligence Results and Discussion 57
5.1 Overview 57
5.2 Testing set 57
5.3 Flow Chart Approach 60
5.4 Expert system and ANN 64
5.5 Highlight 67
Chapter 6 Conclusion 68
6.1 Summary 68
6.2 Guidelines 69
6.3 Future studies 70
References 72
Appendices 77
Appendix-A: Wind Tunnel Results 78
Appendix-B: Expert 2.0 Program 88
Appendix-C: Artificial Neural Network Programming 125
C. 1 ANN Programming Architecture 125
C.2 Matrix 126
C.3 Program 131

List of figures

Fig. 2.1 Wind flow over hills and escarpments (NBCC 2015) 6

Fig. 2.2 Fluid streamlines undergoing channeling effect 7

Fig. 2.3 Illustration of vortex shedding (a), buffeting (b), and aeroelastic forces (c) 13

Fig. 2.4 Wind turbine placement located on the building rooftop (1), building integrated (2) and on building sides (3) as per Stankovic et al, 2005 (a) and as per Stathopoulos et al, 2018 (b) 15

Fig. 2.5 Wind sped profile and turbulence intensities curves for roof slopes 3:10, 5:10, and 7.5:10 (Tominaga et al, 2015) 17

Fig. 3.1 Cross-section of Concordia University atmospheric boundary layer wind tunnel 25

Fig. 3.2 Velocity and turbulence intensity profiles used in the present thesis (Higgins and Stathopoulos, 2020) 26

Fig. 3.3 Building shape models: square, rectangular, U-shaped, T-shaped, and L-shaped buildings (Higgins and Stathopoulos, 2020) 27

Fig. 3.4 Model dimensions and measuring points for the square, rectangular, U-shaped, T-shaped, and L-shaped buildings 29

Fig. 3.5 City clusters with similar building shapes (a), newly implemented building (b), and Boul. René-Lévesque, Montréal (c) in the atmospheric boundary layer wind tunnel of Concordia University (Higgins and Stathopoulos, 2020) 30

Fig. 3.6 ANN architecture programmed in MATLAB 35

Fig. 3.7 Expert system (a) and artificial neural network (b) architecture (Higgins and Stathopoulos, 2020) 34

Fig. 4.1 Channelling requirements (modified after Gandemer and Guyot, 1976, Higgins and Stathopoulos, 2020) 38

Fig. 4.2 Tunnel Louis-Hippolyte Lafontaine model in the atmospheric boundary layer wind tunnel in Concordia University (Higgins and Stathopoulos, 2020) 39

Fig. 4.3 Normalized wind speeds and turbulence intensity per wind direction at the entrance of the valley, mid-point, and wake of the channel (modified after Higgins and Stathopoulos, 2020) 40

Fig. 4.4 Normalized wind velocities and turbulence intensities per wind direction for square (a) and rectangular (b) building shapes 45

Fig. 4.5 Normalized wind velocities and turbulence intensities per wind direction for U-shaped building (a) and T-shaped (b) buildings 46

Fig. 4.6 Normalized wind velocities and turbulence intensities per wind direction for the L-shaped building 47

Fig. 4.7 Normalized wind velocities and normalized turbulence intensities for the rectangular building shape tested at a wind direction of 0^{o} (modified after Higgins and Stathopoulos, 2020) 52

Fig. 5.1 Flow chart approach 60

List of tables

Table 2.1 Davenport terrain classification (Davenport, 1960) 4

Table 2.2 Overall structure, aesthetics, cost and power retrieved from H-rotor, Darrieus, Lotus-shape, O-shape, and HAWT 11

Table 2.3 Wind velocities and turbulence modification due to several urban parameters (Higgins and Stathopoulos, 2019) 20

Table 4.1 Normalized wind velocities V/V_o for the square, rectangular. T-shape, U-shape, and L-shape for the wind directions $\boldsymbol{\theta}$ 0° to 90° (increments of 15°) (modified after Higgins and Stathopoulos, 2020) 50

Table 4.2 Results for the similar building shape city panel (a) and similar height panel (b) 54

Table 5.1 City cluster and René-Lévesque street results for the testing set 59

Table 5.2 Assessment and comparison of turbine locations in a new building implementation in a city configuration (testing set): experimental results, flow chart, expert system and ANN (Higgins and Stathopoulos, 2020) 65

Nomenclature

α	mean wind speed exponent
a_k	expert system input coefficient
A	cross-sectional area, perpendicular to the wind flow
b	bias
E	wind energy
f	frequency
f_n	neural network output
H_h	escarpment height
k	constant based on shape
L	characteristic length
L_h	horizontal distance upwind from the peak to the point where the ground surface lies
n	sample size
σ	variance
ρ	air density
s	standard deviation
St	Strouhal number
Δs	speed-up factor between the modified and undisturbed wind speed due to hill and escarpments
θ	angle between the building's axis of symmetry and the wind direction, referred as the wind direction
t	T-test resut
T	time period
μ	sample mean
U	wind speed
V	wind velocity
$V(z)$	wind velocity at distance x from the escarpment at height z
w_i	neural network input weight
x	given variable

x_i	neural network input variable
x_k	expert system input variable
Z	height above ground
Z_g	gradient height

Superscript

_	average

Subscript

1	location 1
2	location 2
o	upstream
g	gradient height
i	given artificial neural network layer
k	hidden layer of the neural network
n	given expert system rule
x	x-direction
y	y-direction
z	z-direction, height

Abbreviation

AI	artificial intelligence
ANN	artificial neural network
CFD	computational fluid dynamics
HAWT	horizonal axis wind turbine
RMS	root mean square
SW	south west
TI	turbulence intensity
VAWT	vertical axis wind turbine

Chapter 1 Introduction

1.1 Background

Wind energy in urban environment may be maximized by appropriate design strategies. Investigating the factors modifying the turbine efficiency allows the development of design strategies and the development of modeling techniques to improve the wind energy capture. Wind energy E is expressed as Eq. (1.1):

$$E = \frac{1}{2}\rho V^3 AT \tag{1.1}$$

where ρ is the air density (kg/m^3), V is the wind velocity (m/s), A is the surface area of the turbine (m^2) and T is the period of time (s).

As demonstrated in Eq. (1.1), wind energy is a function of the velocity cubed. Thus, wind energy production is augmented by higher wind speeds. As wind turbines efficiency is reduced by higher turbulence intensities, turbine locations in low turbulence zones are preferred. Many combinations of environmental and structural characteristics define wind velocities and turbulent wind flow in urban environment, including roughness, topography, temperature and pressure variations, building shapes, and rooftop features. To optimize urban wind power capture, several features modifying wind velocities and turbulence intensities are investigated through different means (literature and modeling techniques) allowing to construct a complete database. Previous studies using a results database with artificial intelligence (AI) showed encouraging results for predicting meteorological wind modifications (Blanchard et al, 2019) and for predicting thermal comfort index in buildings (Ngarama et al, 2020). Thus, it is interesting to test AI applications on urban wind energy in the aim to predict wind power capture and choose design strategies to maximize power production.

1.2 Objectives

This study attempts to define suitable design strategies and modeling techniques to optimize urban wind energy. Objectives include the development of a database of environmental and building features modifying wind energy capture in urban environment, retrieving guidelines on design strategies to optimize urban wind power energy and the elaboration of accurate modeling techniques for predicting modifications in wind velocities and wind power. Due to lack of study on this issue and as urban wind energy contributes to the development of sustainable buildings, there is a need for deeper investigation.

1.3 Outline

This study will be described into seven different chapters. Chapter 2 focuses on the literature review of the environmental and building features modifying wind velocities and turbulence intensities. This comprehensive assessment is needed for Chapter 3 which describes the modeling techniques methodology for wind tunnel testing and artificial intelligence. Chapter 4 presents and discusses the wind tunnel results for wind speeds and turbulence intensities for channeling, building shapes, and city configurations whereas chapter 5 discusses the results of the testing set obtained through artificial intelligence modeling and the accuracy of each AI system. Chapter 6 presents conclusions on the best design strategies and the use of modeling techniques, and the future works recommended.

Chapter 2 Literature Review

2.1 Overview

Wind turbine power is altered by the turbine efficiency and the upstream wind velocities. Wind turbine efficiency is fluctuating as a result of the wind flow conditions. Knowing the effect of both environmental and building features on wind velocities and turbulence intensities will allow to determine designs optimizing wind power capture. In literature from the past decade, many sources describe the modification in wind velocities and turbulence due to terrain roughness, topography, diurnal and seasonal cycles, climate change, and roof features. From the assessment of these parameters, some guidelines, controversies, and lack of studies on the suitable turbine positioning are expressed. This assessment will generate some guidelines and orient the database building and modeling techniques for predicting wind velocities and power capture.

2.2 Environmental Features

Wind speeds and turbulence are greatly affecting the turbines' wind energy capture. Environmental factors enhancing or reducing wind speeds and turbulence include terrain roughness, topography, seasonal and diurnal cycles, climate change. These are further discussed in the following subsections.

2.2.1 Terrain Roughness

Wind velocity modifications from the upstream velocity V_o due to terrain roughness are calculated from the power law, see Eq. (2.1), and the Davenport classification, see Table 2.1. The power law is defined as:

$$\frac{V_z}{V_{zg}} = (\frac{Z}{Z_g})^{\alpha} \quad \text{Eq. (2.1)}$$

where V is the velocity, z the height above ground, Z_g is the gradient height, α is the mean wind speed exponent, found in Table 2.1.

Table 2.1: Davenport terrain classification (Davenport, 1960)

Terrain Category	Terrain description	Gradient height (m)	Roughness length (m)	Mean speed exponent	Gust speed exponent
1	Open sea, ice, tundra, desert	250	0.001	0.11	0.07
2	Open country with low scrub or scattered trees	300	0.03	0.15	0.09
3	Suburban areas, small towns, well wooden areas	400	0.3	0.25	0.14
4	Numerous tall buildings, city centres, well developed industrial areas	500	3	0.36	0.2

The power law for the suburban or urban terrain and for the open area, at a given wind velocity and height is calculated. Then, the ratio of the modifications in wind velocities for the suburban or urban terrain compared to the open terrain is obtained. The measured velocity V in urban and suburban terrain reduces by a factor of 0.84 to 0.91 compared to the upstream wind velocity V_o at the same height (Higgins and Stathopoulos, 2019). This ratio, V/V_o, will be further referred as the normalized wind velocity. While approaching urban terrain clearly diminishes wind speeds and increases turbulence, suitable topography may enhance wind velocity.

2.2.2 Topography

Topography, especially escarpments and hills, increases wind speeds. The NBCC 2015 presents a formula to express the quantitative increased in wind speeds on from the bottom to the top of hills and escarpments having a length L_h to height H_h ratio higher than 1:10, see Eq. (2.2), Eq. (2.3) and supporting Fig. 2.1:

$$V(z) = V_o(z) \cdot \Delta s + V_o(z) \tag{2.2}$$

$$\Delta s = \Delta s_{max}(1 - \frac{|x|}{kL_h} e^{az/L_h}) \tag{2.3}$$

where *V(z)* is the velocity at distance *x* from the escarpment at height z above the surface, Δs is $2.2\ H_h/L_h$, L_h is horizontal distance upwind from the peak to the point where the ground surface lies, H_h is the height of the escarpment, *x* is the horizontal distance from the peak of the escarpment or hill, *k* and *a* are constants based on the topographic shape; these definitions are illustrated in Fig. 2.1:

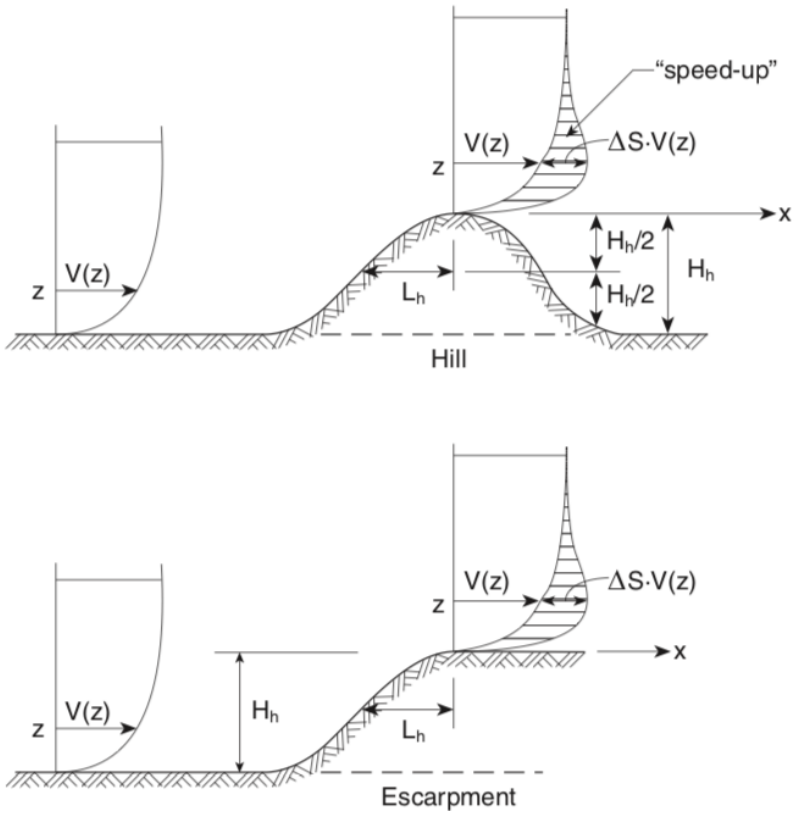

$$V = \Delta S \cdot V(z); \quad \Delta S = \Delta S_{max}\left(1 - \frac{|x|}{kL_h}\right)\exp\left(-az/L_h\right)$$

where

ΔS_{max}= applicable value from the table below
x=horizontal distance from the peak of the hill or escarpment
L_h=horizontal distance upwind from the peak to the point where the ground surface lies at half the height of the hill or escarpment, or $2H_h$ (where H_h=height of hill or escarpment) whichever is greater

Hill or escarpment	Δs_{max} [1]	a	k, where $x < 0$	k, where $x \geq 0$
2-dimensional hill	$2.2H_h/L_h$	3	1.5	1.5
2-dimensional escarpment	$1.3H_h/L_h$	2.5	1.5	4
3-dimensional axi-symmetrical hill	$1.6H_h/L_h$	4	1.5	1.5

[1] For H_h/L_h>0.5, assume H_h/L_h= 0.5and substitute 2 H_h for L_h in the equation for Δs

Fig. 2.1: Wind flow over hills and escarpments (NBCC 2015)

The change in velocity profiles is defined as a function of the hill or escarpment height, length, the horizontal distance from the bottom of the hill or escarpment to the point of measurement, and shape of the topographic region. By computing the maximum and minimum attainable factors k and a as per NBCC 2015, the ratio of the measured velocity to the upstream velocity, V/V_o, ranges between 1.9 to 3.23 (Higgins and Stathopoulos, 2019). Corresponding results were found by works of Winstraw et al (2017) where V/V_o ranged between approximatively 2.0 and 3.0 for hills.

Valleys are also suggested to favour higher wind speeds. Wind velocities are expected to augment at the wake of the valley due to channelling effect (Winstraw et al, 2017). Channeling effect consists in forcing fluid streamlines along a defined axis in a smaller cross-sectional area, resulting in flow acceleration. Fig. 2.2 shows a physical sketch of channeling. As shown in Fig. 2.2, the fluids streamlines are compressed in the middle section:

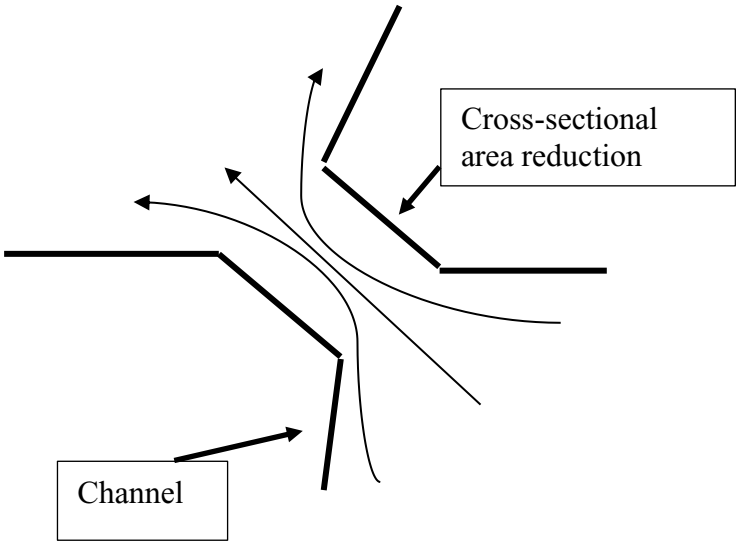

Fig. 2.2: Fluid streamlines undergoing channeling effect

The resulting wind flow acceleration is explained through continuity equation and conservation of mass, which is simplified to:

$$\rho A V_1 = \rho A V_2 \quad (2.4)$$

where ρ is the fluid density (kg/m^3), A is the cross-sectional area (m^2), and V is the velocity (m/s). According to Eq. (2.4) and assuming constant air density, as cross-sectional area decreases, the wind speed increases. Since wind flows through the least resistance path, the flow will be directed through the channel and will be accelerated. Thus, as valleys might show channeling effect, the wind velocities may be significantly increased and yielded in higher power production.

Ridges are also expected to lead to an increased wind speed. Winstraw et al (2017) proposes a wind velocity modification between 1.3 to 3.0 at the summit of ridges. Lower increase in wind velocities on upper slopes and valleys is proposed by Winstraw et al, 2017 (Higgins and Stathopoulos, 2019). As few studies review the effect of topography on wind velocities, the Winstraw's results cannot be compared and analysed easily. Thus, a study on the ratio of the measured velocity V to the upstream velocity V_o of valleys is needed; and an appropriate use of topography may significantly optimize wind power capture.

2.2.3 Diurnal and Seasonal Cycles

Wind turbulence and velocities are expected to be varying through daily and seasonally cycles as reviewed in Heppelmann et al (2016), Winstraw et al (2017) and Englberger and Dornback (2016). Heppelmann et al (2016) demonstrates results of lower wind speeds at nighttime whereas Winstraw et al (2017) hypothesises lower wind speeds in late mornings and afternoons. Recent literature also shows variations in wind power production depending on the seasons, although discrepancies occur on the nature of the variations recorded. Controversies on the effect of diurnal and seasonal cycles on power production may be explained by the differences in geography and temperature locations of the measurement sites (McInnes et al, 2011). Interestingly, high peaks in

wind speed frequencies on a seasonally and diurnal cycle are also observed on the wind spectrum. As many elements suggest, a variation in wind power production among these cycles is expected, although it remains uncertain if diurnal and seasonal cycles increase or decrease wind velocities and turbulence.

2.2.4 Climate Change

With the observed recent changes in mean surface temperatures due to climate change, many studies focus on the modifications in the critical wind directions and velocities (Higgins et Stathopoulos, 2019). Important changes are highlighted in wind trends in various geographical locations. Due to the observed decreasing atmospheric temperature and pressure gradients, modifications in critical wind speeds are documented (McInnes et al, 2011). The increased surface temperature brings modifications in the observed turbulence intensities (McInnes et al, 2011). Klink (1999), Pryor and Barthlemie (2009), McInnes et al (2001) and Jiang (2007) all note different modifications on wind velocities due to climate change: some report increased velocities, other decreased velocities. Discrepancies occur on the precise nature of wind speed modification due to climate change. These discrepancies are believed to be due to measurements taken in different geographical locations (McInnes et al, 2011). Nonetheless, wind velocities and turbulence intensities are expected to change in both magnitude and direction depending on geographical locations. As mentioned by Higgins and Stathopoulos (2019), observed changes in major wind trends, especially on the critical wind directions, turbulence intensities and speeds "are to be taken into account while seeking for optimal energy output for long term projects".

2.3 Building features

Through the aforementioned environmental feature and their effect on wind speeds and turbulence, some information is retrieved for an optimal turbine positioning. Depending on the turbine type, location, and the building roof design, increased wind power may be observed (Higgins and Stathopoulos, 2019). Thus, knowledge of turbine and building features is necessary.

2.3.1 Wind turbine types

Wind turbines are distinguished between vertical axis wind turbines (VAWT) and horizontal axis wind turbines (HAWT). VAWT can retrieve energy from all wind directions whereas HAWT cannot (Stathopoulos et al, 2018). However, an HAWT captures more wind energy than a VAWT at same wind speeds. Most wind turbines do not cope well with turbulence, especially HAWT. It is suggested to use HAWT in open areas and VAWT in higher turbulence areas, as in urban areas. Moreover, in environment with a more than one critical wind direction, VAWT are preferred over HAWT.

Different VAWT types with diverse mechanical components exists. Comparing the different types of turbines and rotors include the analysis of multiple factors counting power capture, production/maintenance cost and efficiency. In urban environment, good aesthetics and low noise levels are important for both the public acceptance and comfort. Table 2.2 summarizes the complexity of the overall turbine structure, aesthetics, cost and power from the main VAWT and rotors types, Savionius, H-Darrieus, Darrieus, Lotus, and O-shaped, compared to the HAWT.

Literature describes three types of VAWT rotors; Savionius, H-Darrieus (H-rotors), and Darrieus, each presenting advantage and inconveniences. Stathopoulos et al (2018) demonstrates the low cost and low efficiency of Savionius rotors compared to Darrieus or the H-Darrieus rotors.

Through literature analysis, it is recommended that Darrieus rotors are used on VAWT on rooftops due to low noise levels and pleasing aesthetics (Stathopoulos et al, 2018). Recent research present innovative types of vertical axis rooftop wind turbines, the lotus-shape and O-shape turbines. Lotus-shaped turbines, although inexpensive, show low power capture according to studies made by Stathopoulos et al (2018). Thus, it has not been recommended to use such turbines in urban environment. O-shaped turbine, developed by Nicolas Orellana, University of Lecaster, is a small VAWT made of complex triangular blades (Evans, 2018). No results on the power output has been yet released, but this turbine might yield in better wind power capture. Comparing the presented VAWT to the HAWT, the overall structure is very complex and has bad aesthetics, although it is less expensive than some VAWT. HAWT allows to retrieve a lot of power from the incoming wind but does not perform well in high turbulence zones.

Table 2.2: Overall structure, aesthetics, cost and power retrieved from H-rotor, Darrieus, Lotus-shape, O-shape, and HAWT

	Savonius	**H-rotor**	**Darrieus**	**Lotus**	**O-shape**	**HAWT**
Overall structure	Simple	Simple	Simple	Simple	More complex	Complicated
Aesthetics	Good	Bad	Good	Very good	Very good	Bad
Cost	Low	Higher	Higher	Low	Low	Low
Power retrieved	Very low	Higher	Higher	Very low	N/A	High

To further increase performance of VAWT having a low power capture, as the VAWT with Savonius rotors, design strategies include the addition of diffusers around the turbine. As stated by Stankovic et al (2005) and Dilimunati et al (2017), diffusers may increase significantly the power of the turbine due to channeling effect. Diffusers may be implemented around the turbine blade

itself or implemented through the architecture of the building. The later design option will be further discussed in turbine placement strategies.

2.3.2 Turbine placement

As stated by Higgins and Stathopoulos, 2019, "maximization of power production of any wind turbine requires to be positioned in low turbulence intensities zones". Knowledge of turbulence intensity definition and mechanisms in urban environments is required to select the turbine location leading to a maximum turbine efficiency.

Turbulence intensity is defined as the numerical appreciation of the unsteadiness of the wind flow. Mechanisms defining turbulence shall be considered to ensure optimal wind turbine functioning. Turbulence may be categorized in the following three forms:

-Vortex shedding (turbulence due to bluff-body itself at the wake of the body)

-Buffeting (turbulence in the approaching flow)

-Aeroelastic forces (turbulence due to the movement of the structure itself)

Fig. 2.3 shows the illustration of wind flow in vortex shedding (a), buffeting (b), and aeroelastic forces (c). Definitions of the previously listed elements are found in bluff-body aerodynamics concepts. Vortex shedding, see Fig. 2.3a, is a form of turbulence due to the bluff body itself causing flow separation at the body edges (Carruther and Houghton, 1976). Vortices are formed in the wake of the body (Carruther and Houghton, 1976). Vortex formation frequency depends on the approaching wind velocity V and shape of the bluff body (Carruther and Houghton, 1976). Exact vortices frequency may be retrieved through the Strouhal number St, defined as the ratio of the characteristic length L times the frequency f to the approaching wind velocity V. In-phase vortices, known as galloping, shall be avoided to prevent resonance (Carruther and Houghton, 1976).

Resonance occurs with the augmented accumulation of energy of in-phase frequencies (Chopra, 2012). If the in-phase frequencies due to vortices and the natural frequency of the structure equates, both significant energies will be added. The structure would then exceed the maximum capacity and will fail. Buffeting, see Fig. 2.3b, consists in turbulence found in the approaching flow caused by upstream obstacles (Carruthers and Houghton, 1976). In urban environment, increased terrain roughness is a form of buffeting. Another form of buffeting is street canyons, defined as the vertical vortex flow between buildings as illustrated in Fig. 2.3b. Skimming flow refers to the streamlines undisturbed by turbulence and free of any flow separation. Aeroelastic forces, see Fig. 2.3c cause turbulence through the movement of the body itself, i.e. aerodynamic damping, and is of interest especially in high-rise buildings (Carruthers and Houghton, 1976, Chopra, 2012). Especially in urban environment, all three turbulence forms are to be considered, as wind flows through many obstacles, thus allowing increased buffeting and vortex shedding. In presence of numerous high-rise buildings, aeroelastic forces should not be neglected.

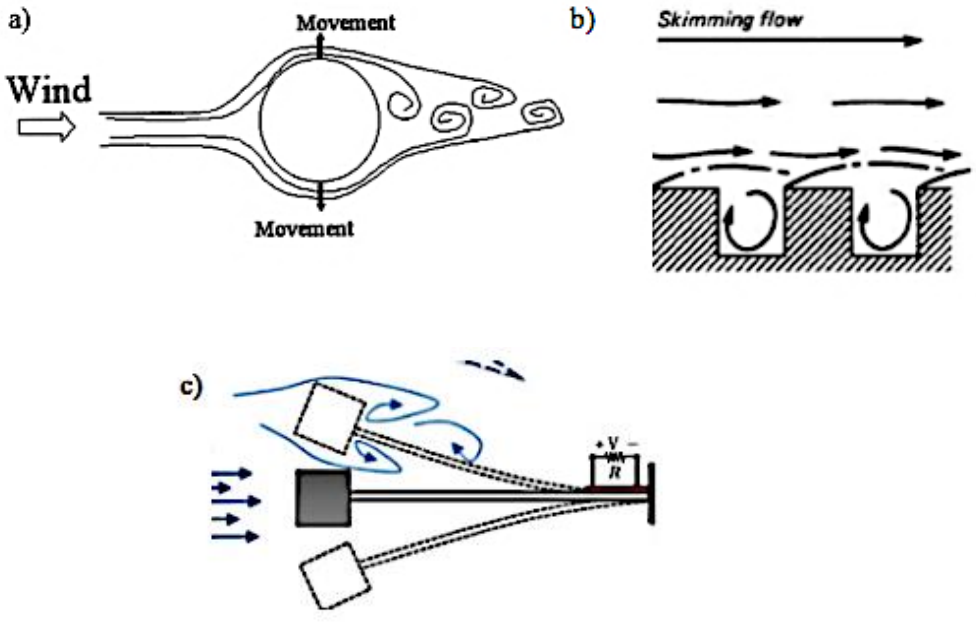

Fig. 2.3: Illustration of vortex shedding (a), buffeting (b), and aeroelastic forces (c)

Moreover, in urban environment, turbulence tends to be increased due to some building features, as arcades and openings (Higgins and Stathopoulos, 2019), and in some particular city configurations presenting urban street canyons and increased terrain roughness, thus turbine placement in these zones should be avoided.

In urban environment, turbines are usually placed in three different manners: on the side of a building, on a building rooftop, and in between two adjacent buildings (Stankovic et al, 2005, Stathopoulos et al, 2018). Fig. 2.4 examines and compares the main building placement strategies as per Stathopoulos et al (2018) in Fig. 2.4a and Stankovic et al (2005) in Fig. 2.4b. Positioning strategies of wind turbines include either on building sides (1), integrated (2) - turbine integration in between two adjacent buildings or in a building core - or on rooftop (3). Proposed turbine placement is similar between paper reviews of Stankovic et al (2005) and Stathopoulos et al (2018) with turbine located on the building rooftop, building integrated, and on the building sides. These three different strategies show different efficiencies. Wind turbines placed on building sides show ratio of the recorded velocity at the turbine V to the upstream velocity V_o of 0.8 whereas rooftop buildings V/V_o ranges between 1.12 to 1.16 and building integrated wind turbines, 1.13 to 1.51 (Stankovic et al, 2005). Significant increase in wind power production in case of a building integrated wind turbine was corroborated in an internal study at Concordia University (Macera et al, 2017). Integrated building turbines ingenuity use some fluid mechanics principles, where the fluids are being forced between two building parts, thus increasing wind speeds by the reduction in the cross-sectional area. Zhou et al (2017) examines the possible building shapes in cases of a turbine implemented in between two adjacent buildings; cubic, cylindrical, half-cylindrical, and composite. Zhou et al (2017) experiment concludes that composite prism shape is the optimal shape to ensure maximum power capture. As the presence of diffusers increases wind speeds and

power in case of building integrated turbine, it is deduced that the turbine itself may be surrounded by diffusers to enhance wind speeds. Dilimulati et al (2017) corroborates the hypothesis and demonstrates a 1.23 to 1.74 power increased for a turbine with blades surrounded by a diffuser.

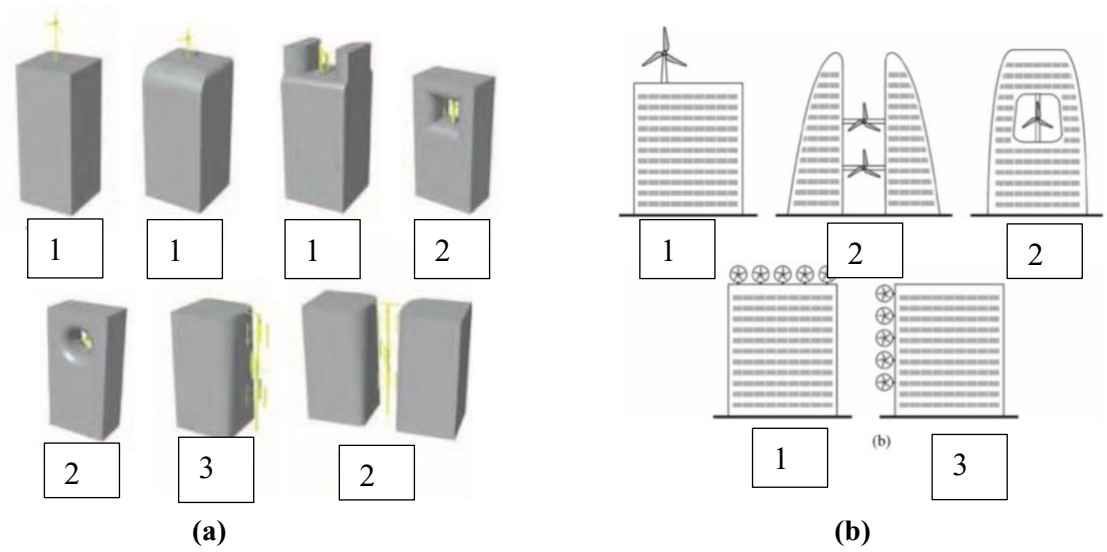

Fig. 2.4: Wind turbine placement located on the building rooftop (1), building integrated (2) and on building sides (3) as per Stankovic et al, 2005 (a) and as per Stathopoulos et al, 2018 (b)

The modification in wind velocities, quantified as V/V_o, found in Stankovic et al (2005) varied as a function of not only turbine positioning but also by the wind critical wind direction(s). Lack of studies on the values of V/V_o due to different building strategies exist; results found in Stankovic et al (2005) cannot be compared. Therefore, experiments on defining modification coefficients are useful in different wind turbine positioning strategies as they address modifications of wind flow properties, turbulence and velocities.

2.3.3 Roof slopes

As aforementioned, building design may change the upstream wind velocity. Especially for roof-mounted VAWT, roof features may modify the energy capture and turbine efficiency, through the

modifications of wind velocities and turbulence intensities. Many studies comment the difference in wind profiles and turbulence intensity curves due to various roof slopes. A thorough analysis shows higher turbulence intensities at roof angles higher than 20 degrees (Ozmen et al, 2016, Tominaga et al, 2015, and Abohela et al, 2015).

By comparing results from Tominaga et al (2015), Ozmen et al (2016) and Abohela et al (2015) there is an agreement that wind flow properties tend to change at a roof angle of 20 degrees. For roof angles higher than 20 degrees, turbulence at the wake of the rooftop is higher and thus the flow reattachment length is longer (Tominaga et al, 2015, Ozmen et al, 2016, Abohela et al, 2015). This is shown in Fig. 2.5, comparing the turbulence intensities and wind speeds profiles:

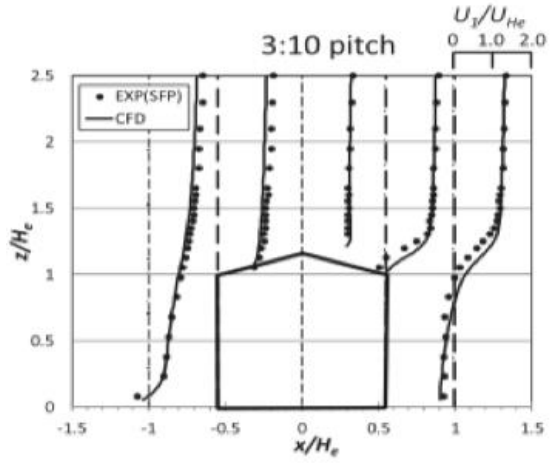
3:10 pitch
U_1/U_{He}
0 1.0 2.0
EXP(SFP)
CFD
z/H_e
x/H_e

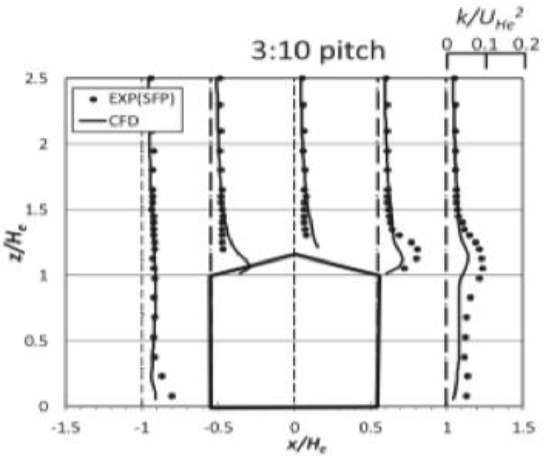
3:10 pitch
k/U_{He}^2
0 0.1 0.2
EXP(SFP)
CFD
z/H_e
x/H_e

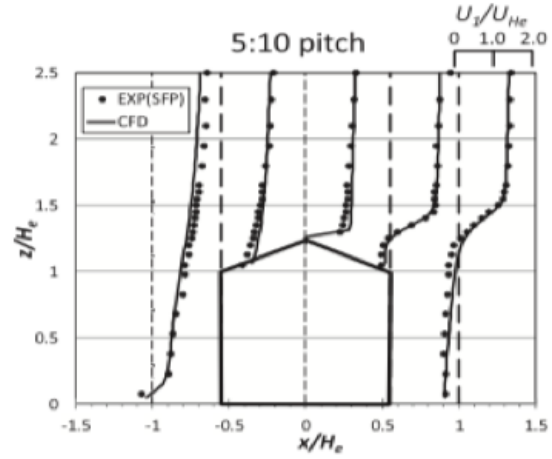
5:10 pitch
U_1/U_{He}
0 1.0 2.0
EXP(SFP)
CFD
z/H_e
x/H_e

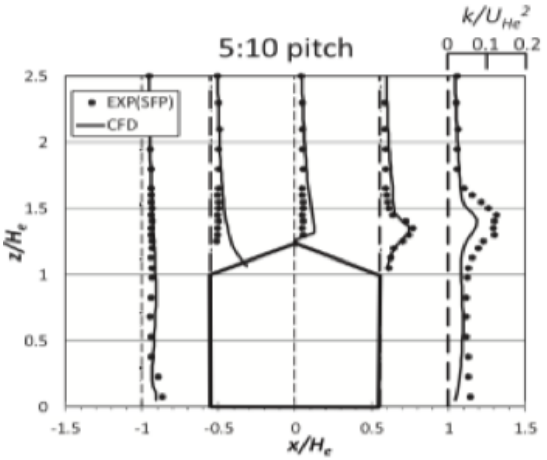
5:10 pitch
k/U_{He}^2
0 0.1 0.2
EXP(SFP)
CFD
z/H_e
x/H_e

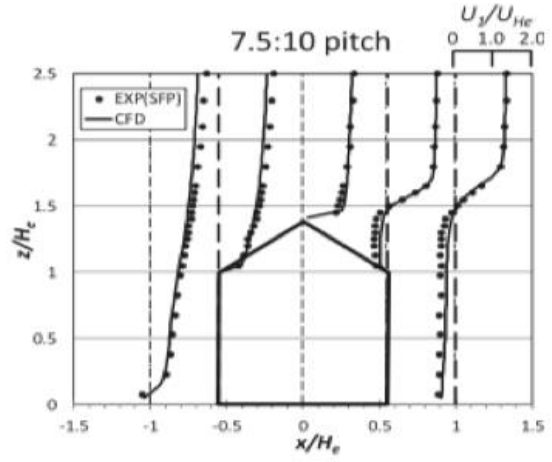
7.5:10 pitch
U_1/U_{He}
0 1.0 2.0
EXP(SFP)
CFD
z/H_e
x/H_e

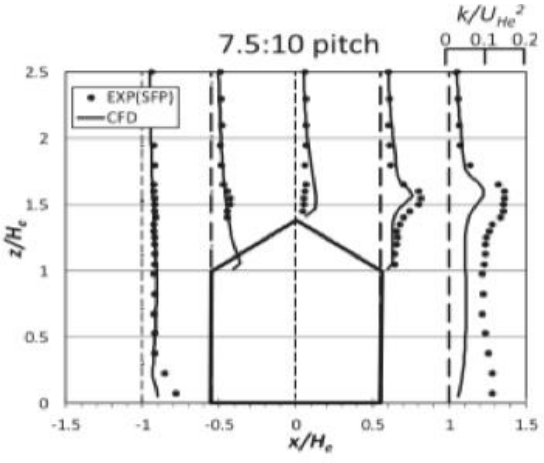
7.5:10 pitch
k/U_{He}^2
0 0.1 0.2
EXP(SFP)
CFD
z/H_e
x/H_e

Fig. 2.5: Wind sped profile and turbulence intensities curves for roof slopes 3:10, 5:10, and 7.5:10 (Tominaga et al, 2015)

Similar studies by Ozmen et al (2016) and Abohela et al (2015) show the same approximative wind speeds profiles and turbulence intensity curves. Ozmen et al (2016) experimental results have shown that roof angles of 15 degrees have a similar wind profile and turbulence intensity curves to the 3:10 roof slope shown in Fig. 2.5. Ozmen et al (2016) results for wind profiles and turbulence intensity curves of roof angles of 30 and 45 degrees resemble those of 5:10 and 7.5:10 roof slopes in Fig. 2.5. Literature suggest that wind flow properties are drastically changing at about 20 degrees roof angle (Ozmen et al, 2016). It is proposed that the wind turbine shall be placed at the middle of the rooftop (Stathopoulos et al, 2018); as shown in the wind profiles where higher wind speeds and lower turbulence is found. Also, the turbine must be a placed 4m above the roof to reach the undisturbed low turbulence region (aiming to the skimming flow region) and maximize the power output (Stathopoulos et al, 2018, Stankovic et al, 2005). As previous reviews agree on the same conclusions, it is deducted that roof angles do not need further analysis.

2.3.4 Roof parapets

Most studies on roof parapets focus on wind pressure coefficients recorded on different parts of the roof (Stathopoulos, 1987). As wind pressure coefficients are related to the average wind speeds, it is deducted that highest average wind speeds are found away from edges and corners. Lower turbulence values might exist away from the edges and corners. However, with the insight from wind pressure coefficients (Stathopoulos, 1987), it is hypothesized that parapets would have a rather small impact on a rooftop wind turbine, as the turbine will be located higher than the turbulent zone.

2.4 Guidelines and Summary

Although compiling and comparing results from previous literature reviews gives insight on the best design strategies to optimize wind power capture, other elements than wind speeds and turbulence intensities should not be neglected in the design process. Public's acceptance, pedestrian comfort, noise level, life cycle cost and analysis should be considered while choosing a design.

Assessment of previous studies discussing the impact of environmental and structural factors on wind velocities and turbulence highlights controversies and lack of studies for some elements. Table 2.3 summarizes, per parameter; effects on turbulence intensity, speed, equations to determine wind velocities, normalized wind velocity V/V_o, and references. Comparison and summarization of terrain roughness, topography, diurnal and seasonal cycles, climate change, roof angle and parapets influence on wind velocities and turbulence intensities from literature are achieved. There is almost no study on the effects of building shapes and city configurations onto wind velocities and turbulence intensities.

Table 2.3: Wind velocities and turbulence modification due to several urban parameters (Higgins and Stathopoulos, 2019)

Category	V	TI	Comment – Equations	V/V_o	Source
Terrain (City Morphology)					
Roughness	↑	↓	$\frac{V_z}{V_{zg}} = (\frac{z}{z_g})^{\alpha}$ Optimized result with $v \geq \frac{5m}{s}$ and $D \geq 130$	0.84 - 0.91	NBCC (2015)
Topography					
Ridges, valeys, and upper slopes			$V(x) = V_z \cdot \Delta s$ $\Delta s = \Delta s_{max}(1 - \frac{\lvert x \rvert}{kLh})e^{\alpha x/Lh}$	3.23 max – 1.9 max	Winstraw (2017), NBCC (2015)
Diurnal Cycle					
Day		↑	Inconsistent		Winstraw (2017), Heppeplman (2016)
Night		↓	Inconsistent		Winstraw (2017), Heppeplman (2016)
Seasons					
		↑	Inconsistent		Winstraw (2017), Emejeamara (2016)
Cimate Change					
			Inconsistent		Pryor (2009), Jiang (2009), McInnes (2011), Klink (1999)
Building Shape and Turbine Placement					
HAWT - Building Integrated Wind Turbine - Composite Prism	↑		Better results on a bidirectional and unidirectional wind, and building placed 0 to 60 degrees from the main wind direction	1.13 - 1.51	Stankovic (2005), Macera (2017), Stathopoulos (2018)
VAWT - Rooftop	↑		Independent from wind direction	1.12 - 1.16	Stankovic (2005), Stathopoulos (2018)
HAWT - Beside building		↓		0.88	Stankovic (2005), Stathopoulos (2018)
Roof slopes					
Roof angle	↑		Lowest turbulence and slight increase in wind speeds with roof angles lower than 20		Ozamen (2016), Tominaga (2015), Abohela (2016)
Parapets					
Parapet height	↓	↑	Following pressure coefficients - expected better results with height lesser than a 1m and away from corners and edges		Stathopoulos (1987)
Building Shape					
Building geometrical shape			No studies		
City configuration - channeling			No studies		

From Table 2.3, optimization of design strategies may be retrieved. Mixing and combining favorable features might lead to a significant increase in power production. From Table 2.3, the following guidelines considering terrain have been provided: in open areas, HAWT shall be use, whereas in urban areas, VAWT are generally preferred to HAWT. Since this thesis focused on urban terrain, the following sets of features might lead to significant increase in urban wind power:

- Geography: when available, in all cases, turbines shall be placed at the peak of a hill or escarpment; it might be beneficial to put turbines in a valley, but there is a lack of study on the effect on wind velocities
- VAWT shall be preferred in cases of rooftop wind turbines as it may cope with all wind directions
- Inclusion of a diffuser around the turbine blades might lead to an increased wind power, but few studies report it. Many advances in wind turbines mechanisms, such as the O-Turbine are being made: these options might lead to non-negligible options
- HAWT shall be preferred in case of building integrated wind turbine, as channeling effect channels the wind into one critical wind direction. HAWT are then more suited for maximizing the power from one critical wind direction
- In cases of HAWT, design shall consider changes in wind direction and speeds due to climate change to ensure full power capture potential in long-term projects
- Power is expected to change on a daily and seasonally manner

Although main features and design strategies are retrieved, some environmental features, especially diurnal, seasonal cycles, and climate change seem to indicate controversies and require further meteorological studies. Few to no studies may give precise values on the modification of

wind velocities of combination of several building components in urban environments, such as building shapes, city configurations, arcades, openings effect on urban wind flow. These would require further investigation. The methodology to determine, model through AI and even approximate the effects of certain urban elements on wind velocities compared to the upstream measured values in the aim to assess different designs will be discussed in Chapter 3.

Chapter 3 Modeling Techniques Methodology

3.1 Overview

In this thesis, AI models attempts to predict the ratio of the upstream wind velocity V_o to the measured wind velocity V as a function of several environmental and building characteristics. Design strategies may be assessed with the aid of AI modeling, as designs showing higher wind velocities are expected to yield in higher wind power. Accurate AI models require the building a sufficiently large and accurate database (Higgins and Stathopoulos, 2020). The present database consists in more than 150 distinct cases. These cases are obtained from both experimental and literature normalized wind velocities V/V_o retrieved from different combination of terrain roughness, topography, buildings shapes and city configurations for various wind directions and turbine locations. Experimental terrain toughness, channeling effect, building shapes, and city panels are obtained through wind tunnel testing in the atmospheric boundary layer wind tunnel of Concordia University. Comparison of wind tunnel results with similar studies found in recent literature is made to validate the results reliability.

3.2 Wind Tunnel Testing

Wind tunnel testing must simulate the flow conditions with the boundary layer in urban environment to ensure accurate experimental measurements. To do so, experiments shall be carried in an atmospheric boundary layer wind tunnel, under the urban or suburban terrain roughness.

3.2.1 Boundary Layer Wind Tunnel

Wind tunnel testing is performed in the Concordia University's Building Aerodynamics Laboratory, shown in Fig. 3.6. The wind tunnel dimensions are, in cross-section, 1.8 m by 1.8 m,

with a depth of 12.2 m (Chavez et al, 2011). Different boundary layers for various terrain exposures may be modeled with the usage of different mix of roughness elements shown in Fig. 3.1, i.e. styrofoam blocks, egg boxes. Concordia atmospheric boundary layer wind tunnel has a turning table allowing to rotate the model and simulate different wind directions. Wind speed and turbulence measurements are recorded by the cobra probe. Cobra probe is calibrated few times per month, ensuring proper measurement accuracy. The obtained results are then transmitted through a software, TFI device Control, which may retrieve, at each designed position, the angles with respect to the XY plane, yaw, pitch and the resultant velocities and turbulence intensities. Moreover, the Cobra probe gives also the "% good", which corresponds to the comparative ratio between the measured results to the real-scale results. Most results included in the thesis showed "% good" above 95%, thus with a measurement error of less than 5%. A statistical analysis on the accuracy of the dataset has been performed.

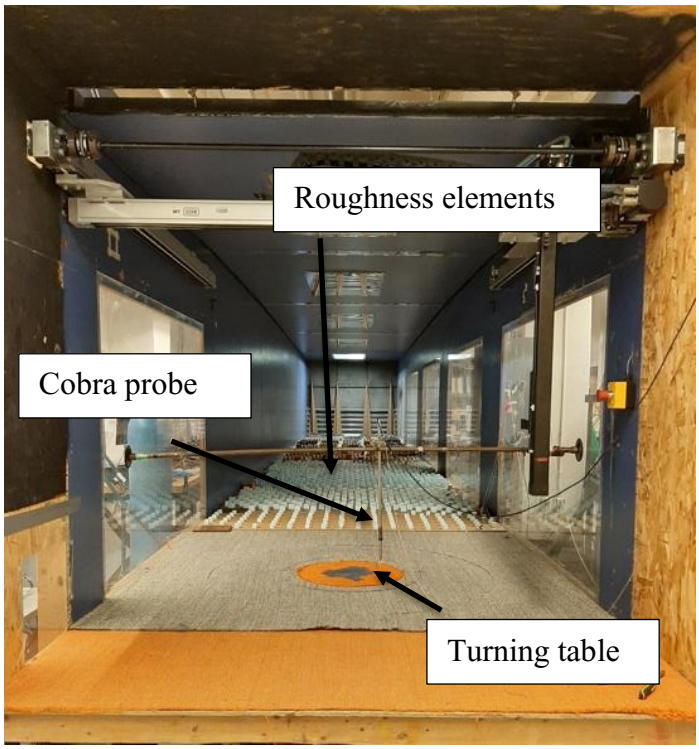

Fig. 3.1: Cross-section of Concordia University's atmospheric boundary layer wind tunnel

3.2.2 Wind Profile

Wind velocity modifications due to terrain roughness are the first elements included in the database. Recalling section 2.3.1, using the power law for the suburban or urban terrain exposure compared to the open area exposure at a given wind velocity and height, the measured velocity V reduces by a factor of 0.84 to 0.91.

Experimental wind profile is set to represent an urban or suburban exposure, as shown in the experimental wind profile in Fig. 3.2. The obtained experimental mean wind speed coefficient α results in 0.2. The mean wind speed coefficient was found through the linearization of the power law, see Eq. (3.1):

$$\ln(V) = \alpha\left(\ln\left(\frac{Z}{Z_g}\right)\right) + \ln\left(V_g\right) \qquad \text{Eq. (3.1)}$$

where V is the wind velocity (m/s), Z is the height above ground, Z_g is the gradient height, V_g is the gradient velocity, and α is the mean wind speed exponent coefficient.

By comparing the power law for a terrain with a mean wind speed coefficient of 0.2 and the power law for the open area, it is found that the experimental terrain reduces the approaching wind velocities by a factor of 0.93.

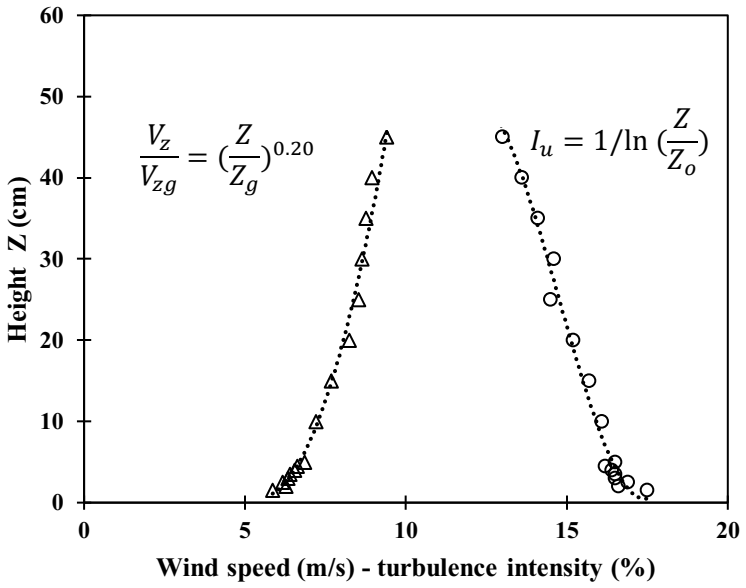

Fig. 3.2: Velocity and turbulence intensity profiles used in the present thesis (Higgins and Stathopoulos, 2020)

3.2.2 Wind Tunnel Parametric Models

In addition to terrain roughness, channelling modifications on wind velocities is added to the database. Considering channeling will allow to more accurately model airflows in between buildings in city configurations and to implement the appropriate modification in wind velocities.

Channeling effect will be studied through the model of the above ground section Tunnel-Louis-Hippolyte Lafontaine. The wind flows through the channel for a total section of 127cm long. Afterwards the channel closes as the tunnel completely goes underground. By measuring the wind velocities and turbulence intensities at the entrance, mid-point and wake of the tunnel for wind directions between 0° and 90°, the effect of channeling may be studied.

To increase the accuracy of the database, commonly found building shapes (square, rectangular, U-shaped, T-shaped, and L-shaped) were tested through wind tunnel experimentation for several wind directions θ, see Fig. 3.3. These building shapes will be tested for roof-mounted wind turbines and turbines located on the building sides.

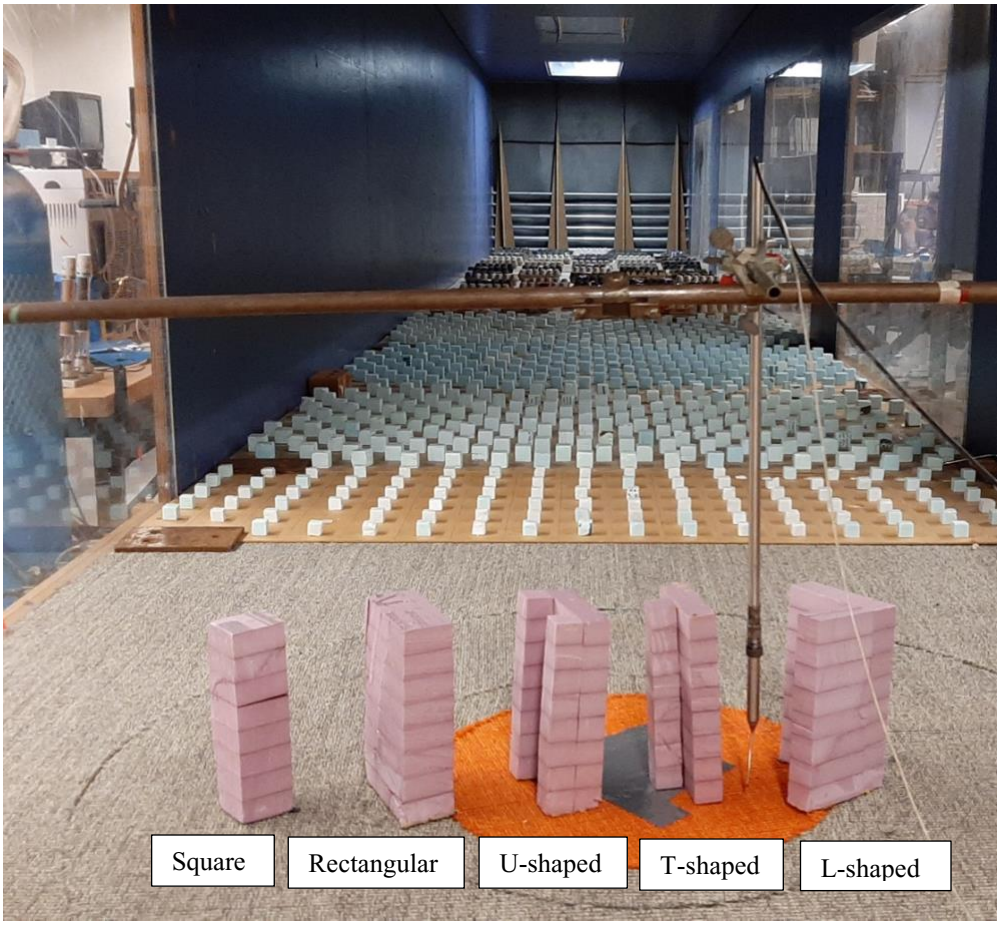

Fig. 3.3: Building shape models: square, rectangular, U-shaped, T-shaped, and L-shaped buildings (Higgins and Stathopoulos, 2020)

For comparison purposes, building model height is kept constant at 20 m, which corresponds to 20 cm, for a geometric scale of 1:100. This scale was chosen as models physically fit in the wind tunnel while respecting the appropriate boundary layer, meaning it "ensures the similarity of the experimental conditions (e.g. turbulence integral scales, wind power spectra, Jensen numbers etc.) with those in the field" (Alrawashdeh and Stathopoulos, 2020). For the turbulence integral scales to reflect the full-scale conditions, the linear scale of building models has to match the longitudinal length scale (Alrawashdeh and Stathopoulos, 2020 and Cook, 1978). If not, the turbulence scales and the turbulence generated by the bluff body will not correspond, leading to the improper

dynamic response of the model (Cook, 1978). As most of the experiments carried out in this study were done in urban environments, turbulence due to buildings and dynamic response of models is of high importance. Apart from turbulence integral scales, the effects of wind frequencies shall be considered in scaling (Jafari et al, 2019). Sometimes wind frequencies are more affected than turbulence integral scales in scaling considerations. Jafari et al, 2019 emphasizes that critical wind frequencies for turbulence range between 0.01 and 1 Hz; matching the reduced turbulence spectrum on low wind frequencies is needed if the model is tested under these conditions. In the scope of this thesis, wind frequency of 1000 Hz will be used, thus overpassing the critical range for turbulence intensity.

To further ensure comparisons in between the building shapes, cross-sectional dimensions were carefully studied. Model dimensions and cases are shown in Fig 3.4. All geometric shapes show a width x of 6 cm, except for the L-shape building which consists of 2 rectangles of width $2x$, and constant 20 cm (scale 1:100) height among all building cross-sectional shapes. Length x is doubled to model the rectangular, T-shaped and U-shaped buildings with the constant width x. To simulate different wind directions θ, building models are rotated along the symmetry axis of the cross-sectional shape. Wind velocities are recorded for wind direction θ between 0^o and 90^o by increments of 15^o for each building shape. Additional cases of -45^o to 0^o and from 90^o to 135^o are added for U-shape and L-shape buildings for turbines located on the building side due to their geometry. Building shapes will be tested for turbines located on the building sides (point d) and for roof-mounted (point e) wind turbines.

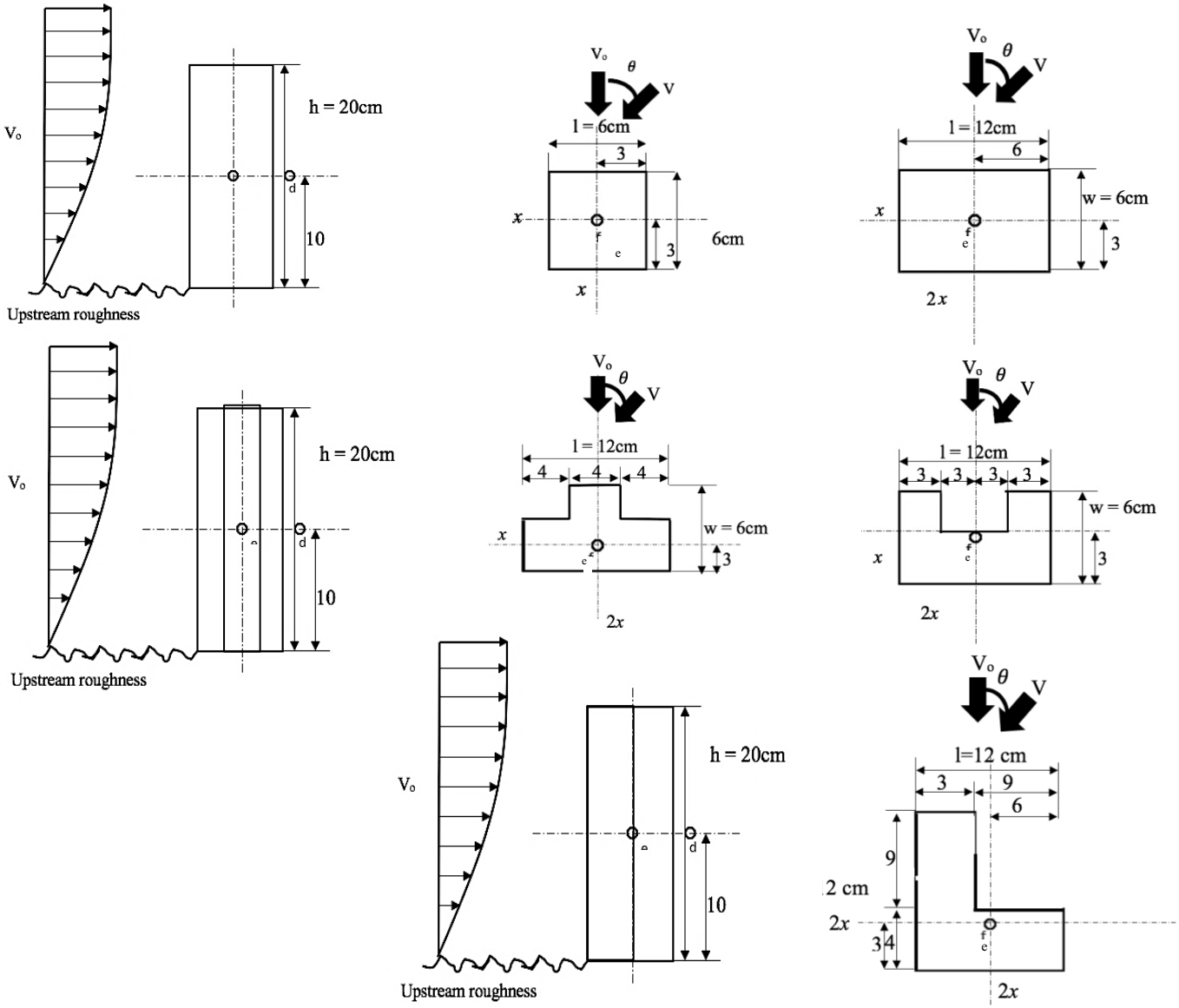

Figure 3.4: Model dimensions and measuring points for the square, rectangular, U-shaped, T-shaped, and L-shaped buildings

After determining and adding the normalized wind velocities due to channeling and building shapes in the database, city configurations are studied, as shown in Fig. 3.5. First, a city configuration with similar building shapes, see Fig. 3.5a, is investigated prior to testing more complete city configuration. Following are experiments included in the testing set. Included in the testing set are the city configurations of Fig. 3.5 (b) and 3.5 (c), where a newly implemented building in a city configuration with similar height buildings (Fig. 3.5b), and the real-case study of Boul. René-Lévesque street in Montréal (Fig. 3.5c) are analyzed for several measurement points.

(a) **(b)** **(c)**

Fig. 3.5: City clusters with similar building shapes (a), newly implemented building (b), and Boul. René-Lévesque, Montréal (c) in the atmospheric boundary layer wind tunnel of Concordia University (Higgins and Stathopoulos, 2020)

3.2.3 Overview

The following parameters are studied through wind tunnel testing, and included in the database:

- Channeling, through the testing of tunnel Louis-Hippolyte Lafontaine
- Building shapes (square, rectangular, U-shaped, T-shaped, and L-shaped)

- City configurations

3.3 Artificial Intelligence

Database was constructed using the normalized wind velocities V/V_o obtained from both literature review and wind tunnel testing. Database is input in an expert system and an artificial neural network and tested using city configurations from Fig. 3.5 (b) and Fig 3.5 (c). Predictive values of the testing set obtained through AI computing will be compared with the wind tunnel experimental values.

3.3.1 Expert System

Expert system is programmed through EXPERT 2.0 Microsoft application platform in C based language. Coding is presented in Appendix B. The programmed expert system retrieves linear relationship between the input variables and the output value, as shown in Fig. 3.6a. For each experimental case, the input parameter x is assigned a weight a_k with the fitting output y. For a complex experiment with n cases, this leads a set of equation of n rules, as defined per Bohlouli et al, 2017 in Eq. (3.2):

$$\sum_{n=1}^{\infty}(a_k x_k)_n = y_n \qquad \text{Eq. (3.2)}$$

where a_k is the coefficient of the variable in the given equation, x is the input variable, and y is the output variable for n rules.

As shown in Fig. 3.6a, in the software knowledge base, the set of all n rules are computed simultaneously, but each output y varies with respect to the weighted input $a_k x_k$ for the n^{th} rule. If the program is run through the interface, the software will retrieve the closest fitting rule n from the given input x and retrieved the output y.

Looking deeper into the variables applied in this study, the input and output parameters and their meaning are discussed. Inputs x are presented in a qualitative form: each parametric value is given in Fig. 3.6 a. These include terrain roughness {urban, suburban}, valley {yes, no}, wind direction {angle θ, corresponding to the wind direction}, shape {building shape: square, rectangular...}, height {building height: dimension}, point {location of the measurement point: middle, wake, entrance, side, rooftop}. The output y_n represents the ratio of the upstream wind velocity V_o to the measured velocity V at height z, namely normalized wind velocity V/V_o.

A linear set of n equations, referred as rules in this context, is constructed and followed by the expert system. It is thus reliable for predicting values following a linear model. For the exercise performed in this thesis, the normalized wind velocity V/V_o will be a function of wind direction θ, measurement point, building shape and channeling. It has to be noted that the linearity is not proven for the aforementioned function. Input variables (wind direction, measurement point, building shape, and channeling) cannot be associated with a defined weight n unless the input and output variables are numerically close. Thus, a large and accurate database allows to assign reliable weight n. To assess the accuracy of the expert system, the output results of the expert system will be compared to the experimental normalized wind velocities obtained through wind tunnel testing, where the input variables will be part of the testing set.

3.3.2 Neural Network

Artificial neural network was programed through MATLAB nntool add-in, in MATLAB language. Coding is presented in Appendix C. Neural network includes many programming models: the most appropriate is the feedforward, as the other models are either based on auto-regression, time-series, or too complex for running the program. Many studies, although focusing other parameters as wind

meteorological data or wind pressure coefficients preferred using a feed-forward system (Blanchard et al, 2019, Bre et al, 2018). However, it may be useful in future work to test and compare different ANN models to ensure the usage of the best fit model.

ANN is solving for the output *f* through hidden layers assigning weight *w* to the input parameters *x*. This allows to draw correlations among the input variables. The solving model is given by Eq. (3.3), for only two sample hidden layers:

$$\sum_{n=1}^{\infty} w_{i,k} x_i (\sum (w_i x_i + b)) = f_n \qquad \text{Eq. (3.3)}$$

Where w_i is the weight given to the input variable by the software for the hidden layer *k*, x_i is the input variable, *b* is the bias, f_n is the output function.

As aforementioned, the ANN solves for the output f_n by assigning weights to the input variables x_i and draws correlations between each layer *i* through multiplying the input variables *x*. Thus, the output f_n results from a polynomial relationship from the input variables *x*, which is defined as a non-linear system.

The input parameters from the expert system had to be transformed in quantitative values to be implemented in the ANN. As shown in Fig. 3.6b, the input parameters are in the following form: terrain {angle θ, corresponding to wind direction}, shape {characteristic length *L*}, obstruction {1,0}, measurement points {x_1, x_2, *z*). The testing and output sets results in the value of the normalized wind velocity, V/V_o. The ANN is programmed to draw exponential correlations, as discussed with Eq. (3.2), as it implements multiple layers between the input parameters. As the normalized wind velocity might not show a linear correlation with the input parameters, possibly the ANN will result in more accurate values.

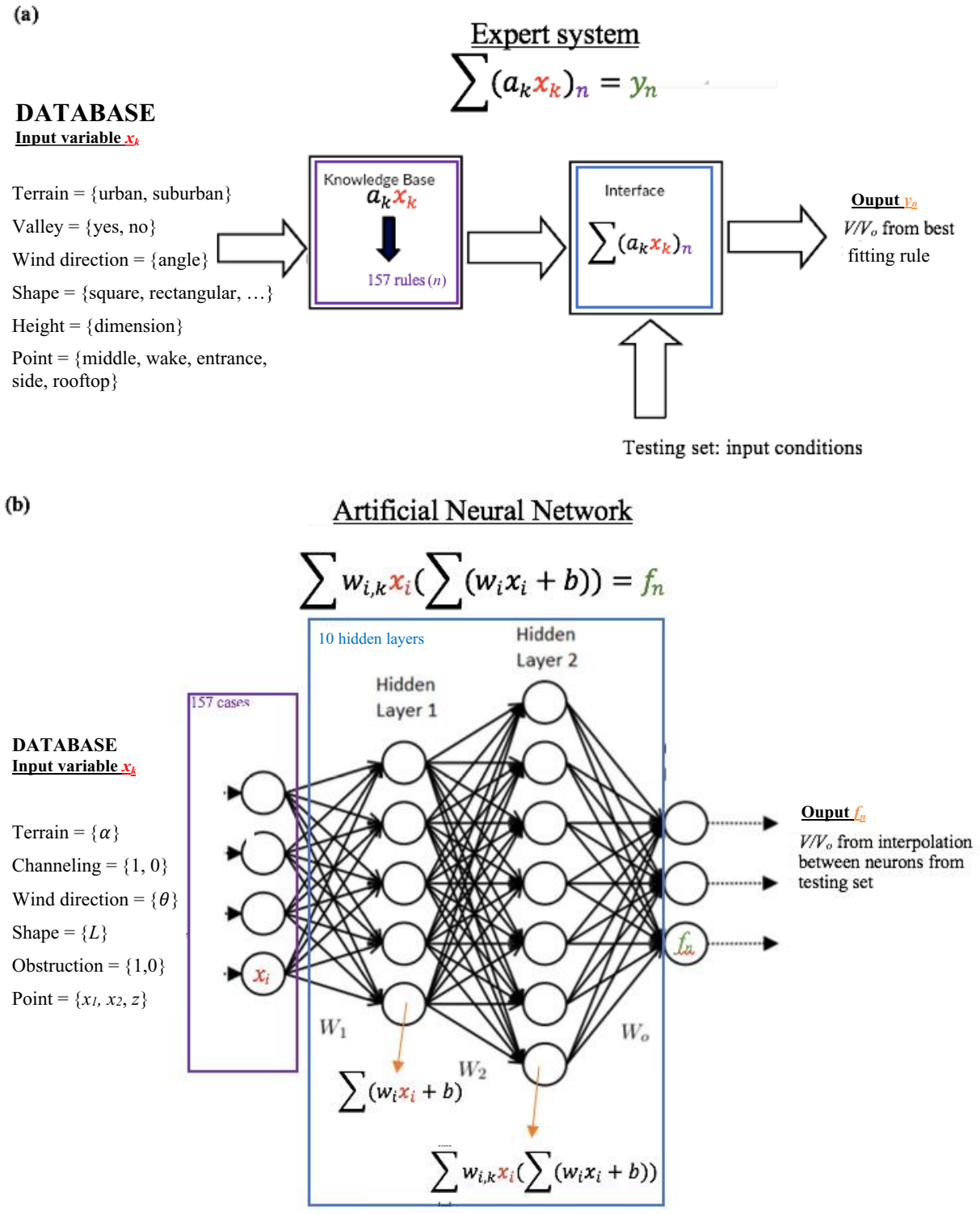

Fig. 3.6: Expert system (a) and artificial neural network (b) architecture (Higgins and Stathopoulos, 2020)

For programming the ANN in MATLAB, the input parameters for all cases were arranged in the form of a matrix. Thoughtful reasoning on the input MATLAB input matrix programming is required. The 157 combinations presented represent the input values and their fitting normalized wind velocities, the target values. The input values corresponded to the previously discussed input parameters. The input matrix was 8x157 and the target values matrix 1x157. Number of layers was randomly selected and compared: 10 hidden layers resulted in the best results. The decision of the number of hidden layers was made through a trial and error process, identifying the minimum number of hidden layers required without impacting the accuracy of the software results. It was found that 10 hidden layers would be adequate for this study. Fig. 3.7 shows the network architecture computed in MATLAB:

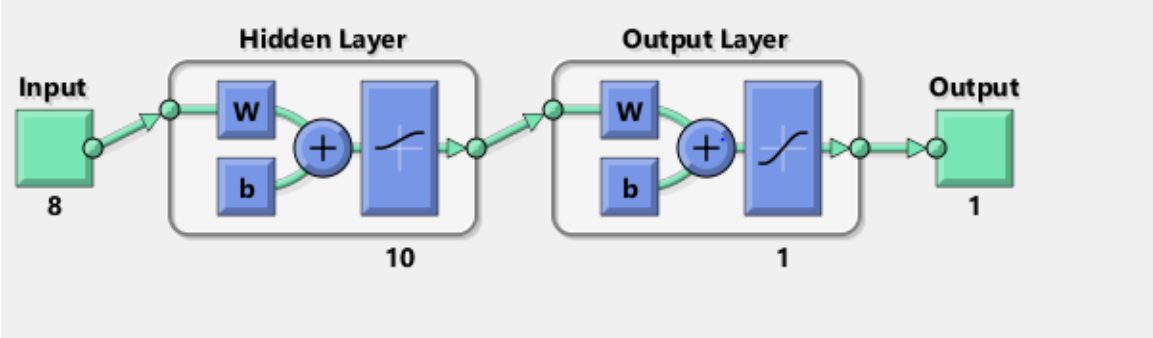

Fig. 3.7: ANN architecture programmed in MATLAB

The system was then trained. Automatically, MATLAB stops the training when the RMS error stops decreasing. Afterwards, the ANN was tested using the data for the new building implementation, as per table 7.10. The sample data was used for the testing of the ANN, a matrix of 8x6. Precise input and target matrix are presented in Appendix C, Table C.22, whereas the sample matrix is presented in Table C.23. The output generated is normalized wind speed due to

the parameters input. The wind speed is normalized from the initial velocity for an open terrain set in the wind tunnel.

In brief, 157 experimental cases are computed in the ANN, thus 157 set of input parameters are resorted in the 10 hidden layers of the ANN software. Thus, multiple interpolations between each input parameters are done, and correlations are made among multiple experimental cases. With software training, the output precision may be increased. As wind speeds is believed to show a non-linear behavior, it is expected for ANN to result in better predicting values than the expert system. Moreover, Blanchard, 2018, showed encouraging results while trying to predict wind speeds from previously collected data samples.

Chapter 4 Wind tunnel results and discussion

4.1 Overview

A database is constructed with the use of literature and wind tunnel results presenting the ratio of the upstream velocity V_o to the measured velocity V at same height z due to various environmental and building features. Lack of studies on the effect of channeling, building shapes, and city configurations on wind velocities and turbulence intensities motivated experiments through wind tunnel testing. Their modifications on the upstream wind velocity for several wind directions θ are presented and analyzed in the subsequent sections.

4.2 Channeling

Channeling effect is the flow acceleration caused by reduction in the cross-section area. According to Gandemer et al, 1987, some dimensional requirements shall be met for channeling effect to be observed. As shown in Fig. 4.1, building height must be higher than 6m; the width of the channel shall be smaller or equal to twice the building height; and the opening length in the channel shall represent less than 5% the length of the channel (Higgins and Stathopoulos, 2020).

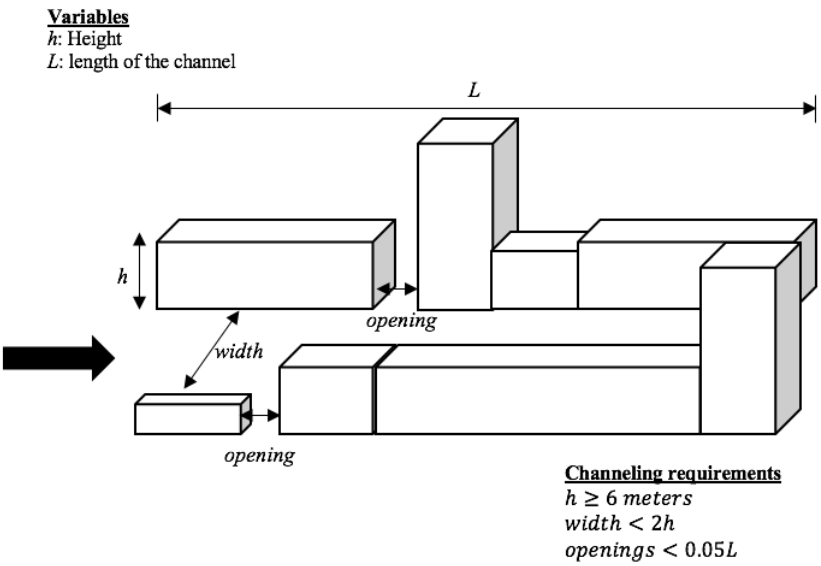

Fig. 4.1: Channelling requirements (modified after Gandemer and Guyot, 1976, Higgins and Stathopoulos, 2020)

For the purpose of this thesis, the model of above ground section of the tunnel Louis-Hippolyte Lafontaine will be used for studying the effect of channeling on wind velocities. Model is shown in Fig. 4.2. Wind flows in the tunnel (channel) for 127 cm, in a geometric scale of 1:100, where the terminal end of the tunnel is closed, as only the above ground section is considered. The tunnel is then considered to represent flow conditions of an open-closed end channel (Higgins and Stathopoulos, 2020). Channel velocities and turbulence intensities are tested at the front (point *a*), midpoint (point *b*, at 63.5 cm distance from the edge) and wake of the tunnel (point *c*). Measurement points *a*, *b*, and *c* were taken at a constant height of 5 mm above the channel floor.

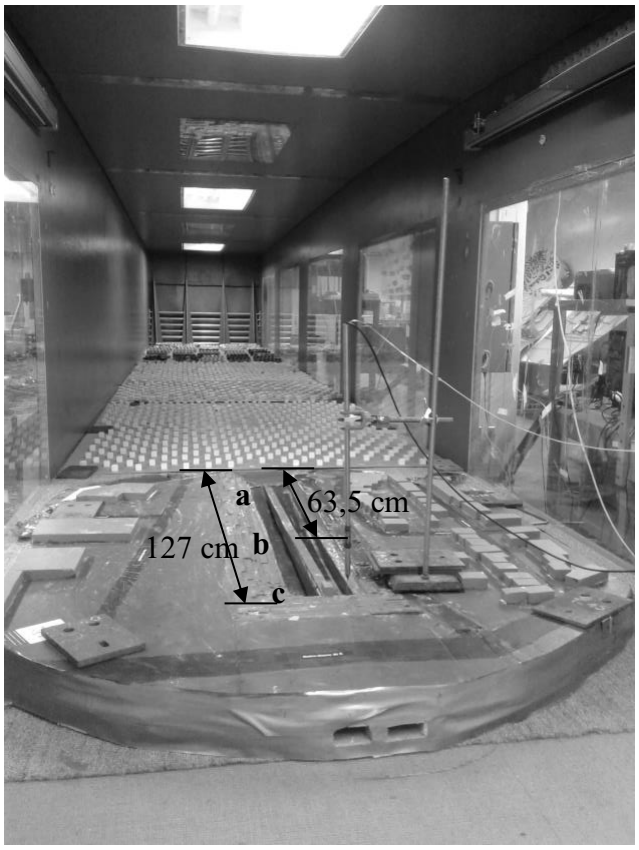

Fig. 4.2: Tunnel Louis-Hippolyte Lafontaine model in the atmospheric boundary layer wind tunnel in Concordia University (Higgins and Stathopoulos, 2020)

Wind tunnel measured velocities V and turbulence intensities $T.I.$ are normalized with the wind velocities V_o and $T.I._o$ obtained with the wind profile at the same height z for the given wind direction θ. Fig. 4.3 shows the obtained normalized wind velocities, V/V_o and turbulence intensities $T.I./T.I._o$ for the wind directions θ.

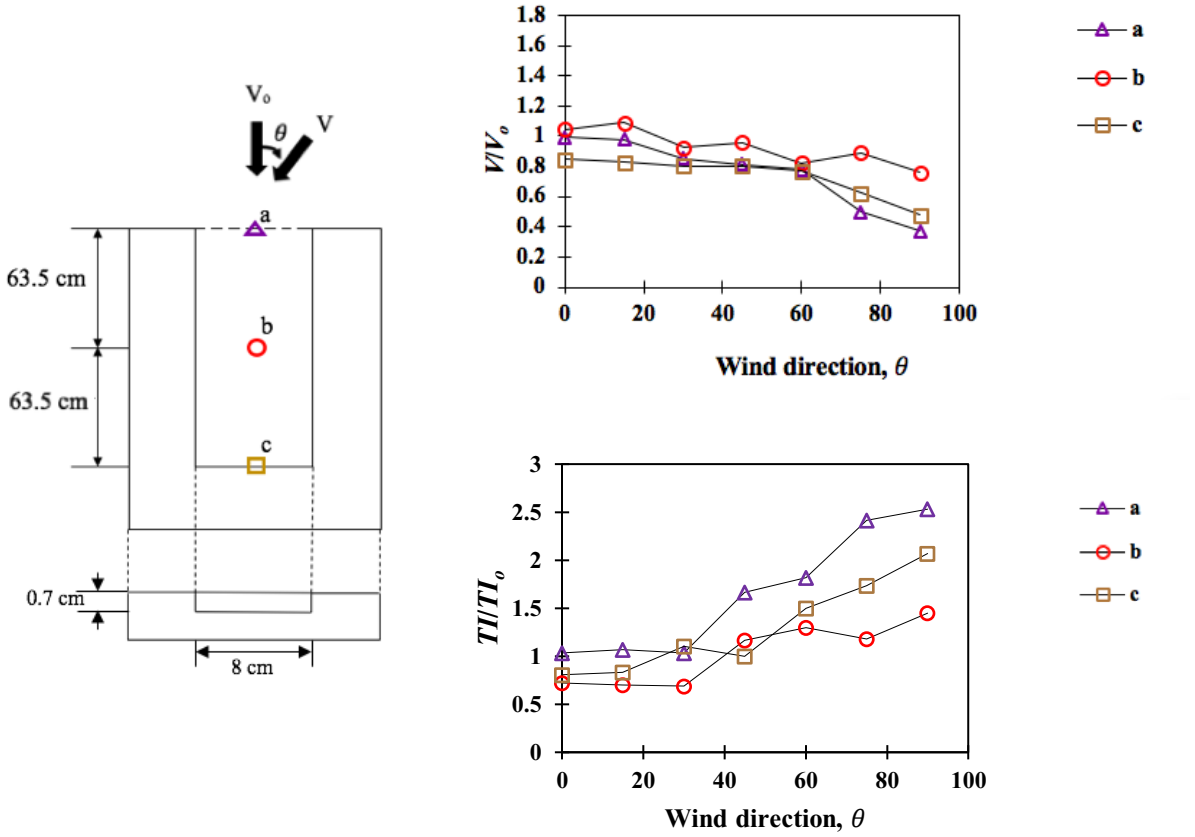

Fig. 4.3: Normalized wind speeds and turbulence intensity per wind direction at the entrance of the valley, mid-point, and wake of the channel (modified after Higgins and Stathopoulos, 2020)

Analyzing Fig. 4.3, an open-closed end channel yields in higher wind speeds and lower turbulence intensities at wind direction θ of 15° for all measurement points *a* (front), *b* (midpoint), and point *c* (wake). For all wind directions, the highest normalized wind velocity is obtained at the midpoint of the channel. Interestingly, at the midpoint (point *b*) of the channel, the lowest turbulence intensities are observed compared to the other point locations. For most of the data, the normalized turbulence intensity $T.I./T.I._o$ increases and the normalized wind velocity V/V_o decreases as the wind direction augments. Lowest normalized wind speeds and highest normalized turbulence intensities with $T.I./T.I._o$ ranging from 1.18 to 2.53 occur at θ=90 and θ=75 for measurement

points *a*, *b*, and *c*. Maximum turbulence intensity at 90º, point c with $T.I/T.I._o$=2.53. Among all wind directions and measurement points, the peak in normalized wind velocity and lowest turbulence intensity is observed at point *b* with θ=15. The measured normalized wind velocity is 1.1. with $T.I./T.I._o$=0.70.

As wind turbine benefit of enhanced wind velocities and lower turbulence, channeling may be beneficial for augmenting power capture. Turbine implementation is suggested at the midpoint of an open-closed end channel for a wind direction θ close to 15º, as the turbine benefits from increased wind velocities and lower turbulence. Less effective turbine placement is located at the entrance and the wake of the open-closed end channel, for wind directions between 45º and 90º. The normalized turbulence intensity $T.I./T.I._o$ is the higher and the normalized wind velocity V/V_o lower, compared to the results obtained at the midpoint of the channel for wind directions up to 45º.

Experimental normalized wind speeds V/V_o found in this experiment show a maximum value of 1.1. These results are more conservative than those observed in open-end channels in the literature. The amplification factors values obtained by Stathopoulos et al (1986), analyzing passageways between buildings showed a maximum amplification factor, referred to V/V_o in the present study, in 1.4. The differences in results is explained by the difference in the channel geometry, as a passageway between buildings is considered an open-end channel (Higgins and Stathopoulos, 2020). Slightly different normalized wind velocities due to channeling in passages in between perpendicular buildings were obtained by Blocken at al, 2008, where V/V_o was recorded up to 1.6. As literature show discrepancies in the modification in wind velocities due to channeling, Huang et al, 2015 observes that wind velocities are increasing due to channeling in pedestrian wind and urban street canyons, but are dependent on the approaching terrain, flow conditions, and wind

directions, making it hard to quantify. In the present study, the measured normalized wind velocities achieve a maximum of 1.1 and are more conservative than those recorded in the literature due to the channel geometry. An open-end channel allows the flow streamlines to remain straight at the wake region, thus to still benefit of the channeling effect, lowering the turbulence and accelerating the flow. In the open-closed end channel, the wind flow will be redirected at the wake, thus increasing the turbulence and lowering the wind velocity *V*.

4.3 Building Shapes

Database includes the normalized wind velocities for various building shapes. Building cross-sectional shapes displays different normalized velocities and normalized turbulence intensities per wind direction θ. Figs. 4.4a and 4.4b the normalized velocities V/V_o and turbulence intensities $T.I./T.I._o$ per wind direction for square and rectangular buildings shapes respectively for turbine located on the building side (point *d*) and roof-mounted wind turbines (point *e*). Similarly to Fig. 4.4a and 4.4b, Figs. 4.5a, 4.5b and 4.6 displays the experimental normalized wind velocities and normalized turbulence intensities for the T-shaped and U-shaped, and the L-shaped building respectively. For turbines located on the building sides, point *d*, measurements are taken at a distance of 2.5 cm (geometric scale 1:100) from the edge of the building. This distance allows space for a standard street-level turbine pals of a diameter of 1.5m to 2m and adds the clearance distance to ensure proper pedestrian passage and noise control (Higgins and Stathopoulos, 2020). Roof-mounted turbines will be located at the center of the roof for point *e*.

From Fig. 4.4a, square buildings show higher normalized velocities at all turbine placement for wind direction θ between 0º and 15º, with a peak at 15º where V/V_o=1.58 at measurement point *d*. Interestingly, the normalized turbulence intensity is among the lowest, with $T.I./T.I._o$=0.83.

Normalized wind velocities V/V_o tend to decrease at wind direction θ higher than 45° for measurement points *d* and *e*. Normalized turbulence intensities tend to increase as the wind direction θ increases for all turbine positions. The highest increase in turbulence intensities is recorded for building sides for wind directions θ between 75° and 90° where the turbulence intensities $T.I./T.I._o$ went from 1.0 to 2.4 approximately. Fig. 4.4b allows to draw conclusions for the rectangular building shape. Rectangular building shapes have similar values in normalized wind velocities ($1.17<V/V_o<1.36$) for all wind directions θ, however, the normalized turbulence intensities show higher variations for measurement points *d* and *e* at wind directions θ higher than 60°. As an example, for point *d*, normalized turbulence intensities for wind directions between 0° and 60° varies between 0.97 and 0.99, whereas the $T.I./T.I._o$ ranges between 0.63 and 0.88 for wind directions higher than 60°. Comparing results for square and rectangular building shapes, it is shown that square building shapes tend to display higher normalized wind velocities than for the rectangular buildings, but turbulence intensities are similar for both building shapes.

Normalized wind velocities for U-shape and T-shape buildings are presented in Fig 4.5a and 4.5b. These building shapes are further tested for point *d* with additional wind directions of -15° to -100° to get the maximum normalized wind velocity along the symmetry of the building. Similar observations may be made as for Fig. 4.6, as the highest normalized velocities V/V_o are obtained on the building sides (point *d*) for T- and U-shaped buildings than for square and rectangular buildings. Maximum normalized wind velocity achieved for point *d* is 1.35 and 1.29 for U-shaped and T-shaped buildings respectively whereas point e shows a maximum of 1.08 and 1.09 for each building. Point *d* also depicts the lowest normalized turbulence intensities, which ranges between 0.75 and 0.98 compared to point *e*, where the normalized turbulence intensities vary between 0.81 and 1.17. Thus, for T- and U-shaped buildings, building sides is the most

suitable turbine location for the optimal wind power capture, consistently with results for square and rectangular buildings.

Similarly to Figs. 4.4 and 4.5, Fig. 4.6 shows the normalized wind velocities as a function of the wind direction θ for the different turbine locations for L-shaped building. This building was further tested with wind directions from -100º up to 135º for the wind velocities V/V_o and turbulence intensities at the building sides (point *d*) due to the differing symmetry of the building. For all turbine locations (points *d* and *e*), the normalized wind speeds are either constant are lower for negative wind directions $-\theta$ compared to positive wind directions θ. As for other building shapes, the highest normalized wind velocities and lowest turbulence intensities are achieved at the building sides, at point *d*.

Is it intriguing to note that results obtained in this study match literature results for rectangular, U-shaped, and L-shaped buildings obtained through CFD analysis. Du et al (2017) studies pedestrian wind on rectangular, U-shaped, and L-shaped buildings and records a peak in wind velocities for a wind direction of 45º, and another peak for L-shaped buildings at a wind direction of 0º. Recalling Fig. 4.4b, Fig. 4.5b, and 4.6, peaks in normalized wind velocities at these aforementioned wind directions for turbines located on the building sides. It suggests CFD as a potential predictive model for assessing urban wind power, but it shall be compared to full-scale studies. As CFD is shown to be accurate in averaging values, not in peak values (as design wind pressures), it is hypothesized that CFD may be used for energy purposes.

a) Square Building

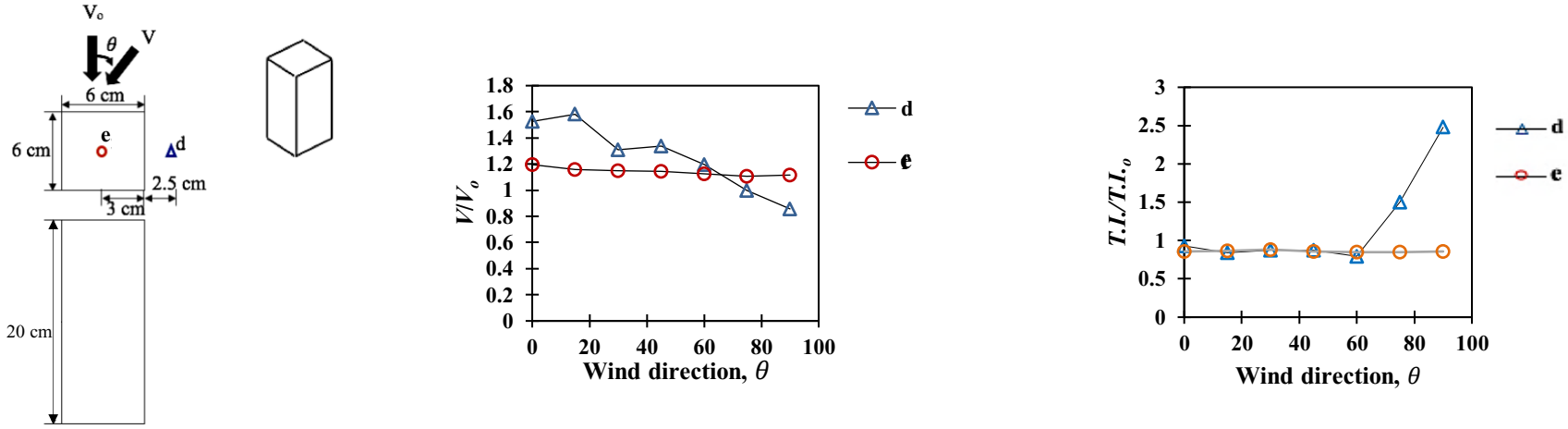

b) Rectangular Building

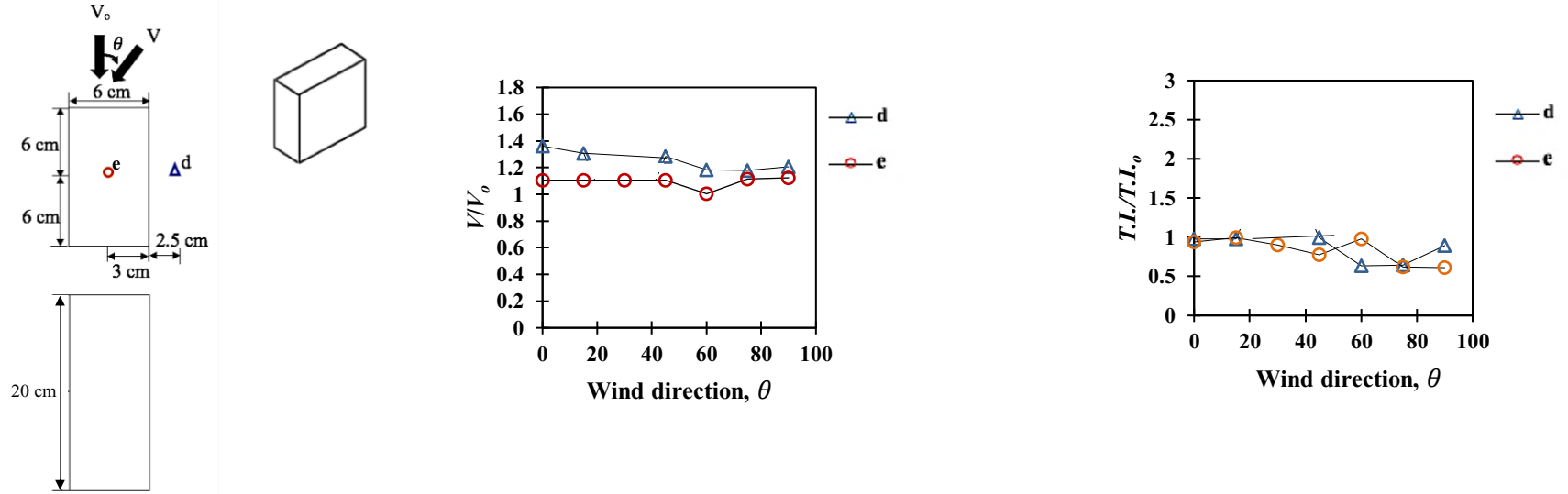

Fig. 4.4: Normalized wind velocities and turbulence intensities per wind direction for square (a) and rectangular (b) building shapes

a) U-shaped Building

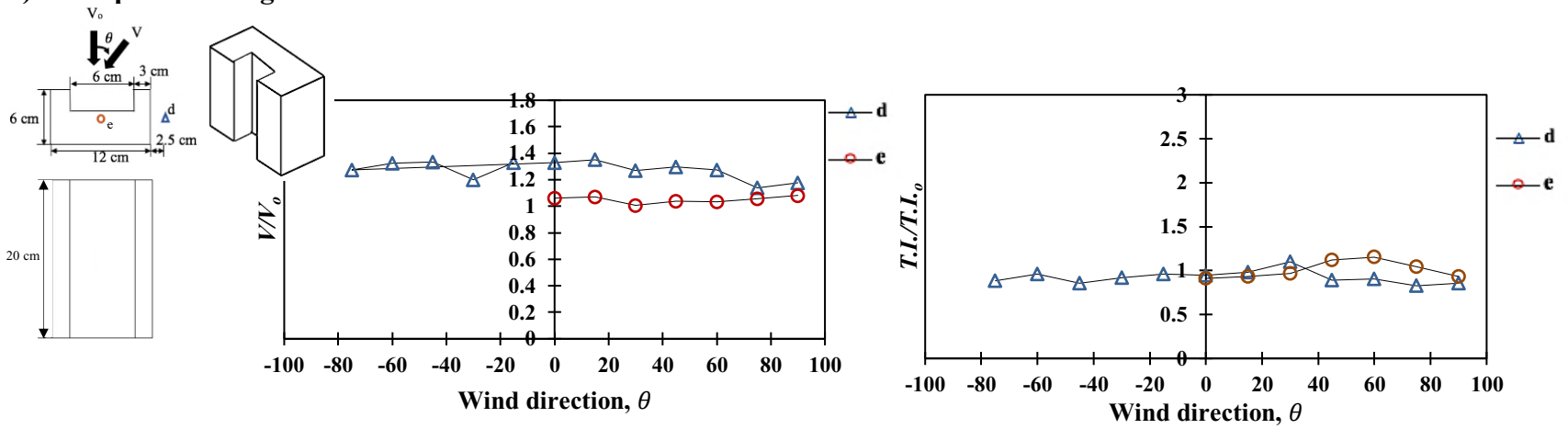

b) T-shaped Building

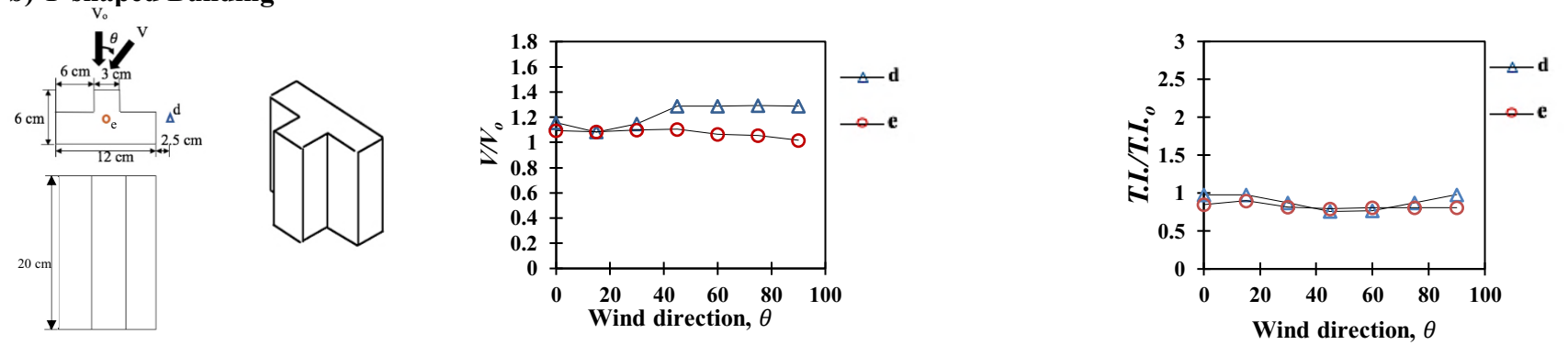

Fig. 4.5: Normalized wind velocities and turbulence intensities per wind direction for U-shaped building (a) and T-shaped (b) buildings

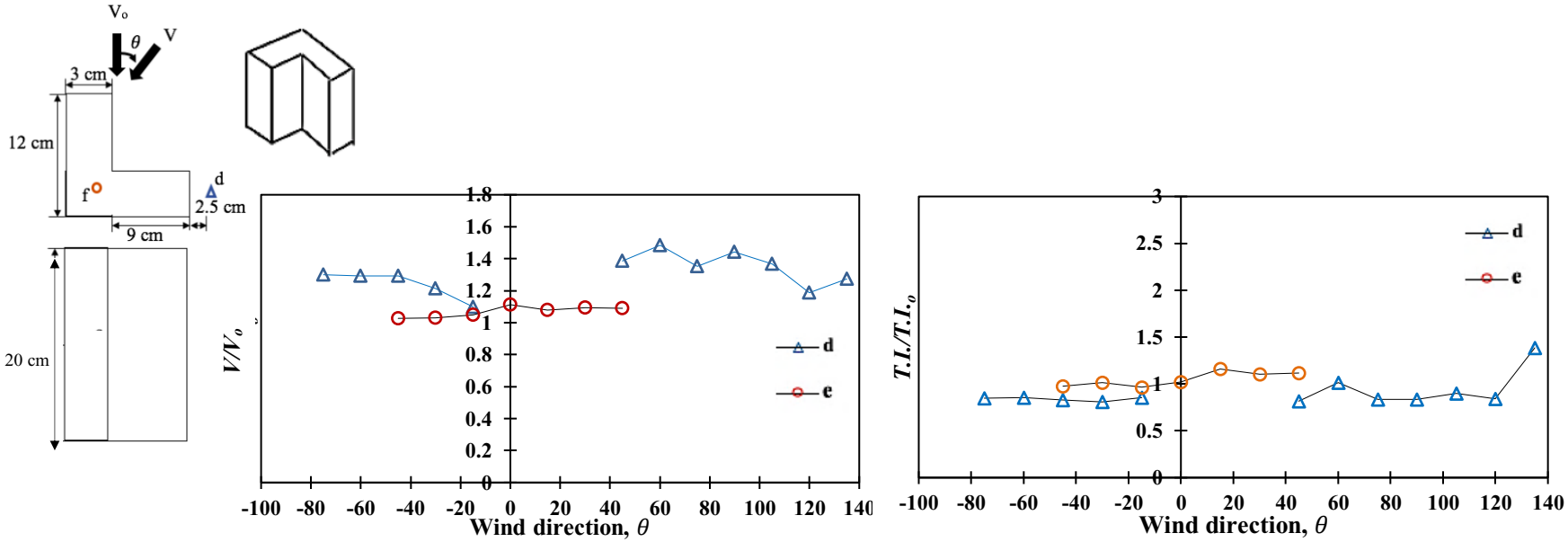

Fig. 4.6: Normalized wind velocities and turbulence intensities per wind direction for the L-shaped building

As Figs. 4.4, 4.5, and 4.6 presents the detailed results for the different normalized wind velocities V/V_o and turbulence intensities $T.I./T.I._o$ per building shapes and wind direction θ, general conclusions are difficulty drawn. Normalized wind velocities for sides and building rooftop are compared in Table 4.1a and Table 4.1b to observe whether building shape influences the normalized wind velocities. Table 4.1a shows the normalized wind velocities V/V_o at point measurement *d* (building sides) for wind direction θ of 0° to 90° for all building shapes. Table 4.5b shows the normalized wind velocities at point measurement *f* (rooftop) for wind direction θ of 0° to 90° for all building shapes.

In Table 4.1a, the square building shape yielded in the highest normalized wind velocities V/V_o for the turbine located on the building side, point *d*, among wind directions between 0° to 30°. The L-shaped buildings show the highest normalized wind velocities for wind directions between 30° to 75°. Although most of the highest normalized wind velocities is measured for the square and L-shaped buildings, most of the other buildings showed normalized wind velocities higher than 1.2. Examples of this the rectangular building shape, although it never reached the highest normalized wind velocity compared to the other building shapes, high normalized at wind directions 0° and 15° where V/V_o=1.36 and 1.31. Similar observations are made for the T-shape, for wind directions θ at 0° (V/V_o=1.32), and 15° (V/V_o=1.35). For most of the wind directions and buildings shapes, normalized turbulence intensities are below 1.0, meaning the turbulence is reduced compared to the upstream wind. This ensures that the above-mentioned locations, buildings shapes and wind directions with higher normalized wind velocities may be used for turbine implementation without having a negative impact on the turbine efficiency.

In Table 4.1b, the square building shape showed significantly higher normalized wind velocities ($1.11 < V/V_o < 1.20$) at wind direction between 0^o and 75^o. The L-shaped building has the highest normalized wind velocity, where V/V=1.11 at wind direction $\theta=0^o$. The L-shaped building showed high normalized wind velocity at $\theta=90^o$, where V/V=1.30. The T-shaped building also showed normalized wind velocities higher than 1.0 in all wind direction for point the turbine located on the rooftop. As stated for point *d*, most of turbulence intensities recorded are below 1.0, thus for the cases yielding in higher normalized wind velocities, if the turbine is to be implemented, the turbine efficiency will be increases compared to the upstream terrain conditions.

Results obtained for mounted-roof turbines may be compared to results from Roy et al, 2012, obtained through CFD analysis. Roy et al, 2012 computed the wind velocities at the roof level of a flat roof square building shape for wind directions of 0^o to 45^o by increments of 15^o. Roy et al, 2012 had the highest normalized wind velocity at a wind direction of 15^o. Then, the higher normalized wind velocities were obtained at wind directions of 0^o, 30^o and 45^o. Recalling Table 4.1b, the same pattern is observed in the scope of the present experiment.

Table 4.1: Normalized wind velocities V/V_o for the square, rectangular. T-shape, U-shape, and L-shape for the wind directions θ 0º to 90º (increments of 15º) (modified after Higgins and Stathopoulos, 2020)

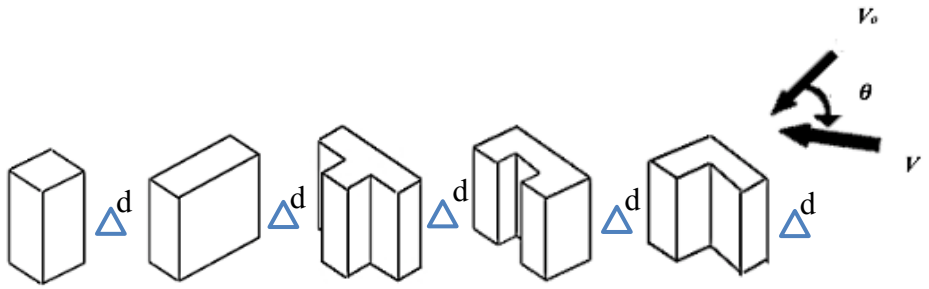

(a) Point measurement *d* (turbine on building side)

Wind direction θ	***V/V$_o$ (T.I./T.I.$_o$)***				
	Square	Rectangular	T-shape	U-shape	L-shape
0	**1.52** (0.93)	1.36 (0.97)	1.15 (0.94)	1.32 (0.97)	1.17 (0.86)
15	**1.58** (0.83)	1.31 (0.97)	1.08 (0.98)	1.35 (0.97)	1.24 (0.91)
30	**1.31** (0.87)		1.15 (1.09)	1.26 (0.87)	**1.31** (0.86)
45	1.34 (0.87)	1.28 (0.99)	1.28 (0.88)	1.30 (0.76)	**1.38** (0.91)
60	1.19 (0.79)	1.18 (0.63)	1.28 (0.91)	1.27 (0.77)	**1.48** (1.04)
75	1.12 (1.49)	1.17 (0.63)	1.28 (0.82)	1.14 (0.88)	**1.35** (0.93)
90	0.85 (2.47)	1.21 (0.88)	1.29 (0.86)	1.17 (0.98)	**1.44** (1.00)

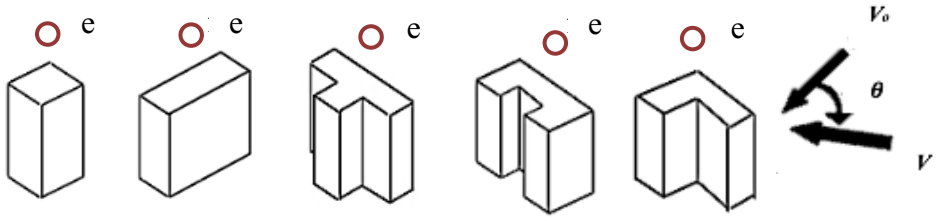

(b) Point measurement *e* (rooftop turbine)

Wind direction θ	***V/V$_o$ (T.I./T.I.$_o$)***				
	Square	Rectangular	T-shape	U-shape	L-shape
0	**1.20** (0.85)	1.06 (0.53)	1.10 (0.91)	1.09 (0.97)	1.02 (0.82)
15	**1.16** (0.86)	1.10 (0.99)	1.10 (0.93)	1.08 (0.90)	1.03 (0.80)
30	**1.15** (0.88)	1.10 (0.89)	1.10 (0.97)	1.09 (0.82)	1.05 (0.85)
45	**1.13** (0.85)	1.10 (0.77)	1.10 (1.12)	1.10 (0.79)	1.11 (0.81)
60	**1.14** (0.84)	1.00 (0.97)	1.00 (1.15)	1.06 (0.81)	1.08 (1.01)
75	1.06 (0.84)	1.11 (0.62)	**1.10** (1.04)	1.05 (0.81)	1.09 (0.83)
90	**1.12** (0.85)	**1.12** (0.61)	**1.12** (0.93)	1.01 (0.81)	1.09 (0.82)

To check on the experimental measurement accuracy and sensitivity, in particular rooftops, another experiment is performed. A sample rectangular building shape is tested for a series of 25 concentrated recording points for of normalized wind velocities V/V_o and normalized turbulence intensities $T.I./T.I._o$ on the rooftop at wind direction θ=0°. The data is tested for a wind data frequency of 1000 Hz. As aforementioned in Chapter 3, wind data experimental frequency stays out of the critical range for turbulence, between 0.01 and 1 Hz, ensuring accuracy in measurements (Jafari et al, 2019). The first point series is taken at a distance of 0.5 cm from the vertical and horizontal model edges. Then, other measurement points are taken at a distance of 1.25 cm for the vertical axis, and a varying distance of 3.5 cm and 2 cm for the horizontal axis. The variation in point measurements towards the middle for the horizontal axis is to better understand the wind behavior for the centered mounted-roof turbine. The obtained wind velocities V/V_o and turbulence intensities $T.I./T.I._o$ are then mapped in a contour graph (see Fig. 4.7a and 4.7b). In Fig. 4.7a, the values for wind velocity V varies up to 0.35 m/s, and might lead to a lower normalize wind velocity, where V/V_o=0.89 or high normalized wind velocities with V/V_o=1.24. Turbulence intensities vary by up to 10 units within the same rooftop, corresponding to normalized turbulence intensities between 0.89 and 1.44. This difference in turbulence intensities shows that the turbine efficiency may be significantly modified depending on its location for a same wind direction.

Thus, measurement precision may impact on the quality of the experimental measured velocities and turbulence intensities, as measurement points are sensitive to the location of the measurement. To ensure a quality of the database, a large amount of measured data may yield in a more accurate set of experimental data.

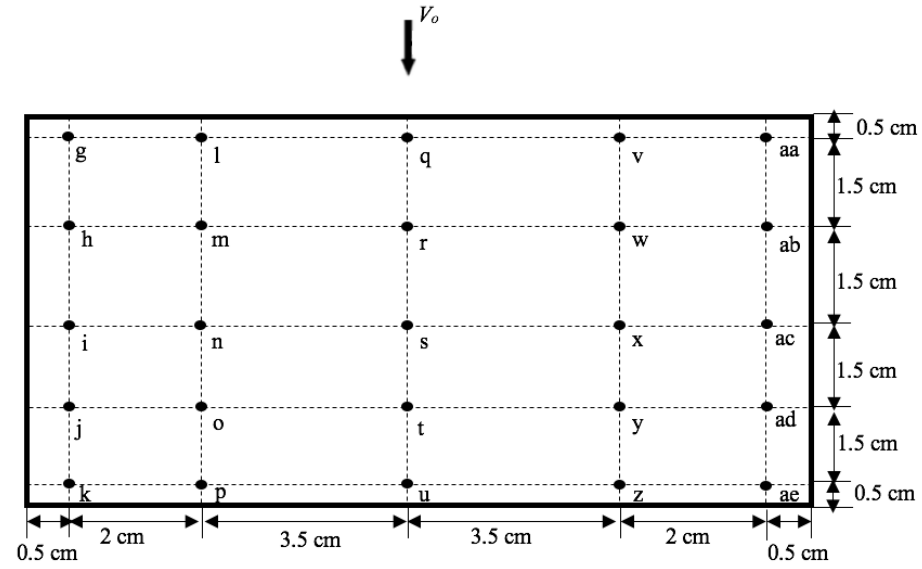

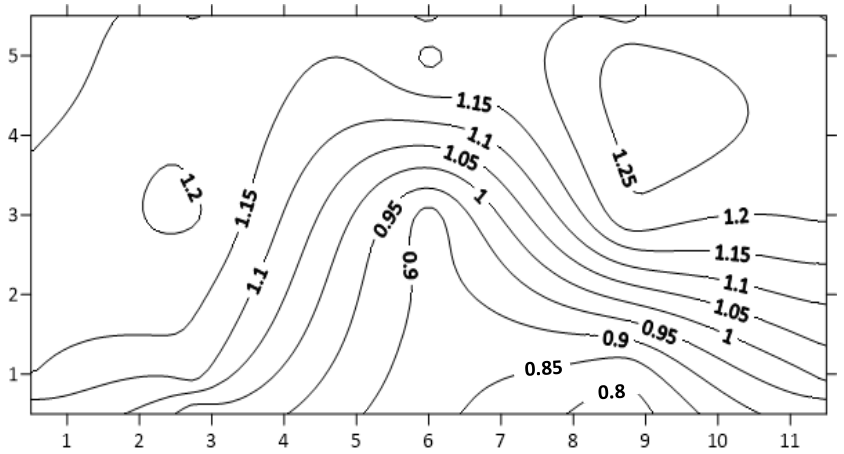

(a) Normalized wind velocities

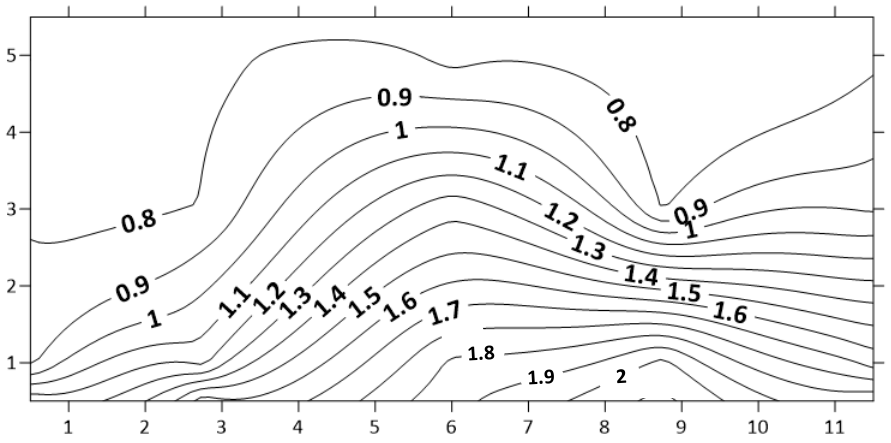

(b) Normalized turbulence intensities

Fig. 4.7: Normalized wind velocities and normalized turbulence intensities for the rectangular building shape tested at a wind direction of 0^o (modified after Higgins and Stathopoulos, 2020)

4.4 Database city configurations

Similar shaped building of city configuration *a* and city configuration *b* with various measurement points are included in the results database. City panels are tested for wind directions of 0^o, 15^o and 90^o. These wind directions were chosen as 0^o and 90^o represent two very different wind flow conditions and see the impact of building obstructions, and 15^o for comparison purposes with the testing set. Table 4.2 shows the wind velocities and turbulence intensities obtained through wind tunnel testing for the wind directions of 0^o, 15^o, 90^o for the measurement points. Results for 90^o for city configuration *b* are not recorded as the results were similar than those at 0^o. For these results, it may be observed that normalized turbulence intensities and normalized wind velocities may increase or decrease depending on the wind direction, due to the building's orientation. As an example, in Table 4.2 for city configuration *a*, the building *al* is blocked by the building *ak*, at wind direction of 0^o resulting in lower wind velocities. However, at a wind direction of 15^o recorded normalized wind velocities for building *al* and *ak* is the same, as building al is not blocking building *ak*. Channeling effect is observed at the pedestrian level for point *ao* and *an*. However, turbulence intensity is very high at point *ao*, thus it would not be suitable for turbine implementation.

In Table 4.2, for city configuration *b*, street-level normalized wind velocities were lower than those recorded at the pedestrian level. It has to be noted that the buildings are 36 cm high (in a geometric scale of 1:50). Therefore, due to the large building height, wind velocities are larger. However, pedestrian wind also shows interesting velocities, and lower turbulence intensities, leading to a potential site for turbine implementation.

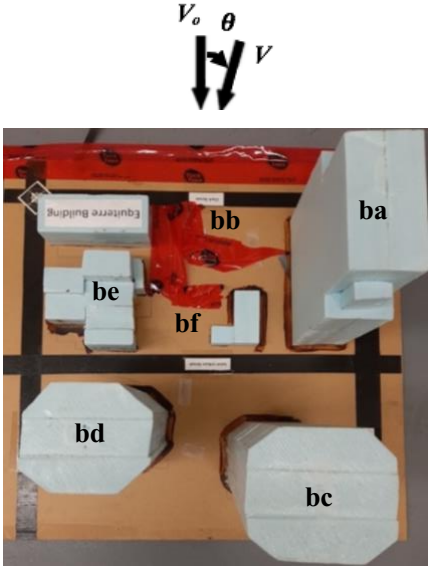

Table 4.2: Results for the similar building shape city panel (a) and similar height panel (b)

Building shape	*Point*	*V/V_o (T.I./T.I.$_o$)*		
		0°	*15°*	*90°*
City configuration (a)				
	ak	1.33 (0.73)	1.04 (0.71)	1.09 (0.79)
	al	1.16 (1.19)	1.04 (1.40)	0.64 (1.40)
	am	1.31 (0.74)	1.20 (0.75)	1.50 (1.10)
	an	1.10 (0.71)	0.5 (0.86)	1.30 (0.98)
	ao	1.09 (1.11)	0.37 (1.22)	
City configuration (b)				
	ba	1.29 (0.73)	1.30 (0.91)	
	bb	0.71 (1.19)	0.92 (0.90)	
	bc	1.31 (0.74)	1.26 (0.96)	
	bd	1.24 (0.71)	1.10 (0.91)	
	be	-	1.33 (1.37)	
	bf	0.85 (1.11)	0.92 (1.22)	

4.5 Database Accuracy Statistical Analysis

To ensure the measurement accuracy of the database, a statistical analysis was performed. From wind tunnel testing, the "% good" is obtained from the Cobra probe measurement, which corresponds to measured accuracy. The values of the % good may be found in Appendix A for all the data points. It may be observed that the measurement accuracy from the "% good" is lower for some locations. It has to be noted that in measurements closer to surfaces, the measurement accuracy decreases significantly, as the turbulence was higher there.

From the measurement accuracies in the total of 157 cases, the mean accuracy obtained is 70%. The variance in the measurement accuracy is calculated as per Eq. (4.1):

$$\sigma^2 = \frac{\sum(x-\mu)^2}{n} \quad \text{Eq. (4.1)}$$

where σ^2 is the variance, x is the sample variable, μ is the mean, n the sample size.

The obtained variance is 900. As the variance corresponds to the variance squared, the standard deviation of the measurement accuracy is 30.1. Thus, measurements are expected to vary along the observed standard deviation.

A T-test was performed over a 98% confidence interval in order to get the range of the measurement accuracies. T-testing is given as per Eq. (4.2):

$$t = \frac{\overline{x}-\mu}{s/\sqrt{n}} \quad \text{(Eq. 4.2)}$$

where t is the t-test result from the t-test table, $\overline{x}$ is the assumed mean, μ is the mean, s the standard deviation, n is the sample size.

For the 98% confidence interval, the sample size is said to vary between 60.6% and 70.4% of the measurement accuracy.

It is important to note that the "% good" in the measurement accuracy is proportional to the turbulence field, thus it is expected that measurements closer to rougher surfaces will impact the overall database mean, standard deviation and variance on the database.

4.6 Summary

From this section, an experimental set of data was designed to check on the impact of channeling, building shapes, and city configurations on the measured wind velocity and turbulence intensity compared to the upstream wind velocity V_o and turbulence intensity $T.I._o$. Channeling effect, building shape, and city configurations were tested for various wind directions θ, mostly between 0^o and 90^o. Results obtained through wind tunnel testing were compared to the results obtained in literature. To further test the accuracy and the analysis reliability, a rectangular building was tested for multiple measurement points on the rooftop for 0^o wind direction.

As there exist large variations in normalized wind velocities on the different cases, a certain form of correlation among building shapes, wind directions, and turbine location was sought. It is observed that highest normalized wind velocities are obtained when the edges and the corners of the buildings are parallel to the wind direction θ when tested for the turbine located on the building sides. This might be due to a flow acceleration caused by flow separation occurring at the edges of the building at the pedestrian level. There seems to have no clear linear correlation between the wind direction, building shape and the measured wind velocity. From the experimental results, determining design strategies to improve the wind energy generated is thus challenging. This suggests that there might exists a non-linear relationship between the building shape, wind direction, and turbine location with the measured normalized wind velocity and might be appropriately modeled through AI.

Chapter 5 Artificial Intelligence Results and Discussion

5.1 Overview

AI applications on urban wind energy is investigated as the evaluation of the different design strategies is difficultly achieved and time-consuming with only the present wind tunnel results. Using the 157 cases presented in Chapter 5, a result database for the normalized wind speeds is compiled and used for the development of the AI programs, the expert system and the artificial neural network (ANN). The accuracy of each method will be compared, analyzed and discussed with the testing set.

5.2 Testing set

City configurations were tested first on similarly-like building shapes city panel and a similar-height city panel. Table 5.1 presents the normalized velocities and normalized turbulence intensities obtained for the similarly-like building shape city panel (*b*) and the similar height buildings city panel (*c*). For comparisons purposes, city configurations were tested for wind direction of 15º, as the real case study in Montreal is tested for its critical wind direction. Montreal's critical wind direction is south-west (SW). As wind direction θ is taken in reference to the building axis of symmetry, the angle between the SW wind and the buildings' axis of symmetry is making an angle of 15º. Thus, buildings are tested for θ=15º. Highest normalized wind velocities were obtained by at the building sides for city configuration *b*. Square and rectangular building showed normalized wind velocities higher than 1.3: the experimental normalized turbulence intensities were below 1.0 in these cases. Analyzing results for city configuration *c*, results showed higher normalized wind velocities for higher buildings (point *ae*, *ag*, and *ai*) compared to the results at street-level. Turbine implementation is thus

recommended in these cases. Looking at points *af* and *aj*, it is shown that channeling effect augments wind velocities significantly: this strategy shall be used in to enhance power capture.

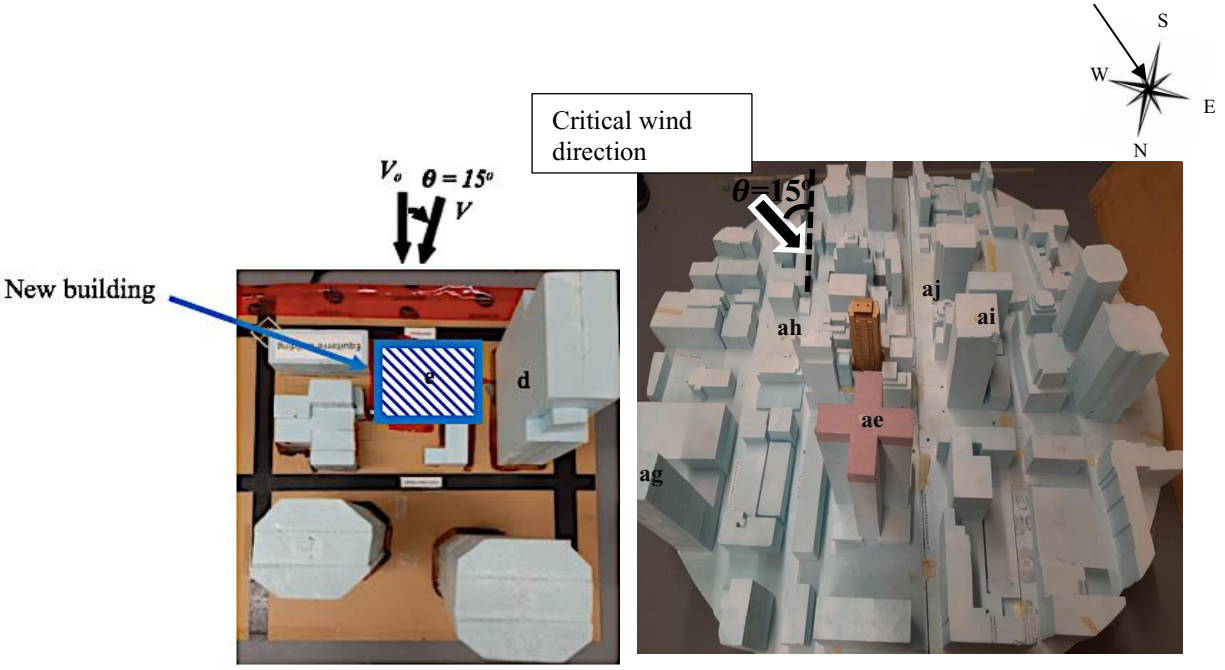

Table 5.1: City cluster and René-Lévesque street results for the testing set

Building shape	***Point***	***V/V_o***
City configuration (b)		
Square	d	1.33
Square	e	1.16
Rectangular	d	1.31
Rectangular	e	1.10
L-shape	d	1.09
L-shape	e	1.07
Boulevard René-Lévesque (c)		
	ae	1.30
	af	0.92
	ag	1.26
	ah	1.10
	ai	1.33
	aj	0.92

Some similarities between city configurations *b* and *c* results and building shapes results from Chapter 4 are observed. As for Chapter 4, city configuration *b* showed higher normalized wind velocities at for a turbine at the street-level than for roof-mounted wind turbines. This shows that modeling techniques may be efficient in predicting normalized wind velocities from the database.

5.3 Flow Chart Approach

A decisional flow chart is elaborated to serve as an aid to estimate the normalized wind velocity V/V_o resulting from the parametric input, and thus optimizing the power capture from an urban wind turbine. The developed approach is used for summarizing the main guidelines for assessing wind velocity changes due to input parameters prior to program AI. The present approach results in the estimated ratio of the measured wind velocity to the upstream measurement.

As described either by literature studies or wind tunnel testing, parameters affecting wind velocities are included in the flow chart approach. According to Stathopoulos et al, 2018, channeling may show a normalized wind velocity V/V_o up to 1.4 and may be used in various city configurations or in buildings. Wind directions between 15º and 45º yields in higher normalized wind speeds, and thus higher turbine power capture. Topographical locations as the summit of hills and escarpments, as well as in valleys may enhance power generation. As an example, preferring implementing a building on top of a mountain or in a valley may result in higher wind speeds. Using building shapes with a characteristic length L close to 1.0, as square, rectangular and L-shape induce a better power production form the turbine according to wind tunnel testing.

Using the previously mentioned conditions, the developed flow chart is shown in Fig. 5.1. The flow chart's starting point is the upstream velocity V_o, obtained from the measured airport velocity, at height z. The upstream velocity will then be adjusted in function of the terrain roughness. The normalized velocity V/V_o is obtained through the power law and with the supporting Davenport classification from Table 2.1, by doing the ratio of the mean speed exponents α ($0.84<V/V_o<0.91$ for suburban/urban terrain with $0.25<\alpha<0.36$). Then, the wind speed may be influenced by channeling. According to Gandemer and Guyot, 1976, recall Fig. 4.1, to have channeling, the openings must represent less than 5% of the length of the channel;

the height of the sides of the channel higher than 6m; and the width of the channel must be smaller than 2 times the height of its sides. If conditions are fulfilled, the normalized wind speed is approximatively 1.10. This value was obtained through wind tunnel testing, and since it more conservative than found by Stathopoulos et al, 2008, wind tunnel values are conserved. Wind velocity may be affected by the building position, either on a hill or an escarpment. A hill or escarpment is described, as per NBCC 2015, recall Fig. 2.1, as height to length ratio larger than 1:10. If this condition is fulfilled, the normalized velocity is given as per the NBCC 2015 Δs, as per Fig. 2.1. If the building may be placed on a valley (same requirements as channeling), the normalized wind velocity V/V_o is around 1.1. For any of the previous locations of the building, if there is only one critical wind direction, HAWT are preferred. If not, or if in highly turbulent environments (i.e. urban terrain), VAWT result in a power wind capture. Wind turbines may be implemented either on the building sides, integrated to the building, or on the rooftop. Depending on the building shape, the building shape, the normalized wind velocities varies as per the table provided in the flow chart in Table 4.1. Generally, square, rectangular and L-shaped buildings show higher wind velocities than U-shaped and T-shaped and are thus recommended.

To assess the flow chart, the square building shape in city configuration *b*. The building is placed in the urban terrain, thus V/V_o=0.84. The building is placed in a channel, thus the normalized velocity retrieved is V/V_o=1.1. The building is not placed on a hill, a mountain or a valley, thus there is no other change in the normalized wind speed to be considered. In Montreal, wind is coming from two main wind directions and is highly turbulent: VAWT is preferred. The turbine tested is located at the pedestrian level, tested for a wind direction of 15^o, near a square building. According to Table 4.1, the resulting normalized wind velocity is 1.58. By multiplying the effect of each element, the normalized wind velocity obtained through the present approach is 1.46, whereas the experimental value is 1.58. For the square building

rooftop, 1.07 and the experimental value s 1.21. Success rates rate for these two later cases is between 88% and 92%.

Variables

V_o: upstream velocity (airport velocity at given height)
α: mean speed exponent (Table 1)
V: measured velocity
L: length of the channel
h: height of the channel sides
l: length in the x-direction of the hill or escarpment
H: height of the hill or escarpment

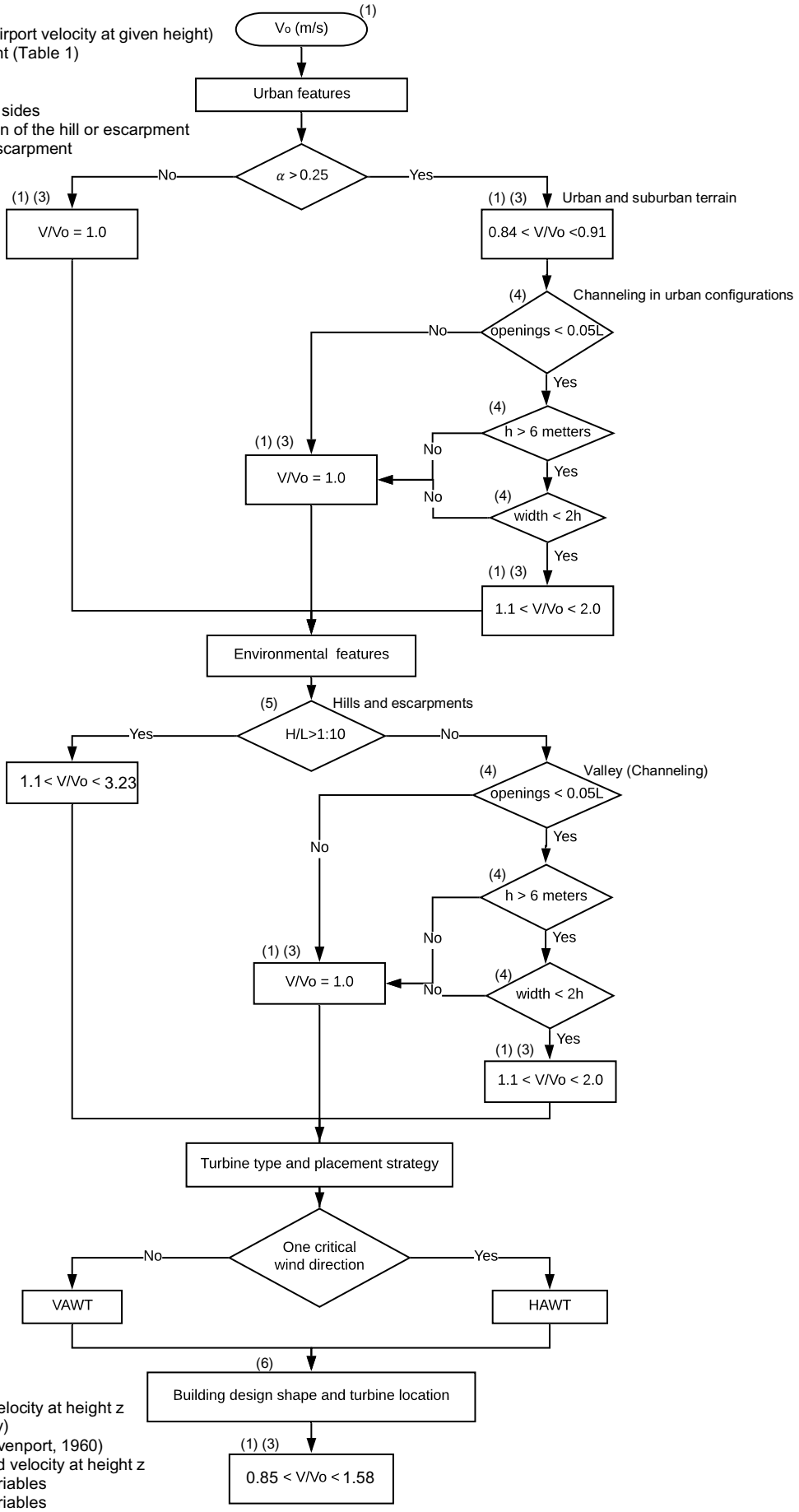

Notes

(1) V_o is the airport wind velocity at height z (approaching wind velocity)
(2) Refer to Table 2.1 (Davenport, 1960)
(3) V is the measured wind velocity at height z
(4) Refer to Fig. 4.1 for variables
(5) Refer to Fig. 2.1 for variables
(6) Refer to table 4.1 for V/V_o

Fig. 5.1: Decisional Flow chart approach

5.4 Expert system and ANN

In this thesis, the AI tools developed, the expert system and the ANN software, are tested with the testing set from city configurations *a* and *b*. The wind tunnel normalized wind velocities V/V_o are compared the normalized wind velocities *V/Vo* retrieved from the expert system and the ANN. Results are presented in Table 5.2. For the first part of the table shows results for city configuration *a,* and the second part of the table shows results for city configuration *b*. Normalized wind velocities V/V_o obtained through flow chart approach, expert system, ANN, and experiments are presented in the first set of columns. The second set of columns presents the respective success rates of the flow chart, expert system and ANN as predictive values. For comparison purposes, city configurations *a* and *b* were tested for wind direction θ=15º, as it corresponds to Montreal critical wind direction.

The experimental normalized wind velocities obtained through wind tunnel testing range from 1.12 to 1.58. The expert system yields in results between 1.07 to 1.33, leading to a minimal success rate of 84.2% and a maximum success rate of 98.2%. The ANN shows normalized velocities from 1.12 to 1.55, which corresponds to a minimal success rate of 93.8% and a maximum success rate of 99.7%. On average, the success rate of city configuration *a* is more accurate with the ANN than with the expert system. For city configuration *b*, the results of normalized wind velocities V/V_o ranges from 0.52 to 1.51 for experimental results. Expert system normalized velocities results were between 0.76 to 1.29. The expert system success rate varies between 71.9% to 98.8%. The ANN shows normalized wind velocities between 0.40 to 1.52, thus the success rate for ANN ranges from 76.9% to 97.6%. In average, the ANN shows higher success rates, than the expert system, leading to better predictive values.

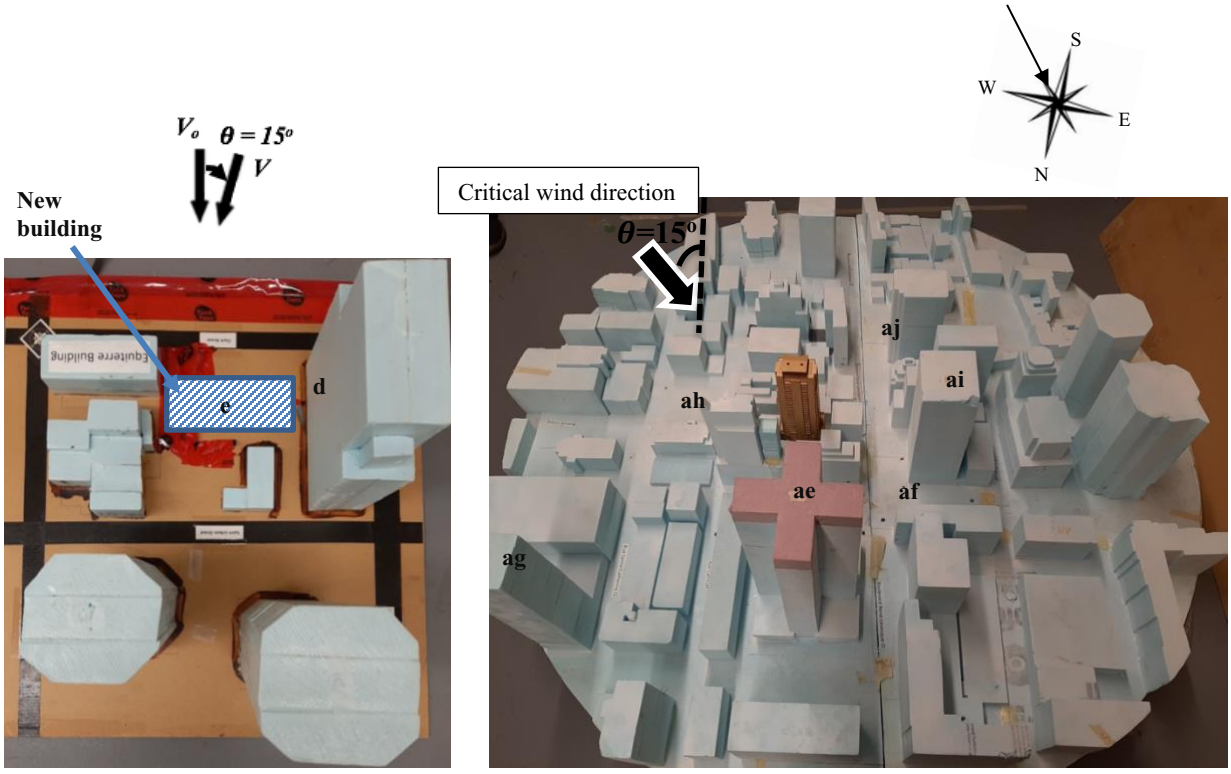

(a) City panel **(b) René-Lévesque street complex**

Table 5.2: Assessment and comparison of turbine locations in a new building implementation in a city configuration (testing set): experimental results, flow chart, expert system and ANN (Higgins and Stathopoulos, 2020)

Training date: Aug. 15, 2019 Testing date: Oct 20, 2019

	Point	***V/V₀***				***Success Rate***		
		Flow Chart	EXPERT	ANN	Experimental	Flow Chart	EXPERT	ANN
	15 degrees – city (a)							
Square	d-	1.46	1.33	1.55	1.58	92.4%	84.2%	**98.1%**
Square	e-	1.07	1.16	1.19	1.21	88.4%	95.8%	**98.1%**
Rectangle	d-	1.21	1.31	1.33	1.25	**96.8%**	95.4%	93.8%
Rectangle	e-	1.01	1.10	1.12	1.12	90.2%	98.2%	**99.7%**
L-shape	d-	1.15	1.09	1.19	1.17	**98.2%**	93.1%	**98.2%**
L-shape	e-	0.95	1.07	1.14	1.13	84.1%	94.7%	**99.4%**
	15 degrees - René-Lévesque – city (b)							
	ae	1.30	1.29	1.52	1.40	**92.8%**	92.1%	92.1%
	af	0.92	0.82	0.55	0.59	54.1%	71.9%	**93.2%**
	ag	1.26	1.29	1.81	1.51	83.4%	**85.4%**	83.4%
	ah	1.10	0.76	0.40	0.52	47.2%	68.4%	**76.9%**
	ai	1.33	1.20	1.45	1.40	95.0%	92.1%	**96.6%**
	aj	0.92	0.82	0.81	0.83	90.2%	**98.8%**	97.6%

From comparing results from Table 5.2 in both city configuration *a* and *b* and the success rates of the expert system and the ANN, it is found that the ANN shows better success rates in most cases than the expert system. As the expert system is better for qualitative predictions rather than quantitative, the expert system may serve as an indicator for the values to be obtained through the ANN for untrained conditions. Expert system may be useful to assess the turbine implementation location in qualitative manner or for designing a new building integrating urban wind energy. Although the ANN shows a better predictive value for the normalized wind velocity, both the ANN and the expert system tend to lose accuracy as the complexity of the city configuration tested increases. Modeling of complex flow conditions with increased turbulent flow represent one of the main difficulties in urban wind studies.

The flow chart approach showed, in most cases tested, a lower success rates then the previously mentioned systems, with an average success rate of 92.1% for city configuration *a* and 77.3% for city configuration *b* from Table 5.2. City configuration *a* from Table 5.2 showed normalized wind velocities varying between 1.00 and 1.4, with a success rate ranging from 88% to 99%. For more complex city configuration, as in city configuration *b* (Boul. René-Lévesque0, flow chart yielded in normalized wind velocities between 0.92 to 1.4, with a success rate between 54% and 100%. The average success rate of the flow chart is lower as the complexity of the city configuration increases. Moreover, the average success rate is lower than with AI software. It is a successful tool for quick preliminary assessment for optimizing the power capture of a turbine in an urban environment, or in case of assessing the reliability of AI output results for untrained conditions.

It is thus more appropriate for a preliminary estimate, and may be used as a guideline, but it remains the less accurate tool presented in this thesis. As it is more friendly user than the other tools, it may be used for quick assessment for designers.

5.5 Highlight

AI models evaluation through a given testing set showed encouraging results for predicting the normalized wind velocities in urban environments. With increasingly complex, success rates of the developed flow chart approach, expert system, and artificial neural network remained with a range of 80% to 99% in most cases. The developed flow chart approach is very effective, up to 98%, and less time consuming for assessing normalized wind velocities, for a preliminary assessment. As city configuration complexity increases, AI modeling techniques tend to lose accuracy. ANN is proven to be slightly more effective than the expert system with the highest success rates for 5 measurement points on a total 6 for city configuration *b* and for 3 measurement points on a total of 6 for city configuration *c*. Due to the high success rates obtained by ANN, it would be interesting to extend the database with the inclusion of meteorological parameters and other parameters. It could possibly correctly predict the wind power production for a turbine in urban environment over a certain period of time.

Chapter 6 Conclusion

6.1 Summary

Optimizing urban wind energy requires the elaboration of predictive models and a sufficient results database to comprehend the urban wind flow and assess design strategies. Database is elaborated from both literature and wind tunnel testing. Literature review on urban wind lack detailing on effects of building shapes and city configuration on wind turbine power production. Thus, a series of experiments on terrain exposure, channeling, building shapes and city configurations was elaborated. Measurements were conducted on a suburban exposure, kept constant through the experimental process. Channeling was tested for wind directions of 0^o to 90^o by increments of 15^o for measurement points placed at the entrance, middle, and wake of the channel. Several shapes, square, rectangular, U-shaped, T-shaped, and L-shaped buildings were tested for wind directions varying between -45^o to 135^o, with increments of 15^o, depending on cases. Results were computed in terms of the ratio of the measured velocity V to the upstream wind velocity V_o at same height z. Wind tunnel results show higher normalized wind velocities V/V_o for square, rectangular, and L-shaped buildings. In addition, few city configurations were tested, and experimental results were all included in a database.

The database was constructed with the 157 cases from the wind tunnel results and literature review. The database was implemented into AI tools. The expert system shows a success rate within 84% to 98% accuracy, and the feedforward ANN has a success rate ranging from 76.9% and 99.4%. The flow chart shows a lower accuracy than the AI tools. Both AI tools and flow chart may be used for preliminary assessment of a turbine. To increase accuracy and diversity of the systems, a larger and more complete database could be elaborated.

Experimental data were compared to CFD literature results. Both seem to indicate the same best building positioning for the highest velocities at the street level. Thus, it is proposed CFD may be used in the future for assessing turbine positioning.

6.2 Guidelines

From this research, some general conclusions and guidelines are retrieved for the AI applications in assessing design strategies for optimizing urban wind capture.

For best turbine locations, considering the literature review and the database:

(1) Use of topography (hills, escarpments, and valleys) to enhance wind velocities;

(2) If possible, use channeling effect in the urban environment for turbine implementation;

(3) Validate the effect of the building shape and the turbine location (rooftop, building sides) to ensure maximum power capture.

On AI applications, to model and assess different design strategies:

(1) Use of the ANN, expert system or as a preliminary assessment by retrieving the modified wind velocity: higher normalized wind velocities are expected to yield in higher wind power production;

(2) Decisional flow chart approach to be used as a quick preliminary assessment

Although this research constitutes a first step towards the development of urban wind energy, some more studies may be valuable to increase the accuracy in modeling urban power capture and improving design strategies.

6.3 Future studies

From this thesis, some elements are suggested to be further studied to improve urban wind power generation. It includes improving the database, studying the different ANN types and the input variables, as well as CFD applications to urban wind energy.

As a limited amount of results were achieved, the database may be increased through testing of many different points on rooftop locations for different wind directions and building shapes. The same could be done for the building sides to determine the optimal location for a possible turbine at the street level. In this study many architectural features have not been discussed in terms of wind speed and turbine locations. These include passageways between buildings, arcades and other architectural configurations. As edges enhance a flow separation and acceleration, it may be suitable to test for these features as a potentially good location for turbine implementation.

As the ANN yielded in accurate results, the neural network may be improved and studied. The network may be compared to other types of neural networks, and perhaps integrate meteorological data to predict the power output of a turbine. As Blanchard, 2019 results show conclusive results for the forecast of turbine power generation, and as results presented in this thesis were conclusive, perhaps the addition of the two inputs may yield in a complete program for prediction of urban power generation. However, special attention shall be kept since the meteorological data shall be presented in terms of time-series, whereas the other parameters presented in this thesis are not time dependent. Therefore, the ANN type shall be carefully chosen, and feedforward may not be the most accurate ANN.

Although this study focused on parameters affecting wind speed and compared results with literature, CFD results, and have been modeled through a data expert system, certain modeling techniques and its suitability was not further explored. Using CFD analysis for mean wind speeds at street level for turbine placement strategies may be further investigated. It has to be noted that CFD analysis is leading in good results for mean wind speeds (not loads) thus may be used for turbine placement insight only. CFD analysis may not be accurate for turbine load determination and design. Moreover, through the development of Google Earth tools for exposure, and though the development of the Expert System presented in this thesis, a powerful tool for decision making in turbine placement and prediction of power production may be produced.

In brief, here are the future works recommended:

(1) Impact on distance between building and the location of street-level turbine on wind power, impact on turbine roof location on wind power capture, and the effect architectural irregularities in buildings on wind velocities and turbulence intensities

(2) On the implementation of different neural networks and the incorporation of meteorological data on predicting urban wind power

(3) Application of Computational Fluid Dynamics in assessing urban wind energy

References

[1] Abohela, I., Hamza, N., Dudeck, S. 2013, "Effect of roof shape, wind direction, building height and urban configuration on the energy yield and positioning of roof mounted wind turbines", *Renewable Energy*, vol. 50, pp. 1106-1118.

[2] Alrawashdeh, A., Stathopoulos, T. 2020. "Wind loads on solar panels mounted on flat roofs: Effect of geomtetric scale", *Journal of Wind and Aerodynamics*, vol. 206.

[3] Baniotopoulos, C., Rebelo C., Simoes da Silva, L., Borri, C., Blocken, B., Hermida, H., Veljokovic, M., Morbiato, T., Borg, R. P., Huber, S., Efthymiou E. 2017. "International Conference on Wind Energy Harvesting" University of Coimbra, Portugal.

[4] Bohlouli, M., Mittas, N., Kakrontzas, G., Theodosiou, T., Angelis, L., Fathi, M. 2017. "Competence assessment as an expert system for human resource management: A mathematical approach", *Expert systems with Applications*, vol 70, pp. 83-102.

[5] Blanchard, T., Samanta, B" 2019. "Wind speed forecasting using neural network", *Wind Engineering*, pp. 1-16.

[6] Blocken B., Moonen, P., Stahtopoulos, T. ASCE, F., Carmeliet, J. 2008, "Numerical study on the existance of Venturi effect in passages between buildings", *Journal of Engineering Mechanics*, vol. 134, issue 12.

[7] Bre, F., Gimenez, J., Fachinotti, V, 2018, "Prediction of wind pressure coefficients on building surfaces using artificial neural networks", *Energy and Buildings,* vol. 158, pp.1429-1441.

[8] Carpentieri, M., Robins, A. G. 2015. "Influence of urban morphology on air flow over building arrays", *Journal of Wind Engineering and Industrial Aerodynamics*, vol.145, pp.61-74.

[9] Carruthers, N. B., Houghton, E. L. 1976. "Wind Forces on Buildings and Structures: an Introduction", New York, United States.

[10] Chopra, Anil K. 2012, "Dynamics of Structures", 4th edition, Boston, United States of America.

[11] Cook, J.1978. “Determination of the model scale factor in wind-tunnel simulations of the adiabatic atmospheric boundary layer”, *Journal of Wind Engineering and Industrial Aerodynamics*, vol. 21, pp.311-321.

[12] Davenport, A.G. 1960. “Rationale for determining design wind velocities”, *ASCE Journal of Structural Division*, vol. 86, pp. 39-68.

[13] Dilimulati, A., Stathopoulos, T., Paraschiovoiu, M. 2017. “Wind Turbine Designs for Urban Applications”, International Conference on Wind Energy Harvesting, Coimbra, Portugal.

[14] Du, Y., Ming Mak, C., Liu, J., Xia, Q., Niu, J., Kwok, K. C. S. 2017. “Effects of lift-u design on pedestrian level wind comfort in different building configurations under three wind directions”, *Building and Environment*, vol. 117, pp. 84-99.

[15] Emejeamara, F. C., Tiomlin, A., Milward-Hopkins, J. 2016, “Urban wind: Characterisation of useful gust and energy capture”, *Renewable Energy*, vol. 81, pp. 162-172.

[16] Englberger, A., Dornbrack, A. 2016, “Impact of the diurnal cycle of the atmospheric boundary layer on wind-turbine wakes: A numerical modelling study”, *Institute of Physics and Atmosphere*, vol. 166, pp. 423-438.

[17] Evans, Pete. 2018, “The Psychology of Climate Change Sketiptcs, and Building a Better Wind Turbine”, *CBC News*.

[18] Gomes, G. Rodriguez, A”, Mendes, P. 2005, “Experimental and numerical study of wind pressures on irregular-plan shapes”, *Journal of Wind Engineering and Industrial Aerodynamics*, Vol. 93, pp.741-756.

[19] Gu, Z., Zhao, W., Lu, H”, Wang, J. 2012, “ Multi-step forecasting for wind speed using a modified EMD-based artificial neural network model”, *Renewable Energy*, vol. 37, pp. 241-249.

[20] Hansen, S. O., Dyrbye, C. 1997. “Wind Loads on Structures”, New York, United States.

[21] Helppelmann, T., Steiner, A., Vogt, S. 2016, “Application of numerical weather prediction in wind power forecasting: Assessment of the diurnal cycle”, *Energy Meteorology*, vol. 26, pp. 319-331.

[22] Higgins, S, Stathopoulos, T. 2020, “Application of AI on urban wind energy” (submitted).

[23] Higgins, S, Stathopoulos, T. 2019, “Design strategies for optimizing wind energy production in urban environment”, CANCAM Conference, Sherbrooke.

[24] Huang, T., Kuo, C., Tzeng, C, Lai, C, 2015, “The influence of high-rise buildings on pedestrian-level wind in surrounding street canyons in an urban renewal project” *Energies*, vol.10, pp. 1942-1957.

[25] Jafari, a., Farzin, G., Emes, M., Arjomandi, M., Cazzolato, B. 2019. “Measurement of unsteady wind loads in a wind tunnel: Scaling of turbulence spectra”, *Jounral of Wind Eginerring and Instrial Aerodynamics,* vol. 193, p.103955.

[26] Jiang, Y. 2009, “Changes in wind speed over China during 1956–2004”, Springer, Vienna.

[27] Klink, K. 1999, “Trends in mean monthly maximum and minimum surface wind speeds in the coterminous United States, 1961 to 1990”, *Climate Research*, vol. 13, pp. 193-205.

[28] Krishnan A., Paraschivoiu, M. 2106. “3D analysis of building mounted VAWT with diffuser shaped shroud”, *Sustainable Cities and Society*, vol. 27, pp.160-166.

[29] Ledo, L., Kosasih, P.B., Cooper, P. 2010. “Roof mounting sit analysis for micro-wind turbines”, *Renewable Energy*, vol. 36, pp. 1379-1391.

[30] Liu, S., Pan, Wuxuan, Zhao, X., Zhang, H., Cheng, X., Long, Z., Chen, Q. 2018. “Influence of surrounding buildings on wind flow around a building predicted by CFD simulations”, *Building and Environment*, vol, 140, pp. 1 -10.

[31] Macera, A., Fiore, L., Lombardo, D., Kansara, D., Villeneuve, A., Higgins, S. 2016, “Building Integrated Wind Turbine”, Concordia University (internal report).

[32] McInnes, K., Erwin, T., Bathols, J. 2011, “Global climate model projected changes in 10 m wind speed and direction due to anthropogenic climate change”, *Atmospheric Science Letters*, vol. 12, pp. 325-333.

[33] Mittal, H., Sharna, A., Gairola, A. 2018. “A review on the study of urban wind at the pedestrian level around buildings”, *Journal of Building Engineering*, Vo. 18, pp. 154-163.

[34] National Building Code of Canada, 2015.

[35] Ngarambe, J., Yun, g. Y., Santamouris, M. 2020, “The use of artificial intelligence (AI) methods in the prediction of thermal comfort in buildings: energy implications of AI-based thermal comfort controls, *Energy and Buildings,* vol. 211, p. 109807.

[36] Ozmen, Y., Baydar, E., Van Beeck, J. 2016, “Wind flow over the low-rise building models with gabled roofs having different pitch angles”, *Building and Environment,* vol. 95, pp. 63-74.

[37] Pryor, S., Barthlemie, R. 2009, "Climate change impacts on wind energy: A review", *Renewable and Sustainable Energy Reviews*, vol. 14, pp. 430-437.

[38] Roy, A. K, Babu, N., Bhargava, P. K. 2012, "Atmospheris boundary layer airflow through CFD simulation on pyramidal roof of square plan shape buildings", 6th National Conference on Wind Enfgineering (NCWE), December 14-15th, 2012, New Dehli.

[39] Saeed, Q., A., Khan, A., Zameer, A., Usman, A. 2017. "Wind power prediction using deep neural network based meta regression and transfer learning", *Applied Soft Computing*, vol. 58, pp. 742-755.

[40] Simiu, E., Sacalan, R. H. 1985. "Wind Effects on Structures", 2nd edition, New Yor, United States.

[41] Stankovic, S. Campbell, N. Harries, A. 2009, "Urban Wind Energy", Earthscan, London.

[42] Stathopoulos, T. 1997. "Computational wind engineering: past achivements and future challenges", *Journal of Wind Engineering and Industrial Aerodynamics*, vol. 68-69, pp. 509-532.

[43] Stathopoulos, T. 2016. "Pedestrian Wind Environment Around Tall Buildings", *Advanced Environmental Wind Engineering*, pp. 101-127.

[44] Stathopoulos, T. 1987, "Wind Pressures on Flat Roofs with Parapets", *Journal of Structural Engineering*, vol. 113, no. 11, pp. 2166-2180.

[45] Stathopoulos, T., Alraweshdeh, H., Al-Quraan, A., Blocken, B., Dilimulati, A., Paraschivoiu, M., Pilay, P. 2018. "Urban wind energy: some views on potiential and challenges", *Journal of Wind Engineering and Industrial Aerodynamics,* vol. 179, pp. 146-157.

[46] Toja-Silvia, F., Kono, T., Peralta, C., Lopez-Garcia, O., Chen, J. 2013. "A review of computational fluid dynamics (CFD) simulations of the wind flow around buildings for urban energy exploitation", *Journal of Wind Engineering and Industrial Aerodynamics*, Vol. 180, pp.66-87.

[47] Tominaga Y., Akabayashi, S-i. Kitahara, T., Arinami, Y. 2015, "Air flow around isolated gable-roof buildings with different roof pitches: Wind tunnel experiments and CFD simulations", *Building and Environment*, vol. 84, pp. 204-213.

[48] Winstral, A., Jonas, T., Helbig, N. 2017, "Statistical downscaling of gridded wind speed data using local topography", *American Meteorological Society*, vol. 18, pp. 335-348.

[49] Zhou, H., Lue, Y., Liu, X., Chang, R., Wang, B. 2017, “Harvesting wind energy in low-rise residential buildings: Design and optimization of building forms”, *Journal of Cleaner Production*, vol. 167, pp. 306-316.

Appendices

Appendix-A: Wind tunnel results

Complete wind tunnel results, including the data accuracy, Cobra probe angles, velocities and turbulence intensities in the different directions for all measurement taken are presented in table format.

Appendix-B: Expert 2.0 Program

Expert system program and software application is explained. Program presented is in EXPERT 2.0 language, as the application has its own coding language.

Appendix-C: Artificial Neural Network Programming

C.1 ANN Programming Architecture

ANN architecture behind the program is discussed.

C.2 Matrix

Programming matrix are presented.

C.3 Program

ANN program is presented, in MATLAB language, as MATLAB has its own programming language.

Appendix-A

Wind tunnel results

Complete wind tunnel results, including turbulence intensities, wind velocities, yaw, pitch and % good results may be found bellow for the Louis-Hippolyte Lafontaine model, square, rectangular, U-shaped, T-shaped, and L-shaped buildings, and the tested city configurations for all measurement points and tested wind directions, included in both the database and the testing set. Tables and the presented results are listed below:

- Table A-A.1 shows the results for Louis-Hippolyte Lafontaine model,
- Table A-A.2, for the square building shape,
- Table A-A.3, for the rectangular building shape,
- Table A-A.4 for the U-shape building,
- Table A-A.5 for the T-shape building,
- Table A-A.6 for the L-shape building,
- Table A-A.7 for the first city configuration, with rectangular buildings,
- Table A-A.8 for the second city configuration, before the building implementation,
- Table A-A.9 for the second city configuration, after the building implementation,
- Table A.A-10 for the roof zones.

These tables may be found in the following pages of Appendix A.

Table A- A.1: Complete wind tunnel valley results

Axis ?	% Good	Vel	U	V	W	Iuvw	Iuu	Ivv	Iww
0 degrees									
d	99.98	5.38	5.22	0.344	0.98	11.7	15.2	9.81	9.11
e	100	6.64	6.56	-0.677	-0.123	10.5	13.6	9.57	7.56
f	99.95	6.29	6.04	-0.128	-1.27	15	17.6	13.4	13.7
15 degrees									
d	99.97	5.25	5.2	0.476	1.01	12.1	15.1	12.4	10.4
e	99.98	6.92	6.82	-0.675	-0.231	10.2	13.4	9.55	10
f	99.96	6.21	6.19	-0.223	-1.34	15.5	17.2	13.1	12
30 degrees									
d	99.98	5.1	4.96	0.231	-0.395	16	19.8	15.8	11.5
e	99.98	5.86	5.05	-0.56	-0.101	10	17.5	14.5	13.5
f	99.99	5.4	4.98	-0.117	-1.02	15	15.4	14	14.6
45 degrees									
d	99.8	5.1	4.96	-0.476	-0.395		16	19.8	15.8
e	99.4	6.07	5.66	-1.71	-0.236	16.9	19	16.8	14.6
f	95.9	5.14	4.78	-0.974	-0.675	24.1	30.6	22.8	17.1
60 degrees									
d	99.1	4.88	4.48	-0.658	-1.12	21.7	20.7	22.7	21.5
e	99.6	5.23	5	-0.495	0.593	18.8	21.2	16.3	18.4
f	94.2	4.95	4.65	-0.647	-0.281	26.4	34.3	21.3	21.4
75 degrees									
d	96.1	3.95	3.59	-0.141	-0.871	25.2	25	27.3	23
e	99.4	5.66	5.15	-1.66	1.08	17.1	19.6	16.3	15.2
f	61.4	3.17	2.77	-0.649	-0.24	35	38.2	40.8	23.4
90 degrees									
d	87.3	3.04	2.71	-0.224	-0.199	30	27	33.2	29.4
e	80.4	4.81	4.07	-2.32	0.189	21	26.4	21.6	12.6
f	25.9	2.35	2.04	-0.557	0.255	36.7	46.4	35.1	25.5

Table A- A.2: Complete wind tunnel results for square building shape

Axis ?	% Good	Vel	Pitch	Yaw	Pstatic	U	V	W	Iuvw	Iuu	Ivv	Iww
0 degrees												
d	96.6	11	-9.6	32.6	2.1	8.86	5.81	-1.97	15	12.7	18.2	13.7
e	46.2	2.6	6	19.3	63.2	2.04	0.822	0.222	36	24.9	37.9	42.9
f	100	10.2	-6.9	6.2	3.3	9.94	1.04	-1.24	12.4	13.2	11.9	12
15 degrees												
d	59.3	11.4	-8.4	42.1	5.5	8.22	7.51	-1.84	13.5	12.1	15.2	13.1
e	20.4	3.19	5.5	29	63.4	2.35	1.45	0.247	33.9	22.3	35.2	41.5
f	100	9.89	-5.6	-6.2	5.6	9.65	-1.1	-0.97	12.5	13.6	13	10.8
30 degrees												
d	99.9	9.43	-5.4	21.2	8.8	8.56	3.38	-0.976	14.1	12.9	15.7	13.6
e	4	3.33	9	20.9	48.5	2.43	1.14	0.476	38.2	22.5	46	41.8
f	100	9.8	-8.7	-2.8	7.8	9.52	-0.529	-1.5	12.8	12.8	15.3	9.68
45 degrees												
d	100	9.64	-5.4	9.5	4.3	9.32	1.56	-1.97	14.1	12.9	15.7	13.6
e	0.9	3.53	21.6	15.1	25	2.52	0.751	1.32	36	20.3	43.5	39.7
f	100	9.75	-8.4	-3.4	8.6	9.48	-0.612	-1.45	12.4	12.6	14.7	9.36
60 degrees												
d	100	8.63	-4	10.1	16.8	8.34	1.58	-0.657	12.8	14	11.8	12.5
e	2.2	3.82	8.5	12.8	14.6	2.91	0.744	0.538	39.6	25.7	43.1	46.8
f	100	9.59	-2.8	1.6	10.2	9.44	0.216	-0.498	12.3	13.5	12.5	10.9
75degrees												
d												
e	18	3.52	2.2	9.8	11.5	2.83	0.587	0.167	40.6	34	42.6	44
f	100	9.44	-0.2	5.7	19.3	9.27	0.893	-0.0632	12.3	13.4	12.4	10.9
90 degrees												
d	57.4	6.18	-2.6	-9.8	-0.2	5.39	-1.54	-0.438	39.9	50.8	37.4	28.3
e	34.4	2.5	2.2	2.4	10.1	2.06	0.0609	0.0925	42.9	41.1	45.3	42.2
f	100	9.53	1.9	-4.9	19.3	9.35	-0.845	0.278	12.4	13.5	13	10.5

Table A- A.3: Complete wind tunnel results for rectangular shape building

Axis ?	% Good	Vel	Pitch	Yaw	Pstatic	U	V	W	Iuvw	Iuu	Ivv	Iww
0 degrees												
d	97.3	9.81	-4.1	-8.2	10.8	9.43	-1.44	-0.731	17.2	20	15.6	15.7
e	77.4	2.98	-5.2	1	65.9	2.59	0.0157	-0.325	33.1	28.7	35.7	34.4
f	100	9.44	12.3	-3.2	14	9.04	-0.537	1.97	13.1	13.1	12.7	13.6
15 degrees												
d	98.8	9.43	-4.3	-8.2	10.4	9.43	-1.43	-0.775	16.1	17.7	14.9	15.7
e	46.2	3.34	-3.8	27.8	68.7	2.67	1.5	-0.322	28.9	24.8	29.4	32.1
f	100	9.41	12	-1.8	16.9	9.04	-0.299	1.93	13.2	13	12.1	14.4
30 degrees												
d	49.7	4.08	0.6	-3.5	2.3	3.5	-0.588	-0.0629	45.4	55.3	43.2	35.5
e	7.5	3.71	1.9	31.5	59.2	2.74	2.02	-0.0975	32.2	27.9	36.9	31.2
f	100	9.41	9.1	-4.1	25.2	9.12	-0.657	1.46	13	13.1	12.8	13
45 degrees												
d	100	9.27	-1.9	7.9	18.5	8.99	1.26	-0.381	14	13.2	12.7	16
e	1.9	2.64	20.9	-4.8	26.9	1.99	-0.158	0.909	37.6	24.9	46.9	37.7
f	100	9.44	3.2	-15.4	23.5	8.94	-2.49	0.501	13.1	13.9	13.9	11.2
60 degrees												
d	100	8.53	1.1	-1.7	29.3	8.4	-0.27	0.121	12.8	14.5	13.4	10.2
e	3.3	2.91	17.5	-2.1	7.3	2.37	-0.165	0.851	32.9	25.4	39.3	32.4
f	100	8.56	1.1	-0.3	23.9	8.32	-0.073	0.133	17.3	18	19.2	14.2
75degrees												
d	100	8.49	2.1	-9.1	27.6	8.28	-1.35	0.259	12.6	15.2	11.7	10.3
e	7.5	3.44	10.9	6.9	-3	2.79	0.304	0.6461	36.1	26	40.3	40.1
f	100	9.5	-3.5	-2.4	23.6	9.34	-0.436	-0.597	12.3	13.3	14	8.98
90 degrees												
d	96.8	8.69	0.5	-20.2	21.9	7.97	-3.02	0.0266	15.9	18.2	14.9	14.3
e	16.6	3.34	4.2	9.2	-6.4	2.67	0.437	0.273	39.9	30	41.9	46.1
f	99.9	9.58	-3.1	-8.5	24.6	9.32	-1.46	-0.534	12.7	14.1	14.3	8.85

Table A- A.4: Complete wind tunnel results for U-shaped building

Axis ?	% Good	Vel	Pitch	Yaw	Pstatic	U	V	W	Iuvw	Iuu	Ivv	Iww
0 degrees												
d	98.9	9.58	-2.9	8.6	21.5	9.24	1.39	-0.535	15.2	15.7	16.4	13.5
e	33.7	1.88	1.5	-10.5	63.4	1.58	-0.325	0.022	25.5	20.7	36.1	39.4
f	99.9	9.04	21.7	7.5	25.2	8.18	1.04	3.3	13.2	13.7	11	14.6
15 degrees												
d	99.3	9.74	-3.2	21	22.2	8.83	3.46	-0.64	15.8	13.9	18.3	14.9
e	40.2	2.12	2	-3.6	67.9	1.8	-0.0934	0.0243	37.7	35.4	36.2	41.2
f	99.8	9.12	21.3	-3.8	21.5	8.31	-0.561	3.29	13.5	13.1	10.6	16.2
30 degrees												
d	97	9.15	-3.3	16.4	17	8.52	2.5	-0.556	17.7	19.5	14	19.2
e	36.7	2.14	0.5	-13.6	72.3	1.78	-0.494	-0.0378	36.1	31.1	35.9	40.8
f	99.7	8.59	20.3	0.1	31.7	7.89	0.0152	2.95	14	14	12.6	15.3
45 degrees												
d	100	9.36	-2.2	9.9	22.9	9.02	1.6	0.423	14.3	14.4	14	14.6
e	34.2	3.06	3.1	-21.7	61	2.4	-1.08	0.0505	35.6	28	35.8	41.6
f	98.8	8.86	9.2	-15.8	25.1	8.2	-2.33	1.35	16.2	17.6	18.4	11.6
60 degrees												
d	99.9	9.19	-0.3	16.6	23.8	8.64	2,59	-0.13	14.6	15.5	12	15.9
e	25.5	3.21	7.5	-9.4	36.8	2.62	-0.613	0.345	37.9	31.7	43.2	38
f	97.7	8.83	9.1	4.4	29.5	8.47	0.675	1.33	16.7	19.7	16.6	13.4
75 degrees												
d	100	8.21	2.8	5.4	35.5	8.05	0.746	0.334	13.3	15.9	12.4	11.1
e	30.1	2.61	6.8	-2.6	21.8	2.2	-0.138	0.302	36.5	32.2	37.7	39.3
f	98.8	9.02	4.2	-1.6	28.2	8.8	-0.257	0.61	15.1	17	16.4	11.3
90 degrees												
d	99.9	8.49	2.2	2.5	33.9	8.34	0.371	0.269	13.8	15.9	13.1	12.1
e	31.9	2.36	-1.1	-4.9	11.4	1.97	-0.219	-0.082	38.5	32.9	36.2	45.3
f	99.7	9.23	1.4	-3.8	26.6	9.06	-0.635	0.198	13.5	15.1	14.8	10.3
-15 degrees												
d	99.3	9.6	-1.7	20	15.4	8.78	3.32	-0.398	15.5	14.2	17.5	14.7
-30 degrees												
d	99.4	8.66	-1.2	19.9	26	7.97	2.91	-0.284	14.8	15	11.3	17.5
-45 degrees												
d	99.9	9.62	-1.7	23.9	22.5	8.63	3.86	-0.398	13.8	13.3	13.5	14.7
-60 degrees												
d	99	9.55	-2.1	30.3	24.1	8.04	4.78	-0.504	15.4	13.7	17	15.4
-75degrees												
d	100	9.2	-0.9	11.8	21.1	8.82	1.85	-0.214	14.2	13.4	14.9	14.3

Table A- A.5: Complete wind tunnel results for T-shaped building

Axis ?	% Good	Vel	Pitch	Yaw	Pstatic	U	V	W	Iuvw	Iuu	Ivv	Iww
0 degrees												
d	99.7	8.33	-5	21.8	37.7	4.43	3.01	-0.803	15.7	14.9	18	13.8
e	88.2	3.57	-2.2	16.4	56.5	3.09	-1.03	-0.192	19.2	26.1	34.8	25.8
f	99.6	9.32	6.4	-1.6	18	8.93	-1.71	0.982	13.6	14.2	14.6	11.9
15 degrees												
d	99.4	7.8	-1.9	23.4	45.4	6.99	3.03	-0.304	15.7	15.8	17.5	13.5
e	81.8	3.66	-2.1	15.7	64.1	3.18	0.94	-0.212	29.3	25.4	34.2	27.4
f	99.6	9.26	5.4	-1.6	19.4	9.02	-0.277	0.834	14.5	14.2	16.5	12.5
30 degrees												
d	100	8.28	-2.6	19	40.5	7.67	-2.6	-0.436	14.1	14	15.5	12.7
e	33	4.86	-1.4	36.5	61	3.69	2.84	-0.279	22.7	19.7	24.4	23.8
f	100	9.38	6.1	2.5	20.5	9.16	0.369	0.964	13.2	13.8	11.7	13.8
45 degrees												
d	100	9.27	-4.3	9.2	30.3	9.01	1.46	-0.748	12.2	13.5	11.8	11.3
e	1.7	5.96	3	37.4	37.9	4.17	3.66	-0.0396	28.3	21.9	34	27.8
f	100	9.43	2.7	-4	20.3	9.24	-0.675	0.43	12.8	13	12.3	13
60 degrees												
d	99.9	9.29	-0.5	11.8	32.1	8.96	1.87	-0.136	12.4	13.5	11.7	12
e	1.3	4.34	16.9	14.1	-29.7	3.21	1.04	1.45	36.7	21.1	44.7	39.9
f	100	9.1	8.5	3.8	32.8	8.84	0.561	1.29	13	13.7	13.2	12
75degrees												
d	99.8	9.32	-1.4	-3.8	27.4	9.13	-0.641	-0.289	14.1	15.3	15.4	11.3
e	5.8	3.46	1.9	4.2	-22.7	2.94	0.19	0.12	34.5	27	38.5	37
f	100	8.99	3.3	0.6	36.3	8.84	0.0653	0.463	13	14.5	13.9	10.3
90 degrees												
d	99.6	9.28	-1.7	-10.1	23.2	8.93	-1.65	-0.33	15.8	18.1	15.8	13
e	13.2	3.17	0.5	3.6	-13.7	2.71	0.118	-0.0165	34.2	27.5	37.5	36.7
f	100	8.68	5.8	-1.6	38.6	8.51	-0.278	0.816	13	14.4	13.8	10.4

Table A- A.6: Complete wind tunnel results for L-shaped building

Axis ?	% Good	Vel	Pitch	Yaw	Pstatic	U	V	W	Iuvw	Iuu	Ivv	Iww
0 degrees												
e	35	2.02	-2.6	-8.4	69.8	1.71	-0.269	-0.146	35.7	30.8	36.9	39
f	98.8	9.49	19.6	-4.3	11.3	8.7	-0.688	3.17	14.8	14.3	11.7	17.8
15 degrees												
e	33.8	1.96	1.1	-2.5	75.5	1.66	-0.0687	-0.0233	36.8	31.2	38.5	40
f	95.6	9.2	20.4	-3.8	11.6	8.39	-0.524	3.2	16.8	19.8	12.5	17.3
30 degrees												
e	26.7	1.89	4.8	0.1	78	1.57	0.02	0.104	38.2	31.6	41	41
f	96.6	9.33	16.7	-16.3	15.8	8.38	-2.42	2.65	16	17.7	12.7	17.1
45 degrees												
d	99.6	10	-0.2	6.4	19.7	9.81	1.1	-0.925	13.1	14.6	12.7	11.8
e	28.3	2.11	5.2	0.5	74.8	1.74	0.0433	0.127	39.7	33.8	44.1	40.7
f	97.1	9.29	9.2	-21.3	21.3	8.31	-3.21	1.45	16.2	16.1	16	16.6
60 degrees												
d	97	10.7	2.6	8.2	2.6	10.3	1.44	0.411	16.3	20.4	12.2	15.3
75 degrees												
d	100	9.75	0.5	15.4	25.6	9.23	2.55	0.0175	13.4	13.7	14.8	11.5
90 degrees												
d	99.7	10.4	-1.4	28	21.5	8.96	4.81	-0.382	14.5	13.4	15.4	14.6
105 degrees												
d	99.6	9.86	-3.1	16.6	12	9.27	2.77	-0.586	13.5	14.2	12.4	14
120 degrees												
d	87.9	8.57	-0.6	7.9	21.5	8.18	1.05	-0.156	22.3	29.3	16.2	19.4
135 degrees												
d	98	9.17	3.5	11.8	24.3	8.75	1.8	0.51	16.1	17.7	16	14.3
-15 degrees												
d	100	7.92	4.8	1.9	42.1	7.76	0.247	0.607	13.7	16	13.4	11.4
e	24.3	1.86	0	-16.9	70.5	1.52	-0.526	-0.0457	35.2	29.3	36.4	39.1
f	100	8.94	8.2	-1.2	20.4	8.67	-0.256	1.22	14	13.8	15.6	12.6
-30 degrees												
d	99.9	8.76	4	19.2	39.3	8.14	2.82	0.55	13	15.2	12.5	11.1
e	32.8	2.13	0.6	-11.5	60	1.77	-0.401	-0.0322	38.1	33.9	40.2	39.8
f	99.9	8.8	5.2	-6	21.8	8.53	-0.99	0.731	14.7	14.4	16.9	12.5
-45 degrees												
d	100	9.33	0.4	9	30.3	9.07	1.43	0.00752	13.3	14.2	14	11.4
e	28.2	2.34	8.4	-1.4	43	1.95	-0.0369	-0.342	38.4	34.2	41.7	38.9
f	100	8.76	4.4	0.8	30.1	8.57	0.0488	0.617	14.1	15.2	15	11.8

60 degrees												
1	100	9.33	0.4	16.1	31	8.8	2.55	-0.00587	13.7	14.2	14.7	12
75 degrees												
d	100	9.38	-1.7	10.5	29.2	9.06	1.65	-0.345	13.6	14.6	14.5	11.6

Table A- A.7: Complete wind tunnel results for the city configurations with rectangular buildings

Axis ?	% Good	Vel	U	V	W	Iuvw	Iuu	Ivv	Iww
0 degrees									
1G	100	8.39	8.14	0.0721	1.33	13.7	15.1	14	11.9
2G	92.9	5.76	5.28	0.38	-0.966	26.7	29.1	26.3	24.5
3G	100	9.11	8.95	0.508	-0.43	13.5	15.6	13.4	11.1
2B	42.5	3.99	3.28	1.35	0.14	43.1	48.3	45	34.9
3B	43.4	3.69	3.02	0.955	-0.038	40.4	40	39.9	41.4
15 degrees									
1G	100	8.37	8.21	-0.0251	-0.237	14.3	15.6	14.7	12.3
2G	98.1	6.14	5.71	-0.664	-1.2	22.8	25.6	21	21.4
3G	100	9.3	8.97	-1.98	-0.153	12.7	14.2	14	9
2B	43.2	2.91	2.36	0.59	-0.3	40	34.2	44.1	41.1
3B	42.2	2.34	1.95	0.415	0.0408	38.4	33.8	43.2	37.6
90 degrees									
1G	100	8.77	8.38	-1.9	1.08	12.7	14.8	13.4	9.22
2G	98.5	5.19	4.88	0.796	-0.0438	23.6	27.9	25.8	15.9
1B	99.4	8.57	8.27	-1.14	-0.26	17.7	21.5	17.9	12.4
2B	99.9	7.56	7.32	-0.89	-0.869	15.7	18.2	17.3	10.2

Table A- A.8: Complete wind tunnel results for the existing building configuration before building implementation

Axis ?	% Good	Vel	Pitch	Yaw	Pstatic	U	V	W	Iuvw	Iuu	Ivv	Iww
0 degrees												
1	100	11.2	-6.2	10.1	7.2	10.8	1.89	-1.22	10.6	11.7	11.1	8.82
2	99.7	6.07	-3	6.7	42.6	5.87	0.644	-0.353	17.3	20.2	16.9	14.2
3	100	10.1	-1.4	-8.6	17.4	9.88	-1.54	-0.254	10.8	11.5	12.5	7.85
4	100	9.56	-4.8	-0.1	20.5	9.44	-0.0244	-0.829	10.3	12.7	9.24	8.46
5	100	7.07	-4	-14.2	28.7	6.68	-1.77	-0.545	16.1	17.2	18.4	11.9
15 degrees												
1	100	11.2	-1.6	6.4	8.2	11	1.21	-0.326	10.3	11.1	9.81	10
2	99	6.13	-7.8	-2.7	38	5.82	-0.344	-0.832	20.4	22.3	20.5	18
3	100	10.3	-4	-19.4	10.9	9.62	-3.44	-0.732	10.9	10.6	13.4	7.92
4	100	8.98	-3.6	-4.3	25	8.98	-0.642	-0.596	12.6	15.2	11.8	10.3
5	99.9	6.71	-7.7	-15.1	30.1	6.25	-1.75	-0.933	17.7	20.2	18.6	13.5

Table A- A.9: Complete wind tunnel results for new building implementation

Square shape - 15 degrees									
Axis ?	% Good	Vel	U	V	W	Iuvw	Iuu	Ivv	Iww
1	100	9.18	8.96	-1.06	0.625	13.3	14.4	14	11.2
2	100	8.84	8.63	0.629	-0.786	14	15.6	14.7	11.4
Rectangular shape									
1	99.8	9.05	8.84	-0.943	0.493	14	16.6	14.7	9.78
2	100	8.07	7.64	-2.21	-0.459	13.2	15.3	13.9	9.72
L-shape									
1	68.1	8.41	7.3	-3.47	0.622	20	21.5	22.8	15
2	86.5	4.34	3.82	1.21	-0.363	27.1	25.9	31.1	23.9
3	99.5	8.13	7.43	2.51	-0.64	17.8	15.4	21	16.4

Table A- A.10: Roof zones results

Axis ?	Vel	Iuvw	Iuu	Ivv	Iww	x	y
aa	10.9	12.4	11.8	10.8	14.3	8.75	5
ab	6.89	34.3	46.8	27.3	24.3	8.75	1
ac	10.5	12.6	11.9	11.3	14.3	11.5	5
ad	8.68	26.7	35.9	23.4	17.4	11.5	1
f	7.49	22	21.1	21.6	23.1	6	3
g	9.66	12.5	12	12.9	12.6	0.5	5.5
h	9.92	12.8	12.2	13.8	12.4	0.5	3
i	9.13	20.5	27	18.6	13.6	0.5	0.5
j	9.77	12.9	11.8	12.6	14.3	2.75	5.5
k	10.3	13	13	13.2	12.7	2.75	3
l	8.19	26.7	35.8	23.7	17.4	2.75	0.5
m	9.7	12.2	11	12.2	13.2	6	5.5
n	7.42	31.5	43.7	25	21.2	6	0.5
o	10.1	11.6	11.4	10.6	12.7	8.75	5.5
p	10.6	12.8	13.4	11.6	13.2	8.75	3
q	6.62	35.7	48.7	28.2	25.4	8.75	0.5
r	10.2	11.8	11.8	10.6	13	11.5	5.5
s	10.3	15.9	20	14	12.6	11.5	3
t	7.78	31.8	42.7	27.2	21.6	11.5	0.5
u	9.46	12.9	12.2	13.6	12.8	0.5	5
v	9.83	14.1	16.1	14.6	11.1	0.5	1
w	10.2	12.5	11.2	12.2	13.8	2.75	5
x	9.6	18.8	24.6	16.6	13.4	2.75	1
y	10.4	12.3	10.6	11.8	14.1	6	5
z	7.48	30.9	41.5	26.7	20.7	6	1

Appendix-B

EXPERT 2.0 Program

EXPERT 2.0 is an application developed by Microsoft allowing its users to program their own Expert System a user-friendly interface. This interface is divided in two parts: the first being the knowledge base and the second, the consultation part. In the knowledge base, the user will indicate its sets of rules, from which the consultation will then return the choice the closet to the set of rules implemented. Expert systems are suitable for a quick check qualitatively on the questioning. EXPERT 2.0 has its own programming language, which is further described in the Help section of the software.

The program implemented on EXPERT 2.0 for the various combinations studied through the experiments performed in the wind tunnel is presented in this Appendix.

1. Urban terrain → wind speed 0.84 V_i
2. Suburban terrain → wind speed 0.91V_i
3. Urban terrain, valley, 0 degrees wind direction, midpoint → 1.04
4. Urban terrain, valley, 15 degrees wind direction, midpoint → 1.09
5. Urban terrain, valley, 30 degrees wind direction, midpoint→ 0.92
6. Urban terrain, valley, 45 degrees wind direction, midpoint→ 0.95
7. Urban terrain, valley, 60 degrees wind direction, midpoint→ 0.82
8. Urban terrain, valley, 75 degrees wind direction, midpoint→ 0.89
9. Urban terrain, valley, 90 degrees wind direction, midpoint→ 0.76
10. Urban terrain, valley, 0 degrees wind direction, entrance → 0.99
11. Urban terrain, valley, 15 degrees wind direction, entrance →0.97
12. Urban terrain, valley, 30 degrees wind direction, entrance→ 0.85
13. Urban terrain, valley, 45 degrees wind direction, entrance→ 0.81
14. Urban terrain, valley, 60 degrees wind direction, entrance→ 0.78
15. Urban terrain, valley, 75 degrees wind direction, entrance→ 0.89
16. Urban terrain, valley, 90 degrees wind direction, entrance→ 0.37
17. Urban terrain, valley, 0 degrees wind direction, wake → 0.84
18. Urban terrain, valley, 15 degrees wind direction, wake → 0.82
19. Urban terrain, valley, 30 degrees wind direction, wake→ 0.80
20. Urban terrain, valley, 45 degrees wind direction, wake→ 0.80
21. Urban terrain, valley, 60 degrees wind direction, wake→ 0.76
22. Urban terrain, valley, 75 degrees wind direction, wake→ 0.62
23. Urban terrain, valley, 90 degrees wind direction, wake→ 0.47
24. Urban terrain, 0 degrees wind direction, square, sides →1.52
25. Urban terrain, 15 degrees wind direction, square, sides →1.58
26. Urban terrain, 30 degrees wind direction, square, sides →1.307
27. Urban terrain, 45 degrees wind direction, square, sides →1.34
28. Urban terrain, 60 degrees wind direction, square, sides →1.19
29. Urban terrain, 75 degrees wind direction, square, sides →1.12
30. Urban terrain, 90 degrees wind direction, square, sides →0.85
31. Urban terrain, 0 degrees wind direction, square, middle →0.36
32. Urban terrain, 15 degrees wind direction, square, middle →0.44
33. Urban terrain, 30 degrees wind direction, square, middle →0.46
34. Urban terrain, 45 degrees wind direction, square, middle →0.49
35. Urban terrain, 60 degrees wind direction, square, middle →0.53
36. Urban terrain, 75 degrees wind direction, square, middle →0.49
37. Urban terrain, 90 degrees wind direction, square, middle →0.35
38. Urban terrain, 0 degrees wind direction, square, rooftop, 24cm →1.20
39. Urban terrain, 15 degrees wind direction, square, rooftop, 24cm →1.16
40. Urban terrain, 30 degrees wind direction, square, rooftop, 24cm →1.15
41. Urban terrain, 45 degrees wind direction, square, rooftop, 24cm →1.14
42. Urban terrain, 60 degrees wind direction, square, rooftop, 24cm →1.11
43. Urban terrain, 75 degrees wind direction, square, rooftop, 24cm →1.11
44. Urban terrain, 90 degrees wind direction, square, rooftop, 24cm →1.12
45. Urban terrain, 0 degrees wind direction, rectangle, sides, 10 cm →1.36
46. Urban terrain, 15 degrees wind direction, rectangle, sides, 10 cm →1.31

47. Urban terrain, 30 degrees wind direction, rectangle, sides, 10 cm →0.56
48. Urban terrain, 45 degrees wind direction, rectangle, sides, 10 cm →1.28
49. Urban terrain, 60 degrees wind direction, rectangle, sides, 10 cm →1.18
50. Urban terrain, 75 degrees wind direction, rectangle, sides, 10 cm →1.17
51. Urban terrain, 90 degrees wind direction, rectangle, sides, 10 cm →1.2
52. Urban terrain, 0 degrees wind direction, rectangle, middle, 10 cm →0.41
53. Urban terrain, 15 degrees wind direction, rectangle, middle, 10 cm →0.46
54. Urban terrain, 30 degrees wind direction, rectangle, middle, 10 cm →0.51
55. Urban terrain, 45 degrees wind direction, rectangle, middle, 10 cm →0.37
56. Urban terrain, 60 degrees wind direction, rectangle, middle, 10 cm →0.40
57. Urban terrain, 75 degrees wind direction, rectangle, middle, 10 cm →0.47
58. Urban terrain, 90 degrees wind direction, rectangle, middle, 10 cm →0.46
59. Urban terrain, 0 degrees wind direction, rectangle, rooftop, 24 cm →1.1
60. Urban terrain, 15 degrees wind direction, rectangle, rooftop, 24 cm →1.1
61. Urban terrain, 30 degrees wind direction, rectangle, rooftop, 24 cm →1.1
62. Urban terrain, 45 degrees wind direction, rectangle, rooftop, 24 cm →1.1
63. Urban terrain, 60 degrees wind direction, rectangle, rooftop, 24 cm →1
64. Urban terrain, 75 degrees wind direction, rectangle, rooftop, 24 cm →1.1
65. Urban terrain, 90 degrees wind direction, rectangle, rooftop, 24cm →1.12
66. Urban terrain, 0 degrees wind direction, U-shape, sides, 10 cm →1.32
67. Urban terrain, 15 degrees wind direction, U-shape, sides, 10 cm →1.35
68. Urban terrain, 30 degrees wind direction, U-shape, sides, 10 cm →1.26
69. Urban terrain, 45 degrees wind direction, U-shape, sides, 10 cm →1.3
70. Urban terrain, 60 degrees wind direction, U-shape, sides, 10 cm →1.27
71. Urban terrain, 75 degrees wind direction, U-shape, sides, 10 cm →1.14
72. Urban terrain, 90 degrees wind direction, U-shape, sides, 10 cm →1.17
73. Urban terrain, 0 degrees wind direction, U-shape, middle, 10 cm →0.26
74. Urban terrain, 15 degrees wind direction, U-shape, middle, 10 cm →0.29
75. Urban terrain, 30 degrees wind direction, U-shape, middle, 10 cm →0.29
76. Urban terrain, 45 degrees wind direction, U-shape, middle, 10 cm →0.42
77. Urban terrain, 60 degrees wind direction, U-shape, middle, 10 cm →0.44
78. Urban terrain, 75 degrees wind direction, U-shape, middle, 10 cm →0.36
79. Urban terrain, 90 degrees wind direction, U-shape, middle, 10 cm →0.32
80. Urban terrain, 0 degrees wind direction, U-shape, rooftop, 24 cm →1.05
81. Urban terrain, 15 degrees wind direction, U-shape, rooftop, 24 cm →1.06
82. Urban terrain, 30 degrees wind direction, U-shape, rooftop, 24 cm →1.00
83. Urban terrain, 45 degrees wind direction, U-shape, rooftop, 24 cm →1.04
84. Urban terrain, 60 degrees wind direction, U-shape, rooftop, 24 cm →1.03
85. Urban terrain, 75 degrees wind direction, U-shape, rooftop, 24 cm →1.05
86. Urban terrain, 90 degrees wind direction, U-shape, rooftop, 24 cm →1.08
87. Urban terrain, -15 degrees wind direction, U-shape, sides, 10 cm →1.33
88. Urban terrain, -30 degrees wind direction, U-shape, sides, 10 cm → 1.2
89. Urban terrain, -45 degrees wind direction, U-shape, sides, 10 cm → 1.33
90. Urban terrain, -60 degrees wind direction, U-shape, sides, 10 cm → 1.32
91. Urban terrain, -75 degrees wind direction, U-shape, sides, 10 cm → 1.28
92. Urban terrain, 0 degrees wind direction, T-shape, sides, 10 cm →1.15

93. Urban terrain, 15 degrees wind direction, T-shape, sides, 10 cm →1.08
94. Urban terrain, 30 degrees wind direction, T-shape, sides, 10 cm →1.15
95. Urban terrain, 45 degrees wind direction, T-shape, sides, 10 cm →1.28
96. Urban terrain, 60 degrees wind direction, T-shape, sides, 10 cm →1.28
97. Urban terrain, 75 degrees wind direction, T-shape, sides, 10 cm →1.28
98. Urban terrain, 90 degrees wind direction, T-shape, sides, 10 cm →1.29
99. Urban terrain, 0 degrees wind direction, T-shape, middle, 10 cm →1.28
100. Urban terrain, 15 degrees wind direction, T-shape, middle, 10 cm →0.5
101. Urban terrain, 30 degrees wind direction, T-shape, middle, 10 cm →0.67
102. Urban terrain, 45 degrees wind direction, T-shape, middle, 10 cm →0.82
103. Urban terrain, 60 degrees wind direction, T-shape, middle, 10 cm →0.6
104. Urban terrain, 75 degrees wind direction, T-shape, middle, 10 cm →0.47
105. Urban terrain, 90 degrees wind direction, T-shape, middle, 10 cm →0.43
106. Urban terrain, 0 degrees wind direction, T-shape, rooftop, 24 cm →1.09
107. Urban terrain, 15 degrees wind direction, T-shape, rooftop, 24 cm →1.08
108. Urban terrain, 30 degrees wind direction, T-shape, rooftop, 24 cm →1.09
109. Urban terrain, 45 degrees wind direction, T-shape, rooftop, 24 cm→1.1
110. Urban terrain, 60 degrees wind direction, T-shape, rooftop, 24 cm →1.06
111. Urban terrain, 75 degrees wind direction, T-shape, rooftop, 24 cm →1.05
112. Urban terrain, 90 degrees wind direction, T-shape, rooftop, 24 cm →1.01
113. Urban terrain, -15 degrees wind direction, L-shape, sides, 10 cm →1.09
114. Urban terrain, -30 degrees wind direction, L-shape, sides, 10 cm →1.21
115. Urban terrain, 45 degrees wind direction, L-shape, sides, 10 cm →1.38
116. Urban terrain, 60 degrees wind direction, L-shape, sides, 10 cm →1.48
117. Urban terrain, 75 degrees wind direction, L-shape, sides, 10 cm →1.35
118. Urban terrain, 90 degrees wind direction, L-shape, sides, 10 cm →1.44
119. Urban terrain, 105 degrees wind direction, L-shape, sides, 10 cm → 1.36
120. Urban terrain, 120 degrees wind direction, L-shape, sides, 10 cm → 1.18
121. Urban terrain, 135 degrees wind direction, L-shape, sides, 10 cm →1.27
122. Urban terrain, 0 degrees wind direction, L-shape, middle, 10 cm → 0.28
123. Urban terrain, 15 degrees wind direction, L-shape, middle, 10 cm →0.27
124. Urban terrain, 30 degrees wind direction, L-shape, middle, 10 cm →0.26
125. Urban terrain, 45 degrees wind direction, L-shape, middle, 10 cm →0.29
126. Urban terrain, -15 degrees wind direction, L-shape, middle, 10 cm →0.26
127. Urban terrain, -30 degrees wind direction, L-shape, middle, 10 cm →0.29
128. Urban terrain, -45 degrees wind direction, L-shape, middle, 10 cm →0.32
129. Urban terrain, 0 degrees wind direction, L-shape, rooftop, 24 cm →1.11
130. Urban terrain, 15 degrees wind direction, L-shape, rooftop, 24 cm →1.07
131. Urban terrain, 30 degrees wind direction, L-shape, rooftop, 24 cm →1.09
132. Urban terrain, 45 degrees wind direction, L-shape, rooftop, 24 cm →1.08
133. Urban terrain, -15 degrees wind direction, L-shape, rooftop, 24 cm →1.03
134. Urban terrain, -30 degrees wind direction, L-shape, rooftop, 24 cm →1.02
135. Urban terrain, -45 degrees wind direction, L-shape, rooftop, 24 cm →1.3

Complex cases combinations:

136. Urban terrain, 0 degrees wind direction, rectangle, rooftop, 9cm →1.04
137. Urban terrain, 0 degrees wind direction, rectangle, side, 1.5 cm → 0.98
138. Urban terrain, 0 degrees wind direction, rectangle, rooftop, 7 cm → 1.14
139. Urban terrain, 0 degrees wind direction, rectangle, rooftop, 1.5 cm → 0.63
140. Urban terrain, 0 degrees wind direction, rectangle, sides, 15 cm → 0.58
141. Urban terrain, 15 degrees wind direction, rectangle, rooftop, 9cm →1.04
142. Urban terrain, 15 degrees wind direction, rectangle, side, 1.5 cm → 1.04
143. Urban terrain, 15 degrees wind direction, rectangle, rooftop, 7 cm → 1.2
144. Urban terrain, 15 degrees wind direction, rectangle, rooftop, 1.5 cm → 0.5
145. Urban terrain, 15 degrees wind direction, rectangle, sides, 15 cm → 0.37
146. Urban terrain, 90 degrees wind direction, rectangle, rooftop, 9cm →1.09
147. Urban terrain, 90 degrees wind direction, rectangle, side, 1.5 cm → 0.64
148. Urban terrain, 90 degrees wind direction, rectangle, rooftop, 7 cm → 1.5
149. Urban terrain, 90 degrees wind direction, rectangle, rooftop, 1.5 cm → 1.3
150. Urban terrain, 0 degrees wind direction, square, rooftop, 30 cm → 1.29
151. Urban terrain, 0 degrees wind direction, square, rooftop, 25 cm → 0.71
152. Urban terrain, 0 degrees wind direction, square, sides, 15 cm → 1.31
153. Urban terrain, 0 degrees wind direction, square, sides, 15 cm → 1.24
154. Urban terrain, 15 degrees win direction, square, rooftop, 30 cm → 1.29
155. Urban terrain, 15 degrees wind direction, square, rooftop, 25 cm → 0.71
156. Urban terrain, 15 degrees wind direction, square, sides, 15 cm → 1.34
157. Urban terrain, 15 degrees wind direction, square, sides, 15 cm → 1.16

Expert 2.0 program:

```
rule(1)
terrain=urban
valley=no
winddirection=no
shape=no
height=no
point=no
then
c1=84, cf=90 ;

rule(2)
terrain=suburban
valley=no
winddirection=no
shape=no
height=no
point=no
then
c1=91, cf=90;

rule (3)
terrain=suburban
valley=yes
winddirection=0
shape=no
height=15
point=wake
then
c1=84, cf=60;

rule(4)
terrain=suburban
valley=yes
winddirection=15
shape=no
height=15
point=wake
then
c1=82, cf=60;

rule (5)
terrain=suburban
valley=yes
winddirection=30
shape=no
height=15
point=wake
then
c1=80, cf=60;
```

rule (6)
terrain=suburban
valley=yes
winddirection=45
shape=no
height=15
point=wake
then
c1=80, cf=60;

rule (7)
terrain=suburban
valley=yes
winddirection=60
shape=no
height=15
point=wake
then
c1=76, cf=60;

rule (8)
terrain=suburban
valley=yes
winddirection=75
shape=no
height=15
point=wake
then
c1=62, cf=60;

rule (9)
terrain=suburban
valley=yes
winddirection=90
shape=no
height=15
point=wake
then
c1=47, cf=60;

rule (10)
terrain=suburban
valley=yes
winddirection=0
sahpe=no
height=15
point=middle
then
c1=84, cf=60;

rule(11)
terrain=suburban
valley=yes
winddirection=15
shape=no
height=15
point=middle
then
c1=82, cf=60;

rule (12)
terrain=suburban
valley=yes
winddirection=30
shape=no
height=15
point=middle
then
c1=80, cf=60;

rule (13)
terrain=suburban
valley=yes
winddirection=45
shape=no
height=15
point=middle
then
c1=80, cf=60;

rule (14)
terrain=suburban
valley=yes
winddirection=60
shape=no
height=15
point=middle
then
c1=76, cf=60;

rule (15)
terrain=suburban
valley=yes
winddirection=75
shape=no
height=15
point=middle
then
c1=62, cf=60;

rule (16)

terrain=suburban
valley=yes
winddirection=90
shape=no
height=15
point=middle
then
c1=47, cf=60;

rule (17)
terrain=suburban
valley=yes
winddirection=0
shape=no
height=15
point=entrance
then
c1=84, cf=60;

rule(18)
terrain=suburban
valley=yes
winddirection=15
shape=no
height=15
point=entrance
then
c1=82, cf=60;

rule (19)
terrain=suburban
valley=yes
winddirection=30
shape=no
height=15
point=entrance
then
c1=80, cf=60;

rule (20)
terrain=suburban
valley=yes
winddirection=45
height=15
shape=no
point=entrance
then
c1=80, cf=60;

rule (21)
terrain=suburban

valley=yes
winddirection=60
shape=no
height=15
point=entrance
then
c1=76, cf=60;

rule (22)
terrain=suburban
valley=yes
winddirection=75
shape=no
height=15
point=entrance
then
c1=62, cf=60;

rule (23)
terrain=suburban
valley=yes
winddirection=90
shape=no
height=15
point=entrance
then
c1=47, cf=60;

rule(24)
terrain=suburban
valley=no
winddirection=0
shape=square
height=100
point=side
then
c1=152, cf=60;

rule (25)
terrain=suburban
valley=no
winddirection=15
shape=square
height=100
point=side
then
c1=158, cf=60;

rule (25)
terrain=suburban
valley=no

winddirection=15
shape=square
height=100
point=side
then
c1=158, cf=60;

rule (26)
terrain=suburban
valley=no
winddirection=30
shape=square
height=100
point=side
then
c1=130, cf=60;

rule (27)
terrain=suburban
valley=no
winddirection=45
shape=square
height=100
point=side
then
c1=134, cf=60;

rule (28)
terrain=suburban
valley=no
winddirection=60
shape=square
height=100
point=side
then
c1=119, cf=60;

rule (29)
terrain=suburban
valley=no
winddirection=75
shape=square
height=100
point=side
then
c1=112, cf=60;

rule (30)
terrain=suburban
valley=no
winddirection=90

shape=square
height=100
point=side
then
c1=85, cf=60;

rule (31)
terrain=suburban
valley=no
winddirection=0
shape=square
height=100
point=middle
then
c1=36, cf=60;

rule (32)
terrain=suburban
valley=no
winddirection=15
shape=square
height=100
point=middle
then
c1=44, cf=60;

rule (33)
terrain=suburban
valley=no
winddirection=30
shape=square
height=100
point=middle
then
c1=46, cf=60;

rule (34)
terrain=suburban
valley=no
winddirection=45
shape=square
height=100
point=middle
then
c1=49, cf=60;

rule (35)
terrain=suburban
valley=no
winddirection=60
shape=square

height=100
point=middle
then
c1=53, cf=60;

rule (36)
terrain=suburban
valley=no
winddirection=75
shape=square
height=100
point=middle
then
c1=49, cf=60;

rule (37)
terrain=suburban
valley=no
winddirection=90
shape=square
height=100
point=middle
then
c1=35, cf=60;

rule (38)
terrain=suburban
valley=no
winddirection=0
shape=square
height=240
point=rooftop
then
c1=120, cf=60;

rule (39)
terrain=suburban
valley=no
winddirection=15
shape=square
height=240
point=rooftop
then
c1=116, cf=60;

rule (40)
terrain=suburban
valley=no
winddirection=30
shape=square
height=240

point=rooftop
then
c1=115, cf=60;

rule (41)
terrain=suburban
valley=no
winddirection=45
shape=square
height=240
point=rooftop
then
c1=114, cf=60;

rule (42)
terrain=suburban
valley=no
winddirection=60
shape=square
height=240
point=rooftop
then
c1=111, cf=60;

rule (43)
terrain=suburban
valley=no
winddirection=75
shape=square
height=240
point=rooftop
then
c1=111, cf=60;

rule (44)
terrain=suburban
valley=no
winddirection=90
shape=square
height=240
point=rooftop
then
c1=112, cf=60;

rule (45)
terrain=suburban
valley=no
winddirection=0
shape=rectangle
height=100
point=side

then
c1=136, cf=60;

rule (46)
terrain=suburban
valley=no
winddirection=15
shape=rectangle
height=100
point=side
then
c1=131, cf=60;

rule (47)
terrain=suburban
valley=no
winddirection=30
shape=rectangle
height=100
point=side
then
c1=56, cf=60;

rule (48)
terrain=suburban
valley=no
winddirection=45
shape=rectangle
height=100
point=side
then
c1=128, cf=60;

rule (49)
terrain=suburban
valley=no
winddirection=60
shape=rectangle
height=100
point=side
then
c1=118, cf=60;

rule (50)
terrain=suburban
valley=no
winddirection=75
shape=rectangle
height=100
point=side
then

c1=117, cf=60;

rule (51)
terrain=suburban
valley=no
winddirection=90
shape=rectangle
height=100
point=side
then
c1=120, cf=60;

rule (52)
terrain=suburban
valley=no
winddirection=0
shape=rectangle
height=100
point=middle
then
c1=41, cf=60;

rule (53)
terrain=suburban
valley=no
winddirection=15
shape=rectangle
height=100
point=middle
then
c1=46, cf=60;

rule (54)
terrain=suburban
valley=no
winddirection=30
shape=rectangle
height=100
point=middle
then
c1=51, cf=60;

rule (55)
terrain=suburban
valley=no
winddirection=45
shape=rectangle
height=100
point=middle
then
c1=37, cf=60;

rule (56)
terrain=suburban
valley=no
winddirection=60
shape=rectangle
height=100
point=middle
then
c1=40, cf=60;

rule (57)
terrain=suburban
valley=no
winddirection=75
shape=rectangle
height=100
point=middle
then
c1=47, cf=60;

rule (58)
terrain=suburban
valley=no
winddirection=90
shape=rectangle
height=100
point=middle
then
c1=46, cf=60;

rule (59)
terrain=suburban
valley=no
winddirection=0
shape=rectangle
height=240
point=rooftop
then
c1=110, cf=60;

rule (60)
terrain=suburban
valley=no
winddirection=15
shape=rectangle
height=240
point=rooftop
then
c1=110, cf=60;

rule (61)
terrain=suburban
valley=no
winddirection=30
shape=rectangle
height=240
point=rooftop
then
c1=110, cf=60;

rule (62)
terrain=suburban
valley=no
winddirection=45
shape=rectangle
height=240
point=rooftop
then
c1=110, cf=60;

rule (63)
terrain=suburban
valley=no
winddirection=60
shape=rectangle
height=240
point=rooftop
then
c1=100, cf=60;

rule (64)
terrain=suburban
valley=no
winddirection=75
shape=rectangle
height=240
point=rooftop
then
c1=110, cf=60;

rule (65)
terrain=suburban
valley=no
winddirection=90
shape=rectangle
height=240
point=rooftop
then
c1=112, cf=60;

rule (66)

terrain=suburban
valley=no
winddirection=0
shape=U
height=100
point=side
then
c1=132, cf=60;

rule (67)
terrain=suburban
valley=no
winddirection=15
shape=U
height=100
point=side
then
c1=135, cf=60;

rule (68)
terrain=suburban
valley=no
winddirection=30
shape=U
height=100
point=side
then
c1=126, cf=60;

rule (69)
terrain=suburban
valley=no
winddirection=45
shape=U
height=100
point=side
then
c1=130, cf=60;

rule (70)
terrain=suburban
valley=no
winddirection=60
shape=U
height=100
point=side
then
c1=127, cf=60;

rule (71)
terrain=suburban

valley=no
winddirection=75
shape=U
height=100
point=side
then
c1=114, cf=60;

rule (72)
terrain=suburban
valley=no
winddirection=90
shape=U
height=100
point=side
then
c1=117, cf=60;

rule (73)
terrain=suburban
valley=no
winddirection=0
shape=U
height=100
point=middle
then
c1=26, cf=60;

rule (74)
terrain=suburban
valley=no
winddirection=15
shape=U
height=100
point=middle
then
c1=29, cf=60;

rule (75)
terrain=suburban
valley=no
winddirection=30
shape=U
height=100
point=middle
then
c1=29, cf=60;

rule (76)
terrain=suburban
valley=no

winddirection=45
shape=U
height=100
point=middle
then
c1=42, cf=60;

rule (77)
terrain=suburban
valley=no
winddirection=60
shape=U
height=100
point=middle
then
c1=44, cf=60;

rule (78)
terrain=suburban
valley=no
winddirection=75
shape=U
height=100
point=middle
then
c1=36, cf=60;

rule (79)
terrain=suburban
valley=no
winddirection=90
shape=U
height=100
point=middle
then
c1=32, cf=60;

rule (80)
terrain=suburban
valley=no
winddirection=0
shape=U
height=240
point=rooftop
then
c1=105, cf=60;

rule (81)
terrain=suburban
valley=no
winddirection=15

shape=U
height=240
point=rooftop
then
c1=106, cf=60;

rule (82)
terrain=suburban
valley=no
winddirection=30
shape=U
height=240
point=rooftop
then
c1=100, cf=60;

rule (83)
terrain=suburban
valley=no
winddirection=45
shape=U
height=240
point=rooftop
then
c1=104, cf=60;

rule (84)
terrain=suburban
valley=no
winddirection=60
shape=U
height=240
point=rooftop
then
c1=103, cf=60;

rule (85)
terrain=suburban
valley=no
winddirection=75
shape=U
height=240
point=rooftop
then
c1=105, cf=60;

rule (86)
terrain=suburban
valley=no
winddirection=90
shape=U

height=240
point=rooftop
then
c1=108, cf=60;

rule (87)
terrain=suburban
valley=no
winddirection=15
shape=U
height=100
point=side
then
c1=133, cf=60;

rule (88)
terrain=suburban
valley=no
winddirection=30
shape=U
height=100
point=side
then
c1=120, cf=60;

rule (89)
terrain=suburban
valley=no
winddirection=45
shape=U
height=100
point=side
then
c1=133, cf=60;

rule (90)
terrain=suburban
valley=no
winddirection=60
shape=U
height=100
point=side
then
c1=132, cf=60;

rule (91)
terrain=suburban
valley=no
winddirection=75
shape=U
height=100

point=side
then
c1=128, cf=60;

rule (92)
terrain=suburban
valley=no
winddirection=0
shape=T
height=100
point=side
then
c1=115, cf=60;

rule (93)
terrain=suburban
valley=no
winddirection=15
shape=T
height=100
point=side
then
c1=108, cf=60;

rule (94)
terrain=suburban
valley=no
winddirection=30
shape=T
height=100
point=side
then
c1=115, cf=60;

rule (95)
terrain=suburban
valley=no
winddirection=45
shape=T
height=100
point=side
then
c1=128, cf=60;

rule (96)
terrain=suburban
valley=no
winddirection=60
shape=T
height=100
point=side

then
c1=128, cf=60;

rule (97)
terrain=suburban
valley=no
winddirection=75
shape=T
height=100
point=side
then
c1=128, cf=60;

rule (98)
terrain=suburban
valley=no
winddirection=90
shape=T
height=100
point=side
then
c1=129, cf=60;

rule (99)
terrain=suburban
valley=no
winddirection=0
shape=T
height=100
point=middle
then
c1=128, cf=60;

rule (100)
terrain=suburban
valley=no
winddirection=15
shape=T
height=100
point=middle
then
c1=50, cf=60;

rule (101)
terrain=suburban
valley=no
winddirection=30
shape=T
height=100
point=middle
then

c1=67, cf=60;

rule (102)
terrain=suburban
valley=no
winddirection=45
shape=T
height=100
point=middle
then
c1=82, cf=60;

rule (103)
terrain=suburban
valley=no
winddirection=60
shape=T
height=100
point=middle
then
c1=60, cf=60;

rule (104)
terrain=suburban
valley=no
winddirection=75
shape=T
height=100
point=middle
then
c1=47, cf=60;

rule (105)
terrain=suburban
valley=no
winddirection=90
shape=T
height=100
point=middle
then
c1=43, cf=60;

rule (106)
terrain=suburban
valley=no
winddirection=0
shape=T
height=240
point=rooftop
then
c1=109, cf=60;

rule (107)
terrain=suburban
valley=no
winddirection=15
shape=T
height=240
point=rooftop
then
c1=108, cf=60;

rule (108)
terrain=suburban
valley=no
winddirection=30
shape=T
height=240
point=rooftop
then
c1=109, cf=60;

rule (109)
terrain=suburban
valley=no
winddirection=45
shape=T
height=240
point=rooftop
then
c1=110, cf=60;

rule (110)
terrain=suburban
valley=no
winddirection=60
shape=T
height=240
point=rooftop
then
c1=106, cf=60;

rule (111)
terrain=suburban
valley=no
winddirection=75
shape=T
height=240
point=rooftop
then
c1=105, cf=60;

rule (112)
terrain=suburban
valley=no
winddirection=90
shape=T
height=240
point=rooftop
then
c1=101, cf=60;

rule (113)
terrain=suburban
valley=no
winddirection=15
shape=L
height=100
point=side
then
c1=109, cf=60;

rule (114)
terrain=suburban
valley=no
winddirection=30
shape=L
height=10
point=side
then
c1=121, cf=60;

rule (115)
terrain=suburban
valley=no
winddirection=45
shape=L
height=100
point=side
then
c1=138, cf=60;

rule (116)
terrain=suburban
valley=no
winddirection=60
shape=L
height=100
point=side
then
c1=109, cf=60;

rule (117)

terrain=suburban
valley=no
winddirection=75
shape=L
height=100
point=side
then
c1=135, cf=60;

rule (118)
terrain=suburban
valley=no
winddirection=90
shape=L
height=100
point=side
then
c1=144, cf=60;

rule (119)
terrain=suburban
valley=no
winddirection=105
shape=L
height=100
point=side
then
c1=136, cf=60;

rule (120)
terrain=suburban
valley=no
winddirection=120
shape=L
height=100
point=side
then
c1=118, cf=60;

rule (121)
terrain=suburban
valley=no
winddirection=135
shape=L
height=100
point=side
then
c1=127, cf=60;

rule (122)
terrain=suburban

valley=no
winddirection=0
shape=L
height=100
point=middle
then
c1=28, cf=60;

rule (123)
terrain=suburban
valley=no
winddirection=15
shape=L
height=100
point=middle
then
c1=27, cf=60;

rule (124)
terrain=suburban
valley=no
winddirection=30
shape=L
height=100
point=middle
then
c1=27, cf=60;

rule (125)
terrain=suburban
valley=no
winddirection=45
shape=L
height=100
point=middle
then
c1=27, cf=60;

rule (126)
terrain=suburban
valley=no
winddirection=15
shape=L
height=100
point=middle
then
c1=26, cf=60;

rule (127)
terrain=suburban
valley=no

winddirection=30
shape=L
height=100
point=middle
then
c1=29, cf=60;

rule (128)
terrain=suburban
valley=no
winddirection=45
shape=L
height=100
point=middle
then
c1=32, cf=60;

rule (129)
terrain=suburban
valley=no
winddirection=0
shape=L
height=240
point=rooftop
then
c1=111, cf=60;

rule (130)
terrain=suburban
valley=no
winddirection=15
shape=L
height=240
point=rooftop
then
c1=107, cf=60;

rule (131)
terrain=suburban
valley=no
winddirection=30
shape=L
height=240
point=rooftop
then
c1=109, cf=60;

rule (132)
terrain=suburban
valley=no
winddirection=45

shape=L
height=240
point=rooftop
then
c1=108, cf=60;

rule (133)
terrain=suburban
valley=no
winddirection=15
shape=L
height=240
point=rooftop
then
c1=103, cf=60;

rule (134)
terrain=suburban
valley=no
winddirection=30
shape=L
height=240
point=rooftop
then
c1=102, cf=60;

rule (135)
terrain=suburban
valley=no
winddirection=45
shape=L
height=240
point=rooftop
then
c1=130, cf=60;

rule (136)
terrain=suburban
valley=no
winddirection=0
shape=rectangle
height=90
point=rooftop
then
c1=104, cf=70;

rule (137)
terrain=suburban
valley=yes
winddirection=0
shape=rectangle

height=15
point=side
then
c1=98, cf=70;

rule(138)
terrain=suburban
valley=no
winddirection=0
shape=rectangle
height=70
point=rooftop
then
c1=114, cf=70;

rule(139)
terrain=suburban
valley=no
winddirection=0
shape=rectangle
height=15
point=rooftop
then
c1=63, cf=70;

rule(140)
terrain=suburban
valley=no
winddirection=0
shape=rectangle
height=150
point=side
then
c1=58, cf=70;

rule (141)
terrain=suburban
valley=no
winddirection=15
shape=rectangle
height=90
point=rooftop
then
c1=104, cf=70;

rule(142)
terrain=suburban
valley=yes
winddirection=15
shape=rectangle
height=15

point=side
then
c1=104, cf=70;

rule (143)
terrain=suburban
valley=no
winddirection=15
shape=rectangle
height=70
point=rooftop
then
c1=120, cf=70;

rule(144)
terrain=suburban
valley=no
winddirection=15
shape=rectangle
height=15
point=rooftop
then
c1=50, cf=70;

rule(145)
terrain=suburban
valley=no
winddirection=15
shape=rectangle
height=150
point=side
then
c1=58, cf=70;

rule(146)
terrain=suburban
valley=no
winddirection=90
shape=rectangle
height=90
point=rooftop
then
c1=109, cf=70;

rule(147)
terrain=suburban
valley=no
winddirection=90
shape=rectangle
height=15
point=side

then
c1=64, cf=70;

rule (148)
terrain=suburban
valley=no
winddirection=90
shape=rectangle
height=70
point=rooftop
then
c1=150, cf=70;

rule(149)
terrain=suburban
valley=no
winddirection=90
shape=rectangle
height=15
point=rooftop
then
c1=130, cf=70;

rule(150)
terrain=suburban
valley=no
winddirection=0
shape=square
height=300
point=rooftop
then
c1=129, cf=70;

rule(151)
terrain=suburban
valley=no
winddirection=0
shape=square
height=250
point=rooftop
then
c1=71, cf=70;

rule(152)
terrain=suburban
valley=yes
winddirection=0
shape=square
height=150
point=side
then

c1=131, cf=70;

rule(153)
terrain=suburban
valley=yes
winddirection=0
shape=square
height=150
point=side
then
c1=124, cf=70;

rule(154)
terrain=suburban
valley=no
winddirection=15
shape=square
height=300
point=rooftop
then
c1=129, cf=70;

rule(155)
terrain=suburban
valley=no
winddirection=15
shape=square
height=250
point=rooftop
then
c1=71, cf=70;

rule(156)
terrain=suburban
valley=yes
winddirection=15
shape=square
height=150
point=side
then
c1=134, cf=70;

rule(157)
terrain=suburban
valley=yes
winddirection=15
shape=square
height=150
point=side
then
c1=116, cf=70;

```
vl(terrain=suburban,urban)
qu(terrain=Terrain?)

vl(valley=yes,no)
qu(valley=Valley?)

vl(winddirection=0,15,30,45,60,75,90,105,120,135,15-,30-,45-)
qu(winddirection=Winddirection?)

vl(shape=sqaure,rectangle,U,T,L)
qu(shape=Shape?)

vl(height=15,200,300,150,240,350,20,30)
qu(height=Height?)

vl(point=rooftop,side,middle,entrance,wake)
qu(point=Point?)
```

Appendix-C

Artificial Neural Network Programming

Artificial neural network consists of a programming procedure inspired by the human brain neurones. ANN may solve complex non-linear problems due to its building architecture. However, development of the program requires values, as it does not cope well with qualitative inputs. Moreover, binary inputs must be avoided as much as possible to ensure an accurate output.

The following sections explore the architecture of the ANN, the input, target and sample matrix implemented in the programmed ANN, and the program coding.

C. 1 ANN Programming Architecture

ANN consists of three sections: the input layer, the hidden layers and the output layer. The input layer consists of the several combinations, or data set, for which the neural network will be trained. The hidden layers are the numbers of neurons, in between the input and output layer, where the system makes connections in order to predict the output. The number of layers is determined through previous knowledge and practice of the programmer. When the number of hidden layers is higher than one, the artificial neural network is referred as a multilayer system, which allows non-linear problem solving. The output layer is trained with the target values: once the neural network properly trained, the output layer may also yield in predictive values. Fig. A-C.1 summarizes the discussed ANN architecture (Bre et al, 2018).

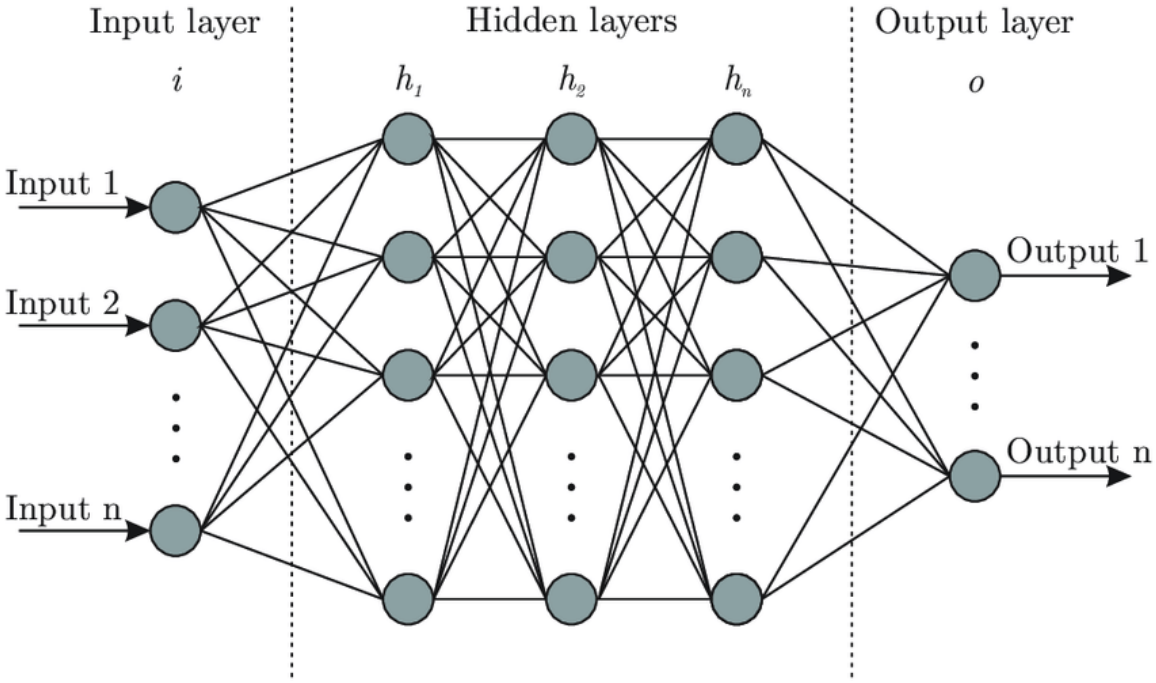

Fig. A- C.1. 1: Neural Network architecture (Bre et al, 2018)

Multiple types of ANN may be implemented. The simplest ANN is the feedforward, where the data is processed through the network. Other types of networks, such as auto-regression, time-series, and more may be more suitable for other problem types, which sometimes require more thoughtful handling. It has to be noted that for the neural network to function adequately, input and target matrix must be set properly, in terms of the correct parameters.

C.2 Matrix

Table A-C.1 presents the transposed input and target matrix. The parameters introduced are the following: terrain exposure, in terms of the mean velocity exponent, $\boldsymbol{\alpha}$, channeling effect, binary numbering, wind direction, the ratio distance within the channel to the total length, the ratio of distance of the point measurement to the total distance of the building façade, the building shape

described as the characteristic length, the obstruction behind the building in terms of binary numbering. Table A-C.2 shows the transposed target matrix:

A- C.2.2: Transposed input and target matrix for the ANN

Input								Target
$\boldsymbol{\alpha}$	Channeling	θ	z	x_1	x_2	L	Obstruction	V.
0.25	0	0	2.5	0.5	0	0	0	0.84
0.36	0	0	2.5	0.5	0	0	0	0.91
0.2	1	0	2.5	0.5	0	0	0	1.04
0.2	1	15	2.5	0.5	0	0	0	1.09
0.2	1	30	2.5	0.5	0	0	0	0.92
0.2	1	45	2.5	0.5	0	0	0	0.95
0.2	1	60	2.5	0.5	0	0	0	0.82
0.2	1	75	2.5	0.5	0	0	0	0.89
0.2	1	90	2.5	0.5	0	0	0	0.76
0.2	1	0	2.5	0	0	0	0	0.99
0.2	1	15	2.5	0	0	0	0	0.97
0.2	1	30	2.5	0	0	0	0	0.85
0.2	1	45	2.5	0	0	0	0	0.81
0.2	1	60	2.5	0	0	0	0	0.78
0.2	1	75	2.5	0	0	0	0	0.89
0.2	1	90	2.5	0	0	0	0	0.37
0.2	1	0	2.5	1	0	0	0	0.84
0.2	1	15	2.5	1	0	0	0	0.82
0.2	1	30	2.5	1	0	0	0	0.8
0.2	1	45	2.5	1	0	0	0	0.8
0.2	1	60	2.5	1	0	0	0	0.76
0.2	1	75	2.5	1	0	0	0	0.62
0.2	1	90	2.5	1	0	0	0	0.47
0.2	1	0	10	0	2	1.11	0	1.52
0.2	0	15	10	0	2	1.11	0	1.58
0.2	0	30	10	0	2	1.11	0	1.31
0.2	0	45	10	0	2	1.11	0	1.34
0.2	0	60	10	0	2	1.11	0	1.19
0.2	0	75	10	0	2	1.11	0	1.12
0.2	0	90	10	0	2	1.11	0	0.85
0.2	0	0	10	0	0.5	1.11	1	0.36
0.2	0	15	10	0	0.5	1.11	1	0.44
0.2	0	30	10	0	0.5	1.11	1	0.46
0.2	0	45	10	0	0.5	1.11	1	0.49

0.2	0	60	10	0	0.5	1.11	1	0.53
0.2	0	75	10	0	0.5	1.11	1	0.49
0.2	0	90	10	0	0.5	1.11	1	0.35
0.2	0	0	24	0	0.5	1.11	0	1.2
0.2	0	15	24	0	0.5	1.11	0	1.16
0.2	0	30	24	0	0.5	1.11	0	1.15
0.2	0	45	24	0	0.5	1.11	0	1.14
0.2	0	60	24	0	0.5	1.11	0	1.11
0.2	0	75	24	0	0.5	1.11	0	1.11
0.2	0	90	24	0	0.5	1.11	0	1.12
0.2	0	0	10	0	2	1.43	0	1.36
0.2	0	15	10	0	2	1.43	0	1.31
0.2	0	30	10	0	2	1.43	0	0.56
0.2	0	45	10	0	2	1.43	0	1.28
0.2	0	60	10	0	2	1.43	0	1.18
0.2	0	75	10	0	2	1.43	0	1.17
0.2	0	90	10	0	2	1.43	0	1.2
0.2	0	0	10	0	0.5	1.43	1	0.41
0.2	0	15	10	0	0.5	1.43	1	0.46
0.2	0	30	10	0	0.5	1.43	1	0.51
0.2	0	45	10	0	0.5	1.43	1	0.37
0.2	0	60	10	0	0.5	1.43	1	0.4
0.2	0	75	10	0	0.5	1.43	1	0.46
0.2	0	90	10	0	0.5	1.43	1	0.47
0.2	0	0	24	0	0.5	1.43	0	1.1
0.2	0	15	24	0	0.5	1.43	0	1.1
0.2	0	30	24	0	0.5	1.43	0	1.1
0.2	0	45	24	0	0.5	1.43	0	1.1
0.2	0	60	24	0	0.5	1.43	0	1
0.2	0	75	24	0	0.5	1.43	0	1.1
0.2	0	90	24	0	0.5	1.43	0	1.12
0.2	0	0	10	0	2	0.98	0	1.32
0.2	0	15	10	0	2	0.98	0	1.35
0.2	0	30	10	0	2	0.98	0	1.26
0.2	0	45	10	0	2	0.98	0	1.3
0.2	0	60	10	0	2	0.98	0	1.27
0.2	0	75	10	0	2	0.98	0	1.14
0.2	0	90	10	0	2	0.98	0	1.17
0.2	0	-15	10	0	2	0.98	0	1.33
0.2	0	-30	10	0	2	0.98	0	1.2
0.2	0	-45	10	0	2	0.98	0	1.33
0.2	0	-60	10	0	2	0.98	0	1.32
0.2	0	-75	10	0	2	0.98	0	1.28

0.2	0	0	10	0	0.5	0.98	1	0.26
0.2	0	15	10	0	0.5	0.98	1	0.29
0.2	0	30	10	0	0.5	0.98	1	0.29
0.2	0	45	10	0	0.5	0.98	1	0.42
0.2	0	60	10	0	0.5	0.98	1	0.44
0.2	0	75	10	0	0.5	0.98	1	0.36
0.2	0	90	10	0	0.5	0.98	1	0.32
0.2	0	0	24	0	0.5	0.98	0	1.05
0.2	0	15	24	0	0.5	0.98	0	1.06
0.2	0	30	24	0	0.5	0.98	0	1
0.2	0	45	24	0	0.5	0.98	0	1.04
0.2	0	60	24	0	0.5	0.98	0	1.03
0.2	0	75	24	0	0.5	0.98	0	1.05
0.2	0	90	24	0	0.5	0.98	0	1.08
0.2	0	0	10	0	2	0.68	0	1.15
0.2	0	15	10	0	2	0.68	0	1.08
0.2	0	30	10	0	2	0.68	0	1.15
0.2	0	45	10	0	2	0.68	0	1.28
0.2	0	60	10	0	2	0.68	0	1.28
0.2	0	75	10	0	2	0.68	0	1.28
0.2	0	90	10	0	2	0.68	0	1.29
0.2	0	0	10	0	0.5	0.68	1	0.5
0.2	0	15	10	0	0.5	0.68	1	0.67
0.2	0	30	10	0	0.5	0.68	1	0.82
0.2	0	45	10	0	0.5	0.68	1	0.6
0.2	0	60	10	0	0.5	0.68	1	0.47
0.2	0	75	10	0	0.5	0.68	1	0.43
0.2	0	90	10	0	0.5	0.68	1	0.4
0.2	0	0	24	0	0.5	0.68	0	1.09
0.2	0	15	24	0	0.5	0.68	0	1.08
0.2	0	30	24	0	0.5	0.68	0	1.09
0.2	0	45	24	0	0.5	0.68	0	1.1
0.2	0	60	24	0	0.5	0.68	0	1.06
0.2	0	75	24	0	0.5	0.68	0	1.05
0.2	0	90	24	0	0.5	0.68	0	1.01
0.2	0	45	10	0	2	0.99	0	1.38
0.2	0	60	10	0	2	0.99	0	1.48
0.2	0	75	10	0	2	0.99	0	1.35
0.2	0	90	10	0	2	0.99	0	1.44
0.2	0	-15	10	0	2	0.99	0	1.09
0.2	0	-30	10	0	2	0.99	0	1.21
0.2	0	105	10	0	2	0.99	0	1.36
0.2	0	120	10	0	2	0.99	0	1.18

0.2	0	135	10	0	2	0.99	0	1.27
0.2	0	0	10	0	0.5	0.99	1	0.28
0.2	0	15	10	0	0.5	0.99	1	0.27
0.2	0	30	10	0	0.5	0.99	1	0.26
0.2	0	45	10	0	0.5	0.99	1	0.29
0.2	0	-15	10	0	0.5	0.99	1	0.26
0.2	0	-30	10	0	0.5	0.99	1	0.29
0.2	0	-45	10	0	0.5	0.99	1	0.32
0.2	0	0	24	0	0.5	0.99	0	1.11
0.2	0	15	24	0	0.5	0.99	0	1.07
0.2	0	30	24	0	0.5	0.99	0	1.09
0.2	0	45	24	0	0.5	0.99	0	1.08
0.2	0	-15	24	0	0.5	0.99	0	1.03
0.2	0	-30	24	0	0.5	0.99	0	1.02
0.2	0	-45	24	0	0.5	0.99	0	1.3
0.2	0	0	9	0	0.5	1.125	0	1.04
0.2	1	0	1.5	0.5	2	0	0	0.98
0.2	0	0	7	0	0.5	1.05	0	1.14
0.2	0	0	1.5	0	0.5	0.8	0	0.63
0.2	1	0	15	0.5	2	0	0	0.58
0.2	0	15	9	0	0.5	1.125	0	1.04
0.2	1	15	1.5	0.5	2	0	0	1.04
0.2	0	15	7	0	0.5	1.05	0	1.2
0.2	0	15	1.5	0	0.5	0.8	0	0.5
0.2	1	15	15	0.5	2	0	0	0.37
0.2	0	90	9	0	0.5	1.125	0	1.09
0.2	1	90	1.5	0.5	2	0	0	0.64
0.2	0	90	7	0	0.5	1.05	0	1.5
0.2	0	90	1.5	0	0.5	0.8	0	1.3
0.2	1	90	15	0.5	2	0	0	1.29
0.2	0	0	30	0	0.5	2.53	0	1.29
0.2	0	0	25	0	0.5	2.54	0	0.71
0.2	1	0	15	0.5	2	0	0	1.31
0.2	1	0	15	0.5	2	0	0	1.24
0.2	0	15	30	0	0.5	2.53	0	1.29
0.2	0	15	25	0	0.5	2.54	0	0.71
0.2	1	15	15	0.5	2	0	0	1.34
0.2	1	15	15	0.5	2	0	0	1.16

Table A-C.2.3 shows the transposed sample matrix for the predicted output results once the program is trained:

A- C.2.3: Transposed sample matrix for the ANN

α	Channeling	θ	z	x_1	x_2	L	Obstruction
0.2	0	15	10	0	0.5	1.11	0
0.2	1	15	10	0.5	2	1.11	0
0.2	0	15	10	0	0.5	1.43	0
0.2	1	15	10	0.5	2	1.43	0
0.2	0	15	10	0	0.5	0.99	0
0.2	1	15	10	0.5	2	0.99	0

With the matrix set for the ANN, the elaboration of the program and its interface will be explained in the nest section.

C.3 Program

Programming the ANN was done by using MATLAB deep learning toolbox, nntool. The presented matrix from section C.2 were implemented in MATLAB toolbox. However, one might attempt to increase its efficiency or review the code. By using the function genFunction(network), the source code for network 1 was found. It has to be noted that ANN coding requires an iterative process. The program below is in MATLAB language:

```
function [Y,Xf,Af] = neural_function(X,~,~)

%NEURAL_FUNCTION neural network simulation function.
%
```

```
% Generated by Neural Network Toolbox function genFunction, 31-Jul-2019 16:52:20.
%
% [Y] = neural_function(X,~,~) takes these arguments:
%
%   X = 0xTS cell, 0 inputs over TS timesteps
%
% and returns:
%   Y = 0xTS cell of 0 outputs over TS timesteps.
%
% where Q is number of samples (or series) and TS is the number of timesteps.

%#ok<*RPMT0>

% ===== NEURAL NETWORK CONSTANTS =====


% ===== SIMULATION ========

% Format Input Arguments
isCellX = iscell(X);
if ~isCellX
  X = {X};
end

% Dimensions
TS = size(X,2); % timesteps

% Allocate Outputs
Y = cell(0,TS);

% Time loop
for ts=1:TS

end

% Final Delay States
Xf = cell(0,0);
Af = cell(0,0);

% Format Output Arguments
if ~isCellX
  Y = cell2mat(Y);
end
end

% ===== MODULE FUNCTIONS ========
```